Dissipation-range fluid turbulence and thermal noise

Dmytro Bandak and Nigel Goldenfeld*
Department of Physics, University of Illinois at Urbana-Champaign, Urbana, Illinois 61801, USA

Alexei A. Mailybaev
Instituto de Matemática Pura e Aplicada–IMPA, Rio de Janeiro, 22460-320, Brazil

Gregory Eyink
Department of Applied Mathematics & Statistics, The Johns Hopkins University, Baltimore, Maryland 21218, USA

(Received 29 July 2021; accepted 26 April 2022; published 29 June 2022)

We revisit the issue of whether thermal fluctuations are relevant for incompressible fluid turbulence and estimate the scale at which they become important. As anticipated by Betchov in a prescient series of works more than six decades ago, this scale is about equal to the Kolmogorov length, even though that is several orders of magnitude above the mean free path. This result implies that the deterministic version of the incompressible Navier-Stokes equation is inadequate to describe the dissipation range of turbulence in molecular fluids. Within this range, the fluctuating hydrodynamics equation of Landau and Lifschitz is more appropriate. In particular, our analysis implies that both the exponentially decaying energy spectrum and the far-dissipation-range intermittency predicted by Kraichnan for deterministic Navier-Stokes will be generally replaced by Gaussian thermal equipartition at scales just below the Kolmogorov length. Stochastic shell model simulations at high Reynolds numbers verify our theoretical predictions and reveal furthermore that inertial-range intermittency can propagate deep into the dissipation range, leading to large fluctuations in the equipartition length scale. We explain the failure of previous scaling arguments for the validity of deterministic Navier-Stokes equations at any Reynolds number and we provide a mathematical interpretation and physical justification of the fluctuating Navier-Stokes equation as an "effective field theory" valid below some high-wave-number cutoff Λ, rather than as a continuum stochastic partial differential equation. At Reynolds number around a million, comparable to that in Earth's atmospheric boundary layer, the strongest turbulent excitations observed in our simulation penetrate down to a length scale of about eight microns, still two orders of magnitude greater than the mean free path of air. However, for longer observation times or for higher Reynolds numbers, more extreme turbulent events could lead to a local breakdown of fluctuating hydrodynamics.

DOI: 10.1103/PhysRevE.105.065113

I. INTRODUCTION

The incompressible Navier-Stokes equation for the fluid velocity field $\mathbf{u}(\mathbf{x}, t)$ as a function of space $\mathbf{x}$ and time t:

$$\partial_t \mathbf{u} + (\mathbf{u}\cdot\boldsymbol{\nabla})\mathbf{u} = -\boldsymbol{\nabla} p + \nu\triangle\mathbf{u}, \quad \boldsymbol{\nabla}\cdot\mathbf{u} = 0, \tag{1.1}$$

since their original introduction [1], have been accepted for more than 100 years as the mathematical model of turbulence in molecular fluids at low Mach numbers and arbitrarily high Reynolds-numbers. These equations have been used as the starting point for statistical theories of turbulence, such as that of Reynolds [2]. In particular, these equations were invoked by Kolmogorov in his celebrated 1941 theory of turbulence (K41), which postulated a universal scaling behavior in the dissipation range of turbulent flow [3] and yielded the exact "4/5 law" [4]. There are rigorous derivations of the Navier-Stokes equations at any fixed Reynolds number, no matter how large, in the limit of small Mach number and small Knudsen number, starting from the Boltzmann equation for low-density gases [5,6] and from stochastic lattice-gas models with no restriction on density [7]. In fact, by a well-known argument of Corrsin using the K41 turbulence theory [8] (see also Ref. [9], Sec. 7.5), the hydrodynamic approximation which underlies the incompressible Navier-Stokes equation becomes increasingly better the higher the Reynolds number, because the Knudsen number decreases as an inverse power of Reynolds number. Mathematically, Leray [10,11] has shown that dissipative weak solutions of incompressible Navier-Stokes equation exist globally in time for any initial data of locally finite energy and also that these solutions remain smooth and unique locally in time for smooth initial data. The global smoothness remains an open question [12] and singularities might possibly appear in finite time for certain initial data at sufficiently high Reynolds number, as conjectured by Leray himself [10,11]. However, the existing rigorous derivations [5–7] show that, even if singularities occur so that Leray solutions are nonunique, nevertheless the empirical velocity field will satisfy *some* Leray solution of incompressible Navier-Stokes equations. The physical and mathematical foundations for basing a theory of turbulence on these equations seems thus quite secure.

*Present address: Department of Physics, University of California San Diego, La Jolla, California 92093, USA.

There are effects intrinsic to molecular fluids that are omitted, however, by the incompressible Navier-Stokes equations, most importantly thermal fluctuations [13,14]. These effects are described instead by an extension of the usual deterministic fluid equations known as *fluctuating hydrodynamics*, originally due to Landau and Lifschitz [15], Ch. XVII. For an incompressible fluid satisfying $\boldsymbol{\nabla}\cdot\mathbf{u}=0$ these equations have the form [16–21]

$$\partial_t\mathbf{u}+(\mathbf{u}\cdot\boldsymbol{\nabla})\mathbf{u}=-\boldsymbol{\nabla}p+\nu\triangle\mathbf{u}+\boldsymbol{\nabla}\cdot\widetilde{\boldsymbol{\tau}}, \tag{1.2}$$

with $\widetilde{\tau}_{ij}(\mathbf{x},t)$ a fluctuating stress prescribed as a Gaussian random field with mean zero and covariance

$$\langle\widetilde{\tau}_{ij}(\mathbf{x},t)\widetilde{\tau}_{kl}(\mathbf{x}',t')\rangle=\frac{2\nu k_BT}{\rho}\left(\delta_{ik}\delta_{jl}+\delta_{il}\delta_{jk}-\frac{2}{3}\delta_{ij}\delta_{kl}\right)\times\delta^3(\mathbf{x}-\mathbf{x}')\delta(t-t'), \tag{1.3}$$

whose realizations are symmetric and traceless, and with Boltzmann's constant $k_B\doteq 1.38\times10^{-23}\ \mathrm{m^2\,kg/s^2}\,K$. These equations can be phenomenologically derived by requiring that the equations with the added stochastic terms have the Gibbs measure

$$P_G[\mathbf{u}]=\frac{1}{Z}\exp\left(-\frac{\rho}{2k_BT}\int_\Omega d^3x\,|\mathbf{u}(\mathbf{x})|^2\right) \tag{1.4}$$

as an invariant measure, in which case Eq. (1.3) is known as the *fluctuation-dissipation relation*. It is very difficult to give Eqs. (1.2) and (1.3), as written, precise mathematical meaning as a stochastic partial differential equation and to show that it has Eq. (1.4) as an invariant measure (e.g., see Ref. [22]). One approach to make mathematical sense of this equation is as an equivalent Onsager-Machlup action or large-deviations rate function [23,24], and in this form it has been rigorously derived for a stochastic lattice gas [7]. However, the common approach of statistical physicists is to regard Eqs. (1.2) and (1.3) as an effective, low-wave-number field theory that should be truncated at some wave-number cutoff Λ which is larger than an inverse gradient length ℓ_∇^{-1} of the fluid but smaller than an inverse microscopic length $\lambda_{\mathrm{micr}}^{-1}$ (in a gas, the inverse mean free path $\lambda_{\mathrm{mfp}}^{-1}$). In fact, there are formal physical derivations of fluctuating hydrodynamics in this sense for compressible fluids starting from molecular dynamics [25–27] and taking the low Mach-number limit yields precisely Eqs. (1.2) and (1.3). Incorporating such a cutoff Λ, the fluctuating hydrodynamic equations become well-defined stochastic ODE's for a finite number of Fourier modes, and the corresponding Fourier truncated measure Eq. (1.4) is easily checked to be time-invariant; see Appendix A.

There have been, however, only a relatively few studies of the effects of thermal fluctuations on turbulent flows and most of these have focused on the role of weak noise in selecting a unique invariant measure for deterministic Navier-Stokes [28–30]. The presence of a new dimensional parameter in the fluctuating hydrodynamics Eqs. (1.2) and (1.3), the thermal energy k_BT, vitiates the similarity analysis of Kolmogorov [3,4], who postulated that the only relevant dimensional parameters in the dissipation range of a turbulent flow are the kinematic viscosity ν and the mean energy dissipation-rate per mass ε. This violation of Kolmogorov's 1941 analysis is in addition to the defect that he later noted himself [31], which is that space-time intermittency introduces dependence upon the outer length scale L of the flow. See Ref. [9] for an extensive review. The interplay between these two additional dimensional parameters, L and k_BT, is one of the major issues addressed in this work. For high Reynolds-number turbulent flows this interplay raises new questions regarding the precise formulation of fluctuating hydrodynamics, even within the "effective field theory" point of view. Arguing from K41 theory, the gradient length ℓ_∇, or largest length below which the velocity field is smooth, should be the Kolmogorov scale $\eta=\nu^{3/4}\varepsilon^{-1/4}$. However, space-time intermittency makes the dissipative cutoff fluctuate [32] (or Ref. [9], Sec. 8.5.5) so that at some points $\ell_\nabla\ll\eta$. In that case, does a cutoff length Λ^{-1} exist which satisfies the necessary conditions $\ell_\nabla\gg\Lambda^{-1}\gg\lambda_{\mathrm{micr}}$? If so, how should Λ be chosen in practice? And, most importantly, what significant effects, if any, does thermal noise have on the dynamics and statistics of incompressible turbulence?

We develop answers to all of these questions in this work and, in particular, argue that thermal noise has profound observable consequences for turbulence. In a following work we shall discuss the inertial range of scales, but here we deal with the dissipation range at scales smaller than the Kolmogorov length η. This range has been the subject of much theoretical and rigorous mathematical work within the framework of the incompressible Navier-Stokes equation for decades, for example, on the rate of decay of the spectrum [33–38] and on intermittency in the dissipation range [36,39,40]. There have also been intensive recent efforts to study the dissipation-range energy spectrum by direct numerical simulations (DNS) of the incompressible Navier-Stokes equations [41–43]. This is part of a larger program to determine the most extreme events and most singular, smallest-scale structures in a turbulent flow, at lengths far below the Kolmogorov scale [44–50]. The underlying science question which drives this work is whether the hydrodynamic equations can remain valid during such extreme turbulent events or whether strong singularities can lead to breakdown of the macroscopic, hydrodynamic description. We shall argue that much of this prior theory and simulation work is called into question for turbulence in real molecular fluids and may require substantial modifications, because effects of thermal noise become significant already at length scales right around the Kolmogorov scale. Laboratory experiments are now attempting to probe these small length scales [42,51,52], but as we shall discuss at length, all current experimental methods lack both the space-time resolution and the sensitivity to measure turbulent velocity fields accurately at sub-Kolmogorov scales. We regard this state of affairs as a crisis in turbulence research, which calls for the development of completely novel experimental techniques.

After the work in this paper was completed, we became aware of a series of remarkable papers published by Robert Betchov starting in the late 1950's [53–55], which anticipated several of our key conclusions. Betchov not only recognized the significant effects that thermal noise could have on dissipation-range statistics and other phenomena in fluid turbulence, such as transition and predictability, but he also developed the framework of fluctuating hydrodynamics for incompressible fluids [54], independent of Landau and Lifschitz [15]. Betchov carried out a novel experimental investigation

with a multi-jet flow created by a perforated box [53], designed to lower as much as possible the space resolution scale of extant hot-wire methods, to test his ideas. Unfortunately, despite improving upon the resolution and especially the accuracy of prior experiments by a couple of orders of magnitude, Betchov's experiments nevertheless lacked the sensitivity required to verify his predicted results. Because he employed linearized equations for his theoretical analysis, Betchov's predictions mainly regarded second-order statistics, such as energy spectra and one-dimensional dissipation, but he studied also experimentally the velocity-derivative skewness and kurtosis. Our analysis goes well beyond that of Betchov, taking full account of the nonlinearity of the fluid equations of motion and associated phenomena such as inertial-range intermittency, which were unappreciated in his day. However, Betchov's pioneering work should be more widely known and many of his ideas are still highly relevant today. We shall therefore compare his conclusions with our own results, which serve to confirm and extend his early insights. In the conclusion Sec. V of our paper we shall briefly review Betchov's experiments and place them in the context of current efforts.

We shall proceed in this paper by developing simple theoretical arguments which are then tested numerically in a reduced dynamical model of turbulence, the Sabra shell model [56,57]. Our numerical results for this model provide, to our knowledge, the first empirical confirmation of Betchov's essential predictions anywhere in the literature. Furthermore, based upon these simulations, we shall then formulate more refined theoretical predictions for the dissipation range of real fluid turbulence. A short report of our most essential physical predictions has been given elsewhere [58], but we provide here full details of our numerical study and, furthermore, address the quite subtle and complex issues surrounding the hydrodynamic description of turbulent flows.

The detailed contents of our paper are as follows: In Sec. II we discuss the incompressible fluctuating hydrodynamics model Eq. (2.1) and its physical and mathematical foundations for describing turbulent fluid flow. This includes the formulation of the basic equations (Sec. II A) and an extended dimensional analysis of turbulence taking into account thermal effects (Sec. II B). In particular, we discuss how thermal noise breaks the scaling symmetry of deterministic incompressible Navier-Stokes Eq. (1.1) and why standard arguments on its validity for molecular fluids thus fail in the dissipation range of turbulent flows (Sec. II C). We make also a preliminary evaluation of the effects of inertial-range intermittency by a phenomenological multifractal approach, to assess possible limitations to a hydrodynamic description of high-Reynolds turbulence (Sec. II D). To test these theoretical ideas we develop in Sec. III a stochastic Sabra shell model of fluctuating hydrodyamics. We justify carefully the use of this "zero-dimensional" model despite some significant differences from fluctuating hydrodynamics in three space dimensions (Sec. III A), and we discuss its meaning and numerical solution as an effective theory for low wave numbers (Sec. III B). The main Sec. IV of our paper presents numerical results on thermal noise effects in turbulence, obtained by simulating the shell model, which confirm our theoretical predictions and motivate additional conjectures for fluid turbulence. After describing the set-up of our turbulence simulations (Sec. IV A), we present results on thermal effects in the statistics of modal energies (Sec. IV B), a comparison of dissipation-range intermittency for the deterministic and stochastic model (Sec. IV C), and a similar comparison of shell-model structure function scaling in the inertial-range as well as the dissipation range (Sec. IV D). Finally, Sec. V summarizes our conclusions and outlines directions for future work.

II. FLUCTUATING HYDRODYNAMICS OF TURBULENT FLOW

A. Formulation of the equations

To keep things simple, we take as flow domain a periodic box or 3 torus, $\Omega = L\mathbb{T}^3$, with volume $V = |\Omega| = L^3$. Then, to discuss steady-state turbulent flow, we shall modify Eq. (1.2) in two ways. First, we shall employ the standard theoretical artifice of adding to the local momentum balance an external body force $\rho\mathbf{f}$ to drive the turbulent flow, assuming that this force is supported in Fourier space at very low wave numbers $\sim 1/L$. Second, and very essentially, we shall assume that the velocity field is comprised of Fourier modes with wave numbers $|\mathbf{k}| < \Lambda$ only, a condition which may be expressed in terms of a projection operator P_Λ:

$$\mathbf{u}(\mathbf{x}) = P_\Lambda \mathbf{u}(\mathbf{x}) := \frac{1}{V}\sum_{|\mathbf{k}|<\Lambda} e^{i\mathbf{k}\cdot\mathbf{x}}\hat{\mathbf{u}}_\mathbf{k},$$

and then the fluctuating hydrodynamic Eq. (1.2) is modified to

$$\partial_t \mathbf{u} + P_\Lambda(\mathbf{u}\cdot\nabla)\mathbf{u} = -\nabla p + \nu\triangle\mathbf{u} + \left(\frac{2\nu k_B T}{\rho}\right)^{1/2}\nabla\cdot\boldsymbol{\eta}_\Lambda + \mathbf{f},$$
$$\nabla\cdot\mathbf{u} = 0. \tag{2.1}$$

Separating out the covariance of the thermal noise facilitates our scaling analysis below. Thus $\boldsymbol{\eta}_\Lambda(\mathbf{x},t)$ is a tensor space-time Gaussian field with mean zero and covariance

$$\langle \eta_{\Lambda ij}(\mathbf{x},t)\eta_{\Lambda kl}(\mathbf{x}',t')\rangle = \left(\delta_{ik}\delta_{jl} + \delta_{il}\delta_{jk} - \frac{2}{3}\delta_{ij}\delta_{kl}\right)\delta^3_\Lambda(\mathbf{x}-\mathbf{x}')\delta(t-t'), \tag{2.2}$$

for

$$\delta^3_\Lambda(\mathbf{x}-\mathbf{x}') = P_\Lambda\delta^3(\mathbf{x}-\mathbf{x}') = \frac{1}{V}\sum_{|\mathbf{k}|<\Lambda} e^{i\mathbf{k}\cdot\mathbf{x}}. \tag{2.3}$$

The kinematic pressure p in Eq. (2.1) is determined by the requirement that $\mathbf{u}$ be solenoidal and obviously satisfies the condition $p = P_\Lambda p$. In contrast to the original Eq. (1.2) with no UV cutoff Λ, which is mathematically ill-defined *a priori*, the Eq. (2.1) is equivalent to a system of Itō stochastic differential equations for the Fourier modes $\hat{\mathbf{u}}(\mathbf{k})$ of the velocity field and its solutions are stochastically well-posed. For example, see the lectures of Flandoli [59]. As usual in discussions of fluctuating hydrodynamics [16–19,25–27], it is assumed that Λ can be chosen to satisfy $1/\ell_\nabla \ll \Lambda \ll 1/\lambda_{\rm micr}$. For a liquid, $\lambda_{\rm micr}$ is the mean interparticle distance $\ell_{\rm intp} \equiv n^{-1/3}$ defined in terms of particle number density n. The condition $\Lambda\ell_{\rm intp} \ll 1$ is a minimal requirement that coarse-graining

cells of size $1/\Lambda$ should contain many molecules. For a low-density gas, the mean-free-path (mfp) length $\lambda_{\rm mfp} \gg \ell_{\rm intp}$ and the condition $\Lambda\lambda_{\rm mfp} \ll 1$ guarantees that terms higher than second-order in gradients can be neglected. We thus take $\lambda_{\rm micr} = \max\{\ell_{\rm intp}, \lambda_{\rm mfp}\}$. For a high Reynolds-number turbulent flow where intermittency effects may cause the gradient length ℓ_∇ to be much smaller than the traditional Kolmogorov length η, it is not trivial that the crucial condition $\ell_\nabla \gg \lambda_{\rm micr}$ should be satisfied. Even if so, one must determine how to choose Λ in this range so that predictions are independent of the choice.

The latter problem is highly nontrivial and currently lacks an analytical solution, even at the physical level of rigor [60]. It is expected that the "bare viscosity" must be chosen to have a cutoff-dependent form ν_Λ so that predictions of the model are independent of Λ. This is due physically to the fact that the effective viscosity is renormalized by hydrodynamic fluctuations from eliminated modes at wave numbers $> \Lambda$. A renormalization group analysis of the fluid in the thermal equilibrium state Eq. (1.4) shows that the dynamics becomes asymptotically free in the infrared for space dimensions $d \geqslant 2$ and described by a linear Langevin dynamics (the Onsager regression hypothesis for long-wavelength, low-frequency velocity fluctuations) [16,17]. This result can be easily understood by estimating the root-mean-square (r.m.s.) velocity u_ℓ at length scale ℓ in an equilibrium fluid with temperature T and mass density ρ by the central limit theorem (cf. Ref. [29]) as $u_\ell \sim (k_B T/\rho\ell^d)^{1/2}$. It follows that the "thermal Reynolds numbers" of such equilibrium velocity fluctuations at length scale ℓ

$$\mathrm{Re}_\ell^{th} := \frac{\ell u_\ell^{th}}{\nu} = \left(\frac{k_B T}{\rho\nu^2\ell^{d-2}}\right)^{1/2}, \tag{2.4}$$

is small at sufficiently large lengths ℓ in space dimensions $d > 2$, which implies that the nonlinear coupling is weak. In principle, the nonlinear coupling becomes large at sufficiently small distances for $d > 2$, but we shall argue later that this length scale is so small that it lies outside the regime of validity of a hydrodynamic description. Current numerical practice in fluctuating hydrodynamics [19] evaluates wave-number-dependent viscosity $\nu(k)$ by fitting molecular dynamics results for velocity-velocity correlations at low frequency and at wave number k to the Lorentzian form predicted by nonlinear fluctuating hydrodynamics (e.g., see Eq. (3.37) in Ref. [17]). The viscosity of a hard-disk fluid with $1/k$ near scales of order the mean free path is found to be well-predicted by the Enskog kinetic theory for dense fluids and scale-dependence due to renormalization by thermal fluctuations is weak; see Ref. [19], Fig. 8.

We remark finally that setting $\nu = 0$ in Eq. (2.1) recovers the truncated Euler dynamics, which has been previously much studied. This ideal system was shown to satisfy a Liouville theorem by Burgers [61] and much later independently by Lee [62]. Quadratic invariants of the ideal incompressible Euler equations such as kinetic energy and helicity are also conserved in detail for individual wave-vector triads, as noted by Onsager [63] and Kraichnan [35], so that these remain invariants of the truncated Euler system. It follows that a Gibbs measure of the form Eq. (1.4) is an invariant measure of the truncated Euler system, as observed by both Lee [62] and Hopf [64]. Furthermore, restoring a positive viscosity $\nu > 0$, the fluctuating hydrodynamics equation preserves that Gibbsian invariant measure, as shown in detail in Appendix A. It is worth remarking that the truncated Euler dynamics possesses other Gibbs-type invariant measures associated to fixed values of helicity in addition to kinetic energy [65], but these measures are no longer invariant in the presence of thermal noise.

B. Dimensional analysis

For our study of the turbulent dissipation range, it is appropriate to nondimensionalize Eq. (2.1) with Kolmogorov dissipation length and velocity scales

$$\eta = \nu^{3/4}\varepsilon^{-1/4}, \quad u_\eta = (\varepsilon\nu)^{1/4}, \tag{2.5}$$

by setting

$$\begin{aligned} &\hat{\mathbf{u}} = \mathbf{u}/u_\eta, \quad \hat{\mathbf{x}} = \mathbf{x}/\eta, \quad \hat{t} = (u_\eta/\eta)t, \\ &\hat{p} = p/u_\eta^2, \quad \hat{\mathbf{f}} = \mathbf{f}/F, \quad \hat{\Lambda} = \Lambda\eta, \end{aligned} \tag{2.6}$$

where F is the typical magnitude of the force per mass (e.g., an r.m.s. value). The equations of motion in dimensionless form become

$$\partial_{\hat{t}}\hat{\mathbf{u}} + P_{\hat{\Lambda}}(\hat{\mathbf{u}}\cdot\hat{\nabla})\hat{\mathbf{u}} = -\hat{\nabla}\hat{p} + \hat{\triangle}\hat{\mathbf{u}} + (2\theta_\eta)^{1/2}\hat{\nabla}\cdot\hat{\boldsymbol{\eta}}_{\hat{\Lambda}} + \mathit{\Gamma}_\eta\hat{\mathbf{f}}, \tag{2.7}$$

with dimensionless temperature and force magnitude:

$$\theta_\eta = \frac{k_B T}{\rho u_\eta^2 \eta^3}, \quad \mathit{\Gamma}_\eta = \frac{F\eta}{u_\eta^2}, \tag{2.8}$$

However, it is more natural to nondimensionalize the large-scale force with inertial-range units of length L and velocity $U = (\varepsilon L)^{1/3}$ [66], so that $\mathit{\Gamma}_\eta = \mathit{\Gamma}_L/\mathrm{Re}^{1/4}$ with

$$\mathit{\Gamma}_L = \frac{FL}{U^2} = \frac{F}{(\varepsilon^2/L)^{1/3}}, \quad \mathrm{Re} = \frac{UL}{\nu} = \frac{\varepsilon^{1/3}L^{4/3}}{\nu}, \tag{2.9}$$

the dimensionless force magnitude at the integral scale and the Reynolds number, respectively. Scaled in this manner and with hats omitted, the fluctuating hydrodynamic Eq. (2.1) becomes

$$\partial_t\mathbf{u} + P_\Lambda(\mathbf{u}\cdot\nabla)\mathbf{u} = -\nabla p + \triangle\mathbf{u} + (2\theta_\eta)^{1/2}\nabla\cdot\boldsymbol{\eta}_\Lambda + \frac{\mathit{\Gamma}_L}{\mathrm{Re}^{1/4}}\mathbf{f}. \tag{2.10}$$

The Reynolds-dependence of the final term just reflects the expectation that the direct effect of large-scale forcing will be negligible in the dissipation range for $\mathrm{Re} \gg 1$.

The thermal noise term is also expected to be small at the Kolmogorov scale. The crucial parameter θ_η is the ratio of the thermal energy to the energy of the Kolmogorov-scale velocity fluctuations u_η in a spatial region of diameter $\sim\eta$. It is interesting to consider concrete numbers corresponding to typical values of physical constants for the turbulent atmospheric boundary layer (ABL), taken from the monograph [67]

$$\begin{aligned} &\varepsilon = 400\ \mathrm{cm}^2/\mathrm{s}^3, \quad \nu = 0.15\ \mathrm{cm}^2/\mathrm{s}, \\ &\rho = 1.2\times10^{-3}\ \mathrm{g/cm}^3, \quad T = 300^\circ\mathrm{K}, \end{aligned} \tag{2.11}$$

which gives

$$\eta = 0.54 \text{ mm}, \quad u_\eta = 2.78 \text{ cm/s}, \quad \theta_\eta = 2.83 \times 10^{-8}. \tag{2.12}$$

The very small value of θ_η arises from the small value of Boltzmann's constant in centimeter-gram-second units, $k_B = 1.38 \times 10^{-16}$ erg/K.

Although this number is very small, it however rises rapidly at length scales $\ell < \eta$. It can be estimated very crudely by assuming an exponential decay for $\ell < \eta$, so that the fluid velocity fluctuation level becomes

$$u_\ell \sim u_\eta \exp(-\eta/\ell). \tag{2.13}$$

Thus,

$$\theta_\ell = \frac{k_B T}{\rho u_\ell^2 \ell^3} \sim \theta_\eta \left(\frac{\eta}{\ell}\right)^3 \exp(\eta/\ell). \tag{2.14}$$

Because θ_ℓ increases so rapidly for decreasing ℓ, one can see that $\theta_\ell \sim 1$ already for $\ell_{\rm eq} \sim \eta/11$. In the ABL, this length is of the order of 49 μm. For comparison, the mean-free-path length of air at room temperature and standard atmospheric pressure is $\lambda_{\rm mfp} = 68$ nm. Thus, thermal noise becomes of the same order as nonlinear terms already at sufficiently large scales where a hydrodynamic description remains valid. Similar estimates hold for other natural turbulent flows, such as the upper ocean mixing layer, and in laboratory experiments performed with a variety of fluids. For example, in the water experiment of Debue *et al.* [51] at $\text{Re} = 3 \times 10^5$ and 20°C, the Kolmogorov scale is $\eta = 0.016$ mm and $\theta_\eta = 2.5 \times 10^{-7}$, so that thermal fluctuations become relevant around length scale $\ell_{\rm eq} \sim \eta/11 = 1.5$ μm which is still much larger than the mean-free-path length of water $\lambda_{\rm mfp} = 0.25$ nm. These cases are typical. We therefore argue that theories of the "far dissipation range" of turbulence which omit thermal noise are of questionable relevance to molecular fluids in Nature.

The example of the ABL and others are reassuring that a cutoff Λ should exist satisfying the fundamental requirement $\ell_\nabla \gg \Lambda^{-1} \gg \ell_{\rm micr}$ for validity of fluctuating hydrodynamics. Since the nonlinearity at length scales $\ell \lesssim \eta$ is weak compared with the thermal noise and the viscous damping, one expects that the velocity fluctuations at those scales should reach thermal equilibrium with a Maxwell-Boltzmann distribution and an equipartition energy spectrum,

$$E(k) \sim \frac{k_B T}{\rho} \frac{4\pi k^2}{(2\pi)^3} \tag{2.15}$$

(see Appendix A). Since this spectrum is growing in k, it must always exceed the spectrum of the turbulent velocity fluctuations at sufficiently high wave number. The physical origin of these large velocity fluctuations is the high speeds of the constituent molecules of the fluid, which are of the order of magnitude of the sound speed $c_{\rm th}$, or about 343 m/s in air and 1481 m/s in water. While these large velocities almost completely cancel in macroscopic spatial averages by the law of large numbers, the central limit theorem fluctuations grow $\sim \ell^{-d/2}$ in space dimension d as the resolved length scale ℓ decreases toward molecular scales. The crossover wave number to see thermal effects can again be crudely estimated by equating the dissipation-range turbulence spectrum with the thermal spectrum

$$u_\eta^2 \eta \exp(-k\eta) \sim \frac{k_B T}{\rho} k^2, \tag{2.16}$$

which implies $\theta_\eta (k\eta)^2 \exp(k\eta) \sim 1$ and yields an estimate of the crossover length $\ell_{\rm eq} \sim 1/k_{\rm eq} \sim \eta/12$ consistent with that found earlier.

At much larger wave numbers than this, the velocity fluctuations should be close to Gaussian, with statistical independence of modes instantaneously in nonoverlapping wave number bands. We therefore propose that the UV truncation wave number Λ of the fluctuating hydrodynamic Eq. (2.1) may be chosen anywhere in the range of k where the equipartition spectrum is achieved and where the high-pass filtered velocity $\mathbf{u}^{>k}(\mathbf{x}, t)$ is a Gaussian random field. Assuming that such a range of wave numbers exists, we expect that the cutoff Λ may be selected arbitrarily in this range and the predictions of the model will be insensitive to the particular choice, as long as the bare viscosity ν_Λ is chosen appropriately. No analytical prescription currently exists for this choice but the prescription will be the same as that for the fluid in thermal equilibrium with the given temperature T, mass density ρ and cutoff wave number Λ. Thus, it should suffice to choose ν_Λ by matching with equilibrium velocity-velocity correlations from molecular dynamics simulations, as in current practice [19]. Note that the equipartition range which we predict slightly beyond the Kolmogorov wave number will be in the "low-wave-number" weak-coupling range of the thermal equilibrium fluid. One can verify this by substituting the definition Eq. (2.8) of θ_η into Eq. (2.4) for $\text{Re}_\eta^{\rm th}$, giving

$$\text{Re}_\eta^{\rm th} = \theta_\eta^{1/2}. \tag{2.17}$$

We see that for θ_η with realistic values, $\text{Re}_\eta^{\rm th} \ll 1$ and thus the nonlinear coupling in the thermal equipartition range should remain negligible for several decades of wave number above $1/\eta$.

The predicted energy spectrum which emerges from our arguments is illustrated in Fig. 1 with a model spectrum proposed by von Kármán [68]

$$E(k) = C_K (\varepsilon L)^{2/3} \frac{L^5 k^4}{[1 + (kL)^2]^{17/6}} \exp(-bk\eta) + Ak^2, \tag{2.18}$$

which has been supplemented with an exponential factor $\exp(-bk\eta)$ to represent decay in the traditional "far dissipation range" and with also an additive contribution from the thermal equipartition spectrum Eq. (2.15) for $A = \frac{k_B T}{\rho} \frac{4\pi}{(2\pi)^3}$. In the plot we have used the parameters Eq. (2.11) and also a typical Reynolds number $\text{Re} = 10^7$ for the ABL taken from Ref. [67]. The exponential-decay factor is consistent with asymptotic predictions [35,38] and rigorous upper bounds [36,37] for deterministic Navier-Stokes dynamics, with the coefficient $b = 7$ chosen consistent with numerical observations [41] and with a conventional value $C_K = 1.6$ of the Kolmogorov constant [69]. Plotted as well with a dashed line is the energy spectrum without thermal noise, obtained by formally setting $T = 0$ in Eq. (2.18). Consistent with our earlier estimates, the two spectra agree up to a wave number $k_{\rm eq} \doteq 10/\eta$ where the equipartition spectrum begins to

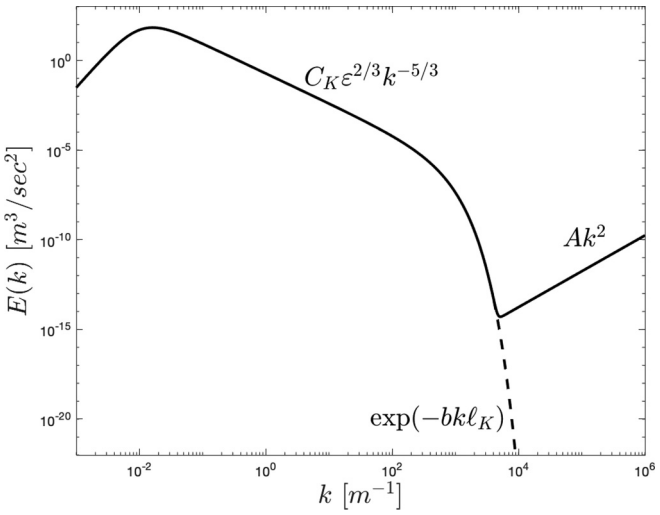

FIG. 1. Plot of the model turbulent energy spectrum Eq. (2.18) for the parameters Eq. (2.11) of the atmospheric boundary layer and for a typical Reynolds number $\mathrm{Re} = 10^7$, as a solid line. The dashed line is the spectrum with no thermal noise.

dominate. Below k_{eq} lies only about half a decade of wave numbers where the traditional exponential decay is manifested. The k^2 energy spectrum that appears at k_{eq} will extend at least up to wave numbers k where the rms velocity $u_{1/k}$ approaches the sound speed c_{th}. The incompressibilty assumption for the model Eq. (2.1) then breaks down and density fluctuations become significant, so that fluctuating compressible equations [25–27] must be employed.

We may observe at this point that our picture of the turbulent energy spectrum was almost entirely anticipated by Betchov in his first paper on the subject [53]. Assuming that the hydrodynamic modes at small scales would reach energy equipartition, he arrived at an expression for the thermal spectrum $E_{\mathrm{noise}}(k)$ identical to our Eq. (2.15), except for an extra overall factor of $3/2$. As previously noted by Hosokawa [28], Betchov did not take into account incompressibility and thus counted 3 degrees of freedom for each independent wave number mode rather than 2. By an argument essentially identical to ours, Betchov then determined the wave number we call k_{eq} by matching $E_{\mathrm{noise}}(k)$ with the turbulent energy spectrum $E(k)$ in the dissipation range. For the latter, he assumed a power-law form $E(k) \sim k^{-n}$, with $n = 7$ predicted by the theory of Heisenberg [33] but with $n = 6$ more consistent with Betchov's own experimental results. Although he did not state a quantitative estimate of k_{eq}, Betchov plotted his theoretical result for $E_{\mathrm{noise}}(k)$ together with his experimental data for $E(k)$ and, extrapolating the latter, they can be observed to cross at a wave number around $10\,\mu$m. In the final sentence of his paper, Betchov concluded that "the gap between turbulence and molecular agitation may not be as wide as is generally appreciated." In his later work [55], he arrived at the more quantitative estimate that $k_{\mathrm{eq}}\eta \doteq 1$ by assuming that the turbulent spectrum drops essentially to zero for $k\eta > 1$. His schematic plot of the atmospheric spectrum, entirely analogous to our Fig. 1, indicated an equilibration scale there of order 1 mm. Betchov ended the paper [55] by noting that, because $\eta \gg \lambda_{\mathrm{mfp}}$, his conclusions differ from those of von Neumann [70], who had argued that thermal noise becomes relevant only for length scales of order the mean free path and that separation of scales is thus "unambiguous" in turbulent flows.

It should be emphasized that these conclusions are very robust and do not depend upon any particular model of the energy spectrum in the turbulent dissipation range, as long as that spectrum decays rapidly in wave number. We made our estimate of the equilibration scale using the model spectrum Eq. (2.18) with exponential decay, but Betchov [53] reached the same conclusion assuming a rapid power-law decay. In the Supplemental Material [71] we show similarly that the "intermediate dissipation range" predicted by Frisch and Vergassola [40] using multifractal phenomenological models [31,72,73] implies also that the equipartition scale is only about an order of magnitude below the Kolmogorov scale. The stretched exponential decay predicted for the dissipation-range spectrum by functional renormalization group arguments [74] will likewise lead to the same result. Of course, all of these arguments are phenomenological and the intuitive superposition of spectra for turbulent and thermal fluctuations depends upon the hypothesis that small scales will achieve the same equilibrium distribution in a turbulent flow as in a laminar one. This hypothesis is supported by the standard presumption of weak turbulent fluctuations in the dissipation range, but it must be tested empirically and could even be false due to rare, intermittent bursts of turbulence that penetrate to very small scales [32].

The physical arguments of Betchov and ourselves which lead to our proposed picture of the turbulent energy spectrum will be corroborated in Sec. III by shell-model simulations. Furthermore, the direct effects of thermal noise will be found to exist in those simulations at length scales much larger than $1/k_{\mathrm{eq}}$ in more refined statistical measures, such as negative-order structure functions or "inverse structure functions" [75], which are more sensitive than the energy spectrum to rare low-amplitude events. Equipartition spectra similar to those predicted here have been observed in superfluid turbulence via numerical simulations of the Gross-Pitaevskii equation [76], where they correspond to a thermal bath of phonons at high wave numbers created by the forward energy cascade. Since superfluids have strictly zero viscosity, there is no exact analog in these simulations of a dissipation range and equipartition spectra there join directly with the Kolmogorov cascade spectra. The same is true for equipartition spectra observed in numerical simulations of decaying turbulence for the truncated Euler system [77,78] where the k^2 spectrum corresponds to thermalized wave-number modes near the spectral cutoff Λ of the model. In contrast to the fluctuating hydrodynamic Eqs. (1.2), which model molecular fluids at mesoscopic scales, the truncated Euler system does not correspond directly to any physical system in nature or in the laboratory. For a more detailed comparison of truncated Euler and related systems with our results in this paper, see Sec. V A.

C. Violation of scale-symmetry of Navier-Stokes

A possible objection can be raised to our claim that the "far dissipation range" of deterministic Navier-Stokes turbulence is physically unachievable, based upon the well-known space-

time scaling symmetry (see Ref. [9], Sec. 2.2; and Ref. [79], Sec. 1.2):

$$\mathbf{u} \to \mathbf{u}' = \lambda \mathbf{u}, \quad \mathbf{x} \to \mathbf{x}' = \lambda^{-1}\mathbf{x}, \quad t \to t' = \lambda^{-2} t, \quad (2.19)$$

which maps an incompressible Navier-Stokes solution $\mathbf{u}(\mathbf{x}, t)$ to another solution $\mathbf{u}'(\mathbf{x}', t')$ with the same Reynolds number $\mathrm{Re}' = \mathrm{Re}$ and with molecular viscosity ν also unchanged. This scale symmetry is equivalent to the familiar principle of hydrodynamic similarity. In the presence of an external body force $\mathbf{f}$, one must also take

$$\mathbf{f} \to \mathbf{f}' = \lambda^3 \mathbf{f}. \quad (2.20)$$

This symmetry of incompressible Navier-Stokes equation is the basis of its rigorous derivation from the Boltzmann equation [5,6] or from lattice gas models [7] through a scaling limit with $\lambda \to 0$. Based on such mathematical treatments, one might conclude that the deterministic Navier-Stokes equation should hold in a turbulent flow to any desired accuracy by simply taking the outer length of the flow large enough and the r.m.s. velocity small enough, at whatever Reynolds number desired.

If, however, a solution of the fluctuating Navier-Stokes Eq. (1.2) in 3D is subjected to the same rescaling Eq. (2.19), then

$$\frac{k_B T}{\rho} \to \frac{k_B T'}{\rho'} = \lambda^3 \frac{k_B T}{\rho}. \quad (2.21)$$

Thus, thermal noise breaks the scaling symmetry of the deterministic Navier-Stokes equation, unless temperature can be decreased as $T \to T' = \lambda^a T$ and density increased as $\rho \to \rho' = \lambda^{-b}\rho$, so that thermal noise satisfies Eq. (2.21) with kinematic viscosity held fixed $\nu(\rho', T') = \nu(\rho, T)$. (For example, for an ideal gas $\nu \propto T^{1/2}/\rho$ and one must take $a = 2,\ b = 1$). The presumed relation Eq. (2.21) is the reason that derivation of the incompressible Navier-Stokes equation through a hydrodynamic scaling limit corresponds to weak noise and leads to a large-deviations framework [7]. However, even this extended scaling symmetry of the fluctuating Eq. (1.2) is physically limited, since at low enough temperature and/or high enough density the fluid will undergo a phase transition to a binary gas-liquid mixture or to a solid state. If one instead keeps the temperature and density fixed, then the thermal noise does *not* become weaker and remains given by the fluctuation-dissipation relation Eq. (1.3) for both the solutions $\mathbf{u}$ and $\mathbf{u}'$, which are no longer statistically similar to each other. This violation of scale-symmetry is generally not observed in fluids because Boltzmann's constant k_B is so small in macroscopic units (centimeter-gram-second or meter-kilogram-second). However, the breaking of hydrodynamic similarity due to thermal noise can be observed in microfluidics, for example in the mixing at fluid interfaces [80].

Specializing these general considerations for the fluctuating hydrodynamic Eq. (1.2) to the case of forced turbulent flow with time-average power input per mass $\varepsilon = \langle \mathbf{u} \cdot \mathbf{f} \rangle$, the scalings Eqs. (2.19) and (2.20) imply that

$$\varepsilon \to \varepsilon' = \lambda^4 \varepsilon. \quad (2.22)$$

In decaying turbulence, the same result holds by Taylor's relation $\varepsilon \sim U^3/L$ [81]. The result Eq. (2.22) then implies that the Kolmogorov velocity and length transform as

$$\begin{aligned} u_\eta = (\nu\varepsilon)^{1/4} &\to u'_\eta = \lambda u_\eta, \\ \eta = \nu^{3/4}\varepsilon^{-1/4} &\to \eta' = \lambda^{-1}\eta, \end{aligned} \quad (2.23)$$

consistent with the scaling Eq. (2.19). It is easy to check that along with the Reynolds number Re, also the dimensionless force amplitudes F_η and F_L defined in Eqs. (2.8) and (2.9) are invariant under the rescaling Eq. (2.19), but that

$$\theta_\eta \to \theta'_\eta = \lambda \theta_\eta \quad (2.24)$$

when keeping ρ and $k_B T$ fixed. This result holds because the kinetic energy of Kolmogorov-scale turbulent fluid eddies increases as λ^{-1}. It is thus possible, in principle, to observe deterministic Navier-Stokes predictions in the dissipation range by taking $\mathbf{u} \to \mathbf{u}' = \lambda \mathbf{u}$ and $\mathbf{x} \to \mathbf{x}' = \lambda^{-1}\mathbf{x}$ with $\lambda \ll 1$. However, in practice, λ must be chosen exponentially small, since the relations Eqs. (2.14) and (2.16) show that deterministic Navier-Stokes predictions for the far dissipation range will hold only up to a wave number $k\eta \sim \ln(1/\theta'_\eta)$ growing as $\ln(1/\lambda)$. For example, in the case of the ABL we argued below Eq. (2.14) that noise would be relevant already at a length scale $\ell \sim \eta/12$. To make the deterministic predictions valid down to $\ell \sim \eta/22$ would require that the integral length be made $4e^{11} = 240\,000$ times larger and r.m.s. velocities 240 000 times weaker [82]!

Based on these considerations, we argue that an extended far-dissipation-range spectrum described by deterministic Navier-Stokes will be practically unobservable both in natural flows and in laboratory experiments. The best hope of achieving a sizable exponential-decay range is probably with a highly viscous fluid at relatively low Reynolds numbers, so that both η and u_η are made as large as possible. In such a moderate Reynolds number turbulent flow, the dimensionless noise parameter θ_η will be as small as possible. This strategy should work best in liquids where viscosity can be increased by lowering temperature, whereas in gases large kinematic viscosity requires either high temperatures or low densities. In any case, there will be a fundamental difficulty in then, say, doubling the wave-number extent of such a far-dissipation-range spectrum, because this would require a further exponential decrease in θ_η, which will be unachievable.

D. Intermittency and validity of fluctuating hydrodynamics

The previous considerations have ignored the phenomenon of small-scale turbulence intermittency, which leads to enhanced fluctuations in the inertial-range that may be described phenomenologically by the Parisi-Frisch multifractal model [9,83]. This model postulates a dimension spectrum $D(h)$ of velocity Hölder exponents h and suggests the existence of viscous cutoff lengths

$$\eta_h \sim L\mathrm{Re}^{-1/(1+h)}, \quad (2.25)$$

depending upon h which can be much smaller than the classical Kolmogorov length η, which corresponds to $h = 1/3$ [32]. This model has been invoked to predict an "intermediate dissipation range" (IDR) of scales [40], as an intermediate asymptotics at high-Re between the inertial range where viscosity effects are negligible and the far dissipation range

where viscosity dominates to produce exponential decay of velocity fluctations. The far dissipation range is itself predicted to suffer extremely large fluctuations, because the intermittency at lower wave numbers is intensely magnified by the exponential drop-off in the spectrum [39]. We should therefore discuss how such intermittency might modify the conclusions in the previous section about the choice of Λ and indeed about the validity of a fluctuating hydrodynamic description of turbulent flow.

We shall exploit here the Parisi-Frisch multifractal model to address these questions. We note that the multifractal concept of an IDR predicts a collapse of spectra at different Re with a certain scaling [40], and this "multiscaling" has been verified in the GOY shell model [84] and to some degree in direct numerical simulations (DNS) of the Navier-Stokes equations; see Ref. [41], Fig. 4. However, there are alternative theoretical ideas about the "near dissipation range" of turbulent flows, for example, from functional renormalization group (FRG) analyses [74,85]. Some recent experimental and DNS studies have given stronger support to the FRG predictions than to the multifractal IDR prediction [42,43,51]. We therefore invoke the multifractal model only as a heuristic to draw qualitative conclusions. We note, however, that several of the results we obtain below can be confirmed independently by rigorous mathematical arguments.

The considerations of Corrsin [8] on the validity of a hydrodynamic description within the K41 theory of turbulence can be easily extended to the multifractal model; see Ref. [86], Sec. III(e). The essential point of Corrsin's analysis is that viscosity ν and microscopic length $\lambda_{\rm micr}$ are not independent quantities but are instead linked by the standard estimate from kinetic theory

$$\nu \sim \lambda_{\rm micr} c_{\rm th}, \tag{2.26}$$

where $c_{\rm th}$ is the thermal velocity/sound speed. Combining Eq. (2.26) with Eq. (2.25) then easily yields

$$\mathrm{Kn}_h := \lambda_{\rm micr}/\eta_h \sim \mathrm{Ma}\,\mathrm{Re}^{-h/(1+h)} \tag{2.27}$$

as an estimate of the "local Knudsen number" at a point with Hölder exponent h, where $\mathrm{Ma} = U/c_{\rm th}$ is the Mach number based on the large-scale flow velocity U. We see that the scale separation required for validity of a hydrodynamic description, as quantified by the fundamental condition $\mathrm{Kn}_h \ll 1$, will become progressively better with increasing Re for $h > 0$ and $\mathrm{Kn}_h \ll 1$ will hold marginally even for $h = 0$ if $\mathrm{Ma} \ll 1$.

There is some evidence that the smallest Hölder exponent in incompressible fluid turbulence is $h_{\rm min} = 0$ [87] (although this conclusion requires the assumption that negative h cannot occur, e.g., Ref. [9], Sec. 8.3, which can be called into question; see Sec. V C). If so, then there is a range of possible wave-number cutoffs Λ satisfying

$$1/\eta_h \ll \Lambda \ll 1/\lambda_{\rm micr}, \quad \text{for all } h, \tag{2.28}$$

as long as $\mathrm{Ma} \ll 1$. Taking into account the thermal noise, we can expect for each h that its effects will be manifested in the length scales just slightly below η_h, where the local energy spectrum (defined, e.g., by a wavelet transform) experiences exponential drop-off. In that case, we may further expect that Gaussian, thermal-equilibrium statistics will hold locally at any length scale $\ell \ll \eta_h$. More precisely, we may consider a locally coarse-grained velocity

$$\bar{\mathbf{u}}_\ell(\mathbf{x}) = \sum_n \mathbf{v}_n G_\ell(\mathbf{x} - \mathbf{x}_n) \Big/ \sum_n G_\ell(\mathbf{x}_n), \tag{2.29}$$

where $G_\ell(\mathbf{r}) = \ell^{-3} G(\mathbf{r}/\ell)$ is a smooth, well-localized kernel function and where the sum $\sum_n$ is over molecules of the fluid with positions $\mathbf{x}_n$ and velocities $\mathbf{v}_n$. Because the microscopic velocity distributions are close to Maxwellian and because of the central limit theorem [29], we expect to observe nearly Gaussian statistics [88]

$$P(\bar{\mathbf{u}}_\ell) \propto \exp\left(-C\frac{\rho \ell^3 |\bar{\mathbf{u}}_\ell - \mathbf{v}|^2}{k_B T}\right), \quad \ell_{\rm intp} \ll \ell \ll \eta_h, \tag{2.30}$$

with $\mathbf{v} = \bar{\mathbf{u}}_{\eta_h}$ locally at each point in space and time, with Hölder exponent $h = h(\mathbf{x}, t)$. Thus, the primary effect of turbulent intermittency should be a strong fluctuation in space and time of the length scale η_h below which Gaussian thermal equipartition sets in. Since the ratio $\eta_h/\lambda_{\rm micr}$ grows with increasing Re, as we have argued earlier, it should be possible to choose a cutoff satisfying Eq. (2.28) without any restriction on Re as long as $\mathrm{Ma} \ll 1$.

Our tentative conclusion is that fluctuating Navier-Stokes equation in the form Eq. (2.1) should be valid with a suitable choice of wave-number cutoff $1/\eta_\eta \ll \Lambda \ll 1/\lambda_{\rm micr}$ for incompressible turbulent flows in the limit $\mathrm{Kn} \ll 1$ and $\mathrm{Ma} \ll 1$. We shall return to this important issue after presenting and discussing our numerical results for the shell model in the following section (see Sec. V C). Most importantly, we have argued that this model predicts a strikingly different behavior than does the deterministic Navier-Stokes equation in the far dissipation range of turbulent flow, at length scales somewhat smaller than the Kolmogorov scale η. Whereas the deterministic equations predict an exponential decay of the energy spectrum [35–38] and consequent enhanced intermittency [36,39], the fluctuating equations predict that the energy spectrum about only an order of magnitude above $1/\eta$ should rapidly bottom out and then rise again with increasing wave number k in a thermal equipartition k^2 spectral range with Gaussian statistics.

III. SABRA SHELL MODEL OF FLUCTUATING NAVIER-STOKES EQUATION

In the preceding section we have made two fundamental claims: first, that turbulence in low Mach-number molecular fluids is described by the incompressible FNS Eqs. (1.2) with a suitable high-wave-number cutoff Λ and, second, that those equations predict a thermal equipartition range a decade or so below the Kolmogorov scale rather than a "far dissipation range" with exponentially decaying energy spectrum. To check the first claim will require novel experimental investigations, which will be discussed later. The second claim is based on physically plausible reasoning, but can be verified by numerical simulations of the FNS equations. Such simulations are possible using existing numerical schemes such as the low Mach number FNS codes in Refs. [18–20], which employ finite-volume spatial discretizations and explicit or semi-implicit stochastic Runge-Kutta integrators in time. Motivated by the present study, such computations have been

carried out and the results will be discussed briefly later. An alternative numerical approach would be based on the lattice Boltzmann method with thermal fluctuations incorporated at the kinetic level [89,90]. Neither of these numerical schemes even with the most powerful current computers can, however, reach Reynolds numbers comparable to those in the atmospheric boundary layer or even in many engineering flows. Such high Reynolds numbers are particularly relevant to the issue whether a hydrodynamic description is valid for the most extreme turbulent events [44–50], since inertial-range intermittency increases with Re. We shall therefore in this paper validate our physical arguments by numerical simulations of a simplified "shell model" of turbulence which can be solved at much higher Reynolds numbers. These models long been used as surrogates of incompressible Navier-Stokes equations, both for physical investigation of high-Re turbulence [91–93] and for comparative mathematical study [94]. Below we discuss the model, introduce a suitable numerical scheme, and then present numerical simulation results on the dissipation range of the model in a statistical steady state of high-Reynolds turbulence.

A. Introduction of the model

The stochastic model that we consider is based upon the deterministic Sabra shell model [56,57,95,96] which describes the evolution of complex shell variables u_n for discrete wave numbers $k_n = k_0 2^n,\ n = 0, 1, 2, \ldots, N$ via the coupled set of ODE's

$$du_n/dt = B_n[u] - \nu k_n^2 u_n + f_n, \tag{3.1}$$

with

$$B_n[u] = i[k_{n+1}u_{n+2}u^*_{n+1} - (1/2)k_n u_{n+1}u^*_{n-1} + (1/2)k_{n-1}u_{n-1}u_{n-2}]. \tag{3.2}$$

Here u_n represents the "velocity" of an eddy of size $1/k_n$, the parameter ν is "kinematic viscosity," and f_n is an external body force to stir the system. Shell models have long been studied as convenient surrogates for the Navier-Stokes equation in the numerical study of high-Reynolds-number turbulence [93,97] but the Sabra model has been especially popular because it enjoys symmetries most similar to those of the incompressible fluid equations, roughly analogous to translation-invariance and scale-invariance. There is no "position space" in the shell model on which a translation group can act, but one can shift phases by defining

$$u^\phi_n(t) = e^{i\phi_n} u_n(t), \tag{3.3}$$

and if the constraint $\phi_{n-2} + \phi_{n-1} = \phi_n$ is satisfied, then u^ϕ is a solution of the Sabra model whenever u is a solution. This result holds as well with a deterministic force, if the latter is also transformed as $f^\phi_n(t) = e^{i\phi_n} f_n(t)$. This symmetry is analogous to the action of space-translations by length displacement $\mathbf{a}$, acting on Fourier modes of the velocity field as

$$\hat{\mathbf{u}}^{\mathbf{a}}(\mathbf{k}, t) = e^{i\mathbf{k}\cdot\mathbf{a}}\hat{\mathbf{u}}(\mathbf{k}, t). \tag{3.4}$$

Other basic symmetries of the inviscid Sabra model are invariance under continuous *time scaling* indexed by a real parameter $\boldsymbol{\tau} > 0$,

$$u^{(\tau)}_n(t) = \tau u_n(\tau t), \tag{3.5}$$

which maps solutions over time interval $[0, T]$ to solutions over the interval $[0, \tau^{-1}T]$ and also under discrete *space scaling* indexed by natural number L,

$$u^{(L)}_n(t) = 2^L u_{n+L}(t), \tag{3.6}$$

where $N^{(L)} = N - L$ and likewise the lowest shell index is shifted from $M = 0$ to $M^{(L)} = M - L$. These are analogous to the scale symmetries of incompressible Euler, according to which for any $\lambda, \tau > 0$ the transformation

$$\mathbf{u}^{(\lambda,\tau)}(\mathbf{x}, t) = \frac{\tau}{\lambda}\mathbf{u}(\lambda\mathbf{x}, \tau t) \tag{3.7}$$

maps every Euler solution $\mathbf{u}$ in the space-time domain $\Omega \times [0, T]$ to another solution $\mathbf{u}^{(\lambda,\tau)}$ in the space-time domain $\lambda^{-1}\Omega \times [0, \tau^{-1}T]$; see Ref. [79], Sec. 1.2. Addition of viscous damping in both shell models and real fluids leaves only the restricted symmetry group with the constraint $\tau = \lambda^2$ and this remaining scaling symmetry is that which leaves the Reynolds number invariant.

Here we add to the deterministic model Eq. (3.1) also *thermal noise* modeled by random Langevin forces

$$du_n/dt = B_n[u] - \nu k_n^2 u_n + \left(\frac{2\nu k_B T}{\varrho}\right)^{1/2} k_n \eta_n(t) + f_n, \tag{3.8}$$

where the complex white-noises $\eta_n(t)$ have covariance

$$\langle \eta_n(t)\eta^*_{n'}(t')\rangle = 2\delta_{nn'}\delta(t - t'), \tag{3.9}$$

for $n = 0, 1, \ldots, N$. Note that the "translation-invariance" symmetry Eq. (3.3) still holds in the presence of thermal noise, but the remaining viscous scaling symmetry Eq. (3.7) with $\tau = \lambda^2$ is broken. This *noisy Sabra model* is motivated as the shell-model caricature of the fluctuating Navier-Stokes Eq. (2.1) at absolute temperature T and mass density ϱ. Note that the "density" ϱ has units of mass, because the shell model is zero-dimensional, describing a scale hierarchy of turbulent eddies at a single point. As usual in statistical physics, we do not attempt to define this stochastic model for infinitely many shells $N = \infty$, but instead truncate at some finite N whose choice is discussed further below. The resulting system of stochastic ODE's is then well-posed globally in time (see Example 3.3 in Ref. [59]). The specific form of the noise term can be justified as that required to make the equilibrium *Gibbs distribution*

$$P_G[u] = \frac{1}{Z}\exp(-\beta\mathcal{E}[u]) \tag{3.10}$$

the unique invariant measure for zero-forcing ($f = 0$), where $\beta = 1/k_B T$ and

$$\mathcal{E}[u] = \sum_{n=0}^{N} \frac{1}{2}\varrho|u_n|^2 \tag{3.11}$$

is the shell-model analog of fluid kinetic energy. In fact, this measure is in detailed balance for the dynamics or time-reversible; see Appendix A for the proof. It is not hard to verify by a modification of this argument that the Langevin forces in Eq. (3.8) are the only possible white-noise terms

that make P_G invariant, a result often called the "Einstein relation" or "fluctuation-dissipation relation" in statistical physics. These are well-known results in the literature on the fluctuating Navier-Stokes equations, here simply extended to the Sabra shell model.

We should note that the infinite-N limit of our model Eqs. (3.8) and (3.9) in the unforced case with $f_n = 0$ has been been previously studied in Ref. [98]. There it was shown that the stochastic dynamical equations with $N \leqslant +\infty$ define a time evolution which is strong in the probabilistic sense (i.e., for individual realizations of the noise) and that the corresponding probability measure Eq. (3.10) with $N = +\infty$ is time-invariant. We do not have any need to consider such an infinite-N limit in our study, although mathematical results of this type do bear upon the N-independence of the statistical predictions of our model, which will be discussed more below. The paper [98] showed also that the unforced, deterministic, inviscid model with $\nu = 0$ makes sense in the limit $N = +\infty$ with initial data chosen from the Gibbs measure Eq. (3.10), which is again time-invariant. This result is likewise not of direct physical interest. The turbulent flows studied here will be described by (weak) solutions of the inviscid shell model dynamics in the limit $\mathrm{Re} \to \infty$, $N - M \to \infty$, as mathematically studied in Refs. [95,96], but these weak solutions will dissipate kinetic energy and will not have P_G as an invariant measure. There are additional invariant measures of the deterministic inviscid dynamics, associated for example to the "helicity" invariant $H = \sum_n (-1)^n k_n |u_n|^2$ [93,97]. However, these measures are not invariant in the presence of viscosity and thermal noise, and are also not of any direct physical interest.

To study our model in the dissipation range, we nondimensionalize variables in analogy to Eq. (2.6), which brings Eq. (3.8) to the form

$$du_n/dt = B_n[u] - k_n^2 u_n + (2\theta_\eta)^{1/2} k_n \eta_n(t) + f_n/\mathrm{Re}^{1/4}, \tag{3.12}$$

where

$$\mathrm{Re} = \frac{U}{\nu k_0}, \quad \theta_\eta = \frac{k_B T}{\varrho u_\eta^2}, \tag{3.13}$$

and the second parameter is the ratio of thermal energies to kinetic energies of Kolmogorov-scale fluid fluctuations. In these units, the shell index now ranges over values $n = M, \ldots, R$, where $M = -\lfloor \frac{3}{4} \log_2(\mathrm{Re}) \rfloor$, $R = N - M$, with $\lfloor x \rfloor$ denoting the integer part of x, and now $n = 0$ corresponds to the Kolmogorov wave number. In a physically reasonable correspondence to real fluid turbulence, the parameter θ_η should be taken extremely small, but fixed independent of Re. In our numerical studies in this work, we shall adopt the precise value in Eq. (2.12) appropriate to the ABL and which has magnitude $\theta_\eta \sim 10^{-8}$, but our results do not depend qualitatively upon the particular choice of this parameter.

The existence of the $R \to \infty$ limit of the model Eq. (3.12), demonstrated in Ref. [98] for $f_n = 0$ and conjectured here with $f_n \neq 0$, is consistent with its much more benign UV-behavior than that of the 3D fluctuating Navier-Stokes model Eq. (2.1). These differences in the two models arise both from the strictly local-in-wave-number couplings of the shell model and also from its lower dimensionality, corresponding to a fluid in space dimension $d = 0$. If the RG analysis of Refs. [16,17] is carried out for the unstirred shell model Eq. (3.8) in thermal equilibrium, then it is found that that the dynamics is UV asymptotically free for $k_n \gg u_{\mathrm{th}}/\nu$, with $u_{\mathrm{th}} := (2k_B T/\varrho)^{1/2}$. The general result Eq. (2.17) implies that $\mathrm{Re}_\eta^{\mathrm{th}} = \theta_\eta^{1/2} \ll 1$ and thus the wave numbers $k_n \eta \gtrsim 1$ are deep in the UV asymptotic-free regime of the thermal Gibbs state. In other words, the modes of the model Eq. (3.12) with shell numbers $n \gtrsim 0$ have dynamics given nearly by uncoupled linear Langevin equations and thus variables u_n, $u_{n'}$ in that range with $n \neq n'$ are statistically independent not only instantaneously but also very nearly independent at unequal times. This statistical independence will be verified to hold in our numerical solutions to very good accuracy. It is therefore possible to increase $R \to R + 1$ while keeping the bare-viscosity as a fixed constant $\nu_L = \nu$ and any resultant change in the stochastic dynamics is unobservable (see Sec. III B 3). As an aside, we remark that, conversely, the IR dynamics of the noisy shell model Eq. (3.8) in the unstirred, thermal equilibrium state at wave numbers $k_n \ll u_{\mathrm{th}}/\nu$ will be strongly coupled and the time-correlations should exhibit nontrivial scaling analogous to that in the $d = 1$ KPZ model [17,99].

It must be emphasized that, as a consequence, our shell model Eq. (3.12) will *underestimate* the effects of thermal noise at high wave numbers. This is due not only to the decrease of thermal noise effects for Sabra compared with increase for Navier-Stokes, but also due to the faster decay of the turbulent energy spectrum in Navier-Stokes without noise. As to the latter, the decay of the energy spectrum in the far dissipation range of deterministic Navier-Stokes turbulence is expected to be exponential (up to a power-law prefactor), based upon physical theory [35,38], rigorous mathematical arguments [36,37], and numerical simulations [41]. In the shell model, on the contrary, physical arguments [100,101], rigorous bounds [95] and numerical simulations [102] support instead a stretched exponential decay:

$$\langle |u_n|^2 \rangle \sim \exp[-c(k_n \eta)^\gamma], \quad \gamma = \log_2 \left(\frac{1+\sqrt{5}}{2} \right). \tag{3.14}$$

This slower decay in the shell-model means that deterministic nonlinear effects will persist to higher wave numbers. In addition, the Gibbs measure Eq. (3.10) for the shell model corresponds to an energy spectrum

$$E_n := \frac{\langle |u_n|^2 \rangle}{2k_n} = A/k_n, \tag{3.15}$$

with $A = k_B T/\varrho$. In contrast to the spectrum Eq. (2.15) for FNS in $d = 3$, which is growing $\sim k^2$ at high-k, the corresponding equipartition spectrum Eq. (3.15) for the noisy shell model is decaying $\sim 1/k_n$. Because of these important differences of our model from reality, any thermal effects that we observe in our shell-model simulations should have appreciably greater analogues in real fluids.

B. Numerical integration method

We now discuss the method for numerical solution of the noisy Sabra model Eq. (3.12) which we shall use for our study of the steady-state statistics in this paper.

1. Slaved Itō-Taylor scheme

We employ here a slaved 3/2-strong-order Itō-Taylor scheme which was proposed by Lord and Rougemont for parabolic stochastic PDE's (see Ref. [103], Sec. 6). Because of the extreme stiffness of the shell model dynamics, it is desirable to use a scheme which explicitly solves the fast viscous dynamics by an integrating factor. The method we employ is a close analog for stochastic equations of the slaved second-order Adams-Bashforth method widely used for numerical simulation of deterministic shell models [104]. The method in Ref. [103] is based on stochastic Itō-Taylor expansions and is a slaved version of the 3/2-strong-order method of Platen and Wagner [105]; see Ref. [106], Sec. 10.4 for a detailed discussion. The method of Lord-Rougemont [103] used a Fourier-Galerkin method for spatial discretization that kept Fourier modes $|n| \leqslant N$, which brings it very close to the formulation of the shell models. It must be emphasized once again however that our view of the noisy Sabra model as an "effective low-wave-number theory," although standard in the statistical physics literature, is quite different from the framework of stochastic PDE's, which requires a limit $N \to \infty$. This difference will inform our discussion of convergence issues further below.

To state the numerical scheme explicitly, we write the noisy Sabra model Eq. (3.8) in the form

$$du_n = a_n dt + b_n dW_n, \quad n = 0, 1, \ldots, N, \tag{3.16}$$

with

$$a_n := B_n[u] - \nu k_n^2 u_n + f_n, \quad b_n := \left(\frac{2k_B T}{\varrho}\right)^{1/2} k_n. \tag{3.17}$$

The method of Ref. [103] solves this system approximately for a discrete set of times t_k, $k = 0, 1, 2, \ldots$ by the iteration

$$\begin{aligned} u_n(t_{k+1}) = e^{-\nu k_n^2 \Delta t} \Big\{ & u_n(t_k) + \Delta t[B_n(t_k, u(t_k)) + f_n(t_k)] + \frac{1}{2}(\Delta t)^2 \big(\nu k_n^2 [B_n(t_k, u(t_k)) + f_n(t_k)] + \dot{f}_n(t_k)\big) \\ & + \frac{i}{2}(\Delta t)^2 [k_{n+1}(a_{n+2} u_{n+1}^* + u_{n+2} a_{n+1}^*) - (1/2) k_n (a_{n+1} u_{n-1}^* + u_{n+1} a_{n-1}^*) \\ & + (1/2) k_{n-1}(a_{n-1} u_{n-2} + u_{n-1} a_{n-2})] + b_n \big[(1 + \nu k_n^2 \Delta t)\Delta W_n(t_k) - \Delta Z_n(t_k)\big] \\ & + i[k_{n+1}(b_{n+2} \Delta Z_{n+2}(t_k) u_{n+1}^* + u_{n+2} b_{n+1} \Delta Z_{n+1}^*(t_k)) - (1/2) k_n (b_{n+1} \Delta Z_{n+1}(t_k) u_{n-1}^* + u_{n+1} b_{n-1} \Delta Z_{n-1}^*(t_k)) \\ & + (1/2) k_{n-1}(b_{n-1} \Delta Z_{n-1}(t_k) u_{n-2} + u_{n-1} b_{n-2} \Delta Z_{n-2}(t_k))] \Big\}, \end{aligned} \tag{3.18}$$

for $n = 0, 1, \ldots, N$, where

$$\Delta W_n(t_k) := \int_{t_k}^{t_{k+1}} dW_n(t) = W_n(t_{k+1}) - W_n(t_k), \tag{3.19}$$

$$\Delta Z_n(t_k) := \int_{t_k}^{t_{k+1}} dt\ [W_n(t) - W_n(t_k)]. \tag{3.20}$$

The derivation of this scheme is sketched briefly in Appendix B, for completeness. In a practical implementation the pairs of complex random variables $\Delta W_m(t_k)$, $\Delta Z_m(t_k)$ have real and imaginary parts which can be generated from independent $N(0, 1)$ random variables by the method in Ref. [106], Sec. 10.4, Eq. (4.3). For all of our tests of convergence of this scheme we used the same model parameters employed in the long-time steady-state simulation, discussed in detail in the next Sec. IV A.

The convergence proofs in the mathematical literature for this method and related ones [103,107,108] employ a joint limit $\Delta t \to 0$ and $N \to \infty$ and require a noise spectrum rapidly converging $b_n \to 0$ as $n \to \infty$. By contrast, the spectrum defined in Eq. (3.17) that corresponds to thermal noise has in fact diverging b_n, with $b_n \to \infty$ as $n \to \infty$. However, we do not take the limit $N \to \infty$ but consider instead a fixed large N, which makes our model a system of stochastic ODE's, for which standard convergence proofs in the limit $\Delta t \to 0$ apply [106]. Our selection criterion for N is that it must lie in the range of shell numbers n where the statistics are Gibbsian thermal equilibrium at temperature T, with energy equipartition and independent Gaussian distributions of the shell variables u_n. We shall show in Sec. IV C for fixed individual realizations of the shell model state vector u which are chosen from the long-time, turbulent steady state that such an equipartition range in fact appears for all $n \geqslant N_e$, with some N_e, when these data u are evolved under the stochastic dynamics Eq. (3.8) for a very short time $\tau_e \sim 1/k_{N_e} u_{N_e}$. Here $N_e = N_e(u)$ depends upon the state vector u which is selected. We shall show furthermore that, for the range of integration times considered (300 large-eddy turnover times), there is a maximum value $N_e^\star = \max_t N_e[u(t)]$ over all times t. In our convergence tests below we shall select as initial data u a particular realization $u^\star$ such that $N_e^\star = N_e(u^\star)$, which corresponds to one of these most intense "bursts" which we encountered in our long numerical run. See Sec. IV C where this state $u^\star$ is more completely described and, also, Supplemental Material [71]. We only note here that this state $u^\star$ was found to have $N_e^\star = N_e(u^\star) = n_\eta + 6$, with n_η the Kolmogorov shell number, in a simulation with shell number cutoff $N = n_\eta + 7 = 22$. Thus, only the two highest wave-number shells remained in thermal equilibrium for this intense bursting event $u^\star$. This is presumably the most stringent test case for convergence of our numerical scheme, which should require the smallest time step Δt and largest truncation shell number N. However, we have tested convergence of our numerical scheme as well for other initial data $u(0)$

selected from the turbulent steady state and found very similar results.

2. Strong convergence in Δt

To check strong (pathwise) convergence in the time step Δt in the model with $N = 22$ shells, we must compare numerical solutions with different time steps Δt for the same realization of the complex Brownian motions $W_n(t)$. This requires a statistically consistent choice of the random variables $\Delta W_n(t_k)$, $\Delta Z_n(t_k)$ for the different step sizes Δt. We create such a consistent set by first constructing these pairs by the method of Ref. [106], Sec. 10.4, for the smallest time step $\Delta t = \delta t$. We then construct consistent values for $\Delta t = 2\,\delta t$, by the combinations

$$\Delta W_n^{(1)}\big(t_k^{(1)}\big) = \Delta W(t_{2k+1}) + \Delta W(t_{2k}), \tag{3.21}$$

$$\Delta Z_n^{(1)}\big(t_k^{(1)}\big) = \Delta Z(t_{2k+1}) + \Delta Z(t_{2k}) + \Delta t\,\Delta W(t_{2k}), \tag{3.22}$$

where $t_k = k(\delta t)$ and $t_k^{(1)} = k(2\delta t)$, for $k = 0, 1, 2, \ldots$. Equations (3.21) and (3.22) follow easily from the definition Eqs. (3.19) and (3.20). This procedure may be iterated p times to produce consistent sets of random increments $\Delta W_n^{(p)}(t_k^{(p)})$, $\Delta Z_n^{(p)}(t_k^{(p)})$ for any time step of the form $\Delta t = 2^p\,\delta t$, with $t_k^{(p)} = k(2^p\,\delta t)$ for $k = 0, 1, 2, \ldots$.

As discussed in the previous section, we use as initial condition for our pathwise convergence study the state $u^\star$ from the strong "burst" which propagated to the highest shell. We define error as the expectation over noise realizations $\mathbb{E}$ of the norm $\|\cdot\|$ of the difference $u^{\Delta t}(t) - u^{\delta t}(t)$, where $u^{\Delta t}(t)$ is the numerical solution starting from $u^\star$ using time step Δt and $u^{\delta t}(t)$ is the reference state obtained by integration with the finest time step δt, which we take as the "exact solution." To make our convergence criterion most sensitive to the largest wave numbers, we used the enstrophy norm associated to the space h_2^1, or

$$\|u\|_{\text{ens}} := \sqrt{\sum_{n=0}^{N} k_n^2 |u_n|^2}. \tag{3.23}$$

However, we obtained similar results with norms for other spaces such as energy norm for the space l_2 and sup-norm for the space l_∞ and also for individual shells n. We took $t = 10^{-3} t_\eta$, where $t_\eta = \eta/u_\eta$ is the Kolmogorov time, since this choice of time t was large enough to obtain appreciable evolution at the highest shells. The results which are plotted in Figure 2 show convincingly that the strong order of convergence of the method is 2.

This is consistent with the mathematical theory [103], which establishes at least $\frac{3}{2}$-order (see also Appendix B), but better than we had initially expected. We furthermore found the method to be strong order 2 for all other initial data that we considered. To illuminate this unexpectedly large convergence rate, we estimated the local truncation error $T(\Delta t)$ by calculating the error in the method with a single step $\mathbb{E}[\|u^{\Delta t}(\Delta t) - u^{\delta t}(\Delta t)\|_{h_2^1}]$, for each stepsize Δt. The results, plotted in Fig. 3 show the scaling $T(\Delta t) \propto (\Delta t)^{5/2}$ that was expected. This would produce a global error scaling as $(\Delta t)^{3/2}$ in a number of steps $N_{\text{steps}} \propto \frac{1}{\Delta t}$, if these errors accumulated without cancellation. The observed scaling of global error is explained if the errors at each step are in fact uncorrelated and of different signs, so that, by the central limit theorem, the total error then scales as $(\Delta t)^{5/2}\sqrt{N_{\text{steps}}} \propto (\Delta t)^2$.

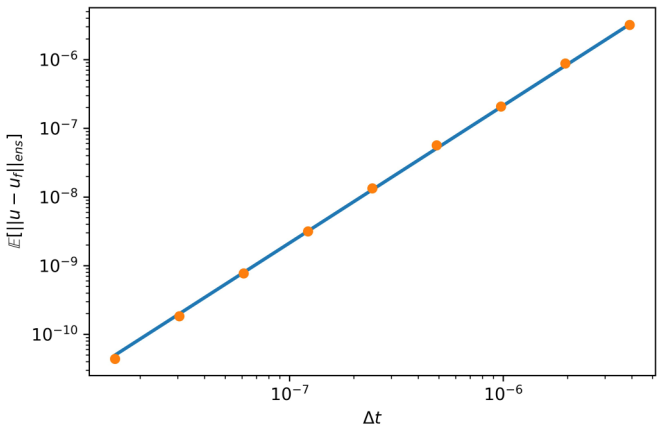

FIG. 2. Test of order of convergence of the numerical scheme, starting with a strong burst as the initial conditions. Solid orange dots (●) correspond to expectation values of the enstrophy norm Eq. (3.23) of the error; solid cyan line (—) corresponds to least-squares fit of a function $c\Delta t^2$, where c was determined to be 7.434.

In conclusion, our numerical scheme Eq. (3.18) converges pathwise with order at least 3/2 (and effectively 2) as $\Delta t \to 0$ for a choice of the cutoff $N > N_e^\star$.

3. Independence of wave-number truncation N

We next verify that the statistical evolution of the shell modes u_n for $n \leqslant N_e^\star$ is independent of the choice of cutoff $N \geqslant N_e^\star$. More precisely, we study the transition probability density

$$P_N[u, t\,|u(0), 0] = \mathbb{E}(\delta\{u - U_N[t; u(0), W]\}), \tag{3.24}$$

where $U_N[t; u(0), W]$ is the (strong) solution of our stochastic shell model Eq. (3.8) for number of shells $N \geqslant N_e[u(0)]$ with

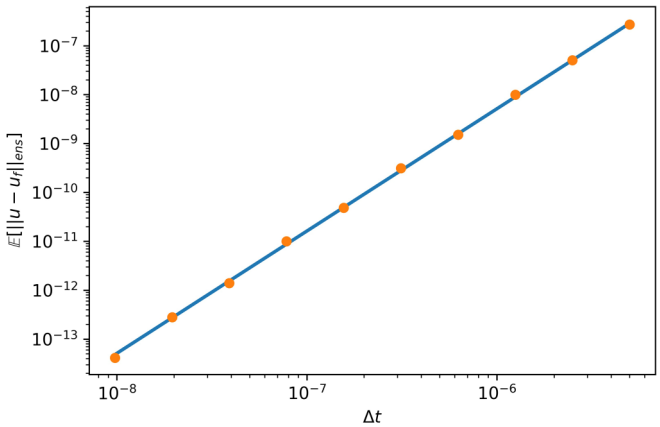

FIG. 3. Scaling $(\Delta t)^{\frac{5}{2}}$ for the local truncation error $T(\Delta t)$. Solid orange dots (●) correspond to expectation values of the enstrophy norm Eq. (3.23) of the error; solid cyan line (—) corresponds to least-squares fit of a function $c\Delta t^{5/2}$, where c was determined to be 6.710.

initial data $u(0)$ and with the particular realization $W = (W_n : n = 0, 1, \ldots, N)$ of the random Brownian motions over the time-interval $[0, t]$, and $\mathbb{E}[\cdot]$ again denotes expectation over those random Brownian motions. We present evidence that this transition probability for the set of modes $[u_n(0) = u_n^\star : n = 0, 1, \ldots, N_e^\star]$ is independent of the choice of cutoff $N \geqslant N_e^\star$ and also independent of the initial data $[u_n(0) : n = N_e^\star + 1, \ldots, N]$ of the modes with $n > N_e^\star$ when those are selected at random from the thermal Gibbs distribution for those shells. If this result holds, then we have a well-defined stochastic Markov evolution for the modes $[u_n(0) : n = 0, 1, \ldots, N_e^\star]$, which is independent of the cutoff N. This gives a precise mathematical meaning to the stochastic shell-model Eq. (3.8) as a "low-wave-number effective theory."

The transition probability density Eq. (3.24) of the entire state vector $(u_n : n = 0, 1, \ldots, N_e^\star)$ is obviously too unwieldy to investigate in its entirety, so we consider instead reduced or marginal PDF's of u_n for specific shell numbers $n \leqslant N_e^\star$. We focus our attention on the shell modes with n near to $N_e^\star$, since those must be most affected by the change in truncation N. Here we present results for $n = N_e^\star$ itself, but comparable results are found also for $n < N_e^\star$. For the time lapse t in the transition PDF Eq. (3.24) we chose $t = t_\eta$, one Kolmogorov time. This time should be sufficient for the influence of truncation N to propagate through the entire dissipation range. Once the transition PDF Eq. (3.24) has been verified to be independent of N for times $t \leqslant t_\eta$, then this independence of course extends to the transition PDF's for *all* times $t > 0$ by the Chapman-Kolmogorov equation. Here we presume that N-independence of the transition probability for the most singular event, $u(0) = u^*$, implies independence for any other choices of $u(0)$.

For the study of effects of truncation, we used the same model parameters and time step Δt that were employed in the long-time steady-state simulation, discussed in detail in the next Sec. IV A. Increasing N from its original value $N = N_e^\star + 1$ would require a smaller time step and this would have been numerically expensive. We therefore chose to make the much more demanding test of *reducing* the cutoff N to the value $N = N_e^\star$, taking $u_{N_e^\star+1} = 0$ as boundary condition, and then comparing the transition PDF for the reduced value $N = N_e^\star$ with that for the original value $N = N_e^\star + 1$. We emphasize that for the intense burst event $u^\star$, only the highest two modes with $n = N_e^\star,\ N_e^\star + 1$ remained in thermal equilibrium, so that our reduction to $N = N_e^\star$ leaves only a single mode in equipartition. Plotted in Fig. 4 are the reduced transition PDF's for the real part $x_{N_e^\star} = \mathrm{Re}(u_{N_e^\star})$ with both $N = N_e^\star$ and $N = N_e^\star + 1$, calculated by averaging over 8×10^4 independent samples of the Brownian motions $W = (W_n : n = 0, 1, \ldots, N_e^\star + 1)$. The two PDF's are identical within Monte Carlo error, a strong evidence for statistical decoupling of mode $u_{N_e^\star+1}$ from the dynamics of the modes u_n with $n \leqslant N_e^\star$. We obtained analogous results (not shown here) for the marginal transition PDF of the imaginary part $y_{N_e^\star} = \mathrm{Im}(u_{N_e^\star})$ and for the similar variables $x_n,\ y_n$ with $n < N_e^\star$.

These independence results support the claim that we have a well-defined stochastic dynamics whenever the cutoff N is selected larger than $N_e^\star$, in agreement with the idea that the shell modes in thermal equilibrium are UV asymptotically

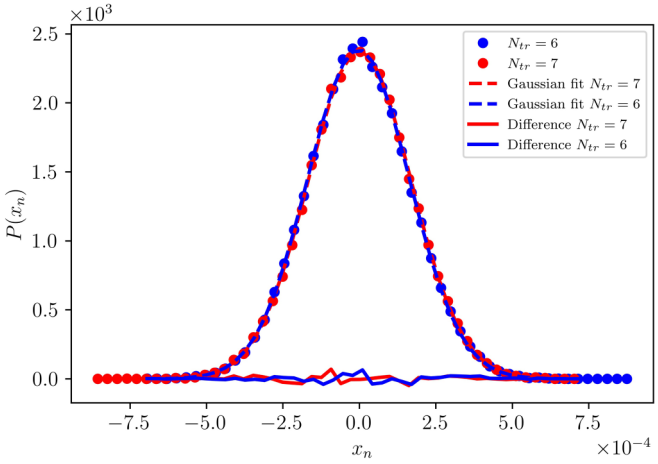

FIG. 4. Comparison of the two marginal transition PDFs $P_N(x_{N_e^\star}, t|u^\star, 0)$ for the variable $x_{N_e^\star} = \mathrm{Re}(u_{N_e^\star})$ with the truncation wave numbers $N = N_e^\star$ and $N = N_e^\star + 1$.

free. These results in fact suggest that a convergence result should hold for the idealized mathematical limit $N \to \infty$. This is hinted also by the rigorous results in Ref. [98] for the unforced, thermal equilibrium dynamics. Of course, even if such a limit result could be proved for the forced model, it would still not suffice to justify it physically, unless it could be shown even further that convergence is practically attained for a value of $N_e^\star = \log_2(\Lambda/k_0)$ corresponding to a length scale Λ^{-1} still much greater than λ_{mfp}. Our results for the Sabra model are thus encouraging, because $N_e^\star = n_\eta + 6$ corresponds to a length scale only 64 times smaller than η. In the case of the ABL with $\eta = 0.54$ mm these events of most extreme intermittency would correspond to a length about 8.4 μm, which is still 124 times greater than the mean-free-path length of air, $\lambda_{\mathrm{mfp}} = 68$ nm.

IV. NUMERICAL SIMULATION RESULTS

A. Setup of the simulations

We undertook to perform our simulations of the noisy Sabra model in dimensionless form with the dissipation scaling Eq. (3.12), so that $\varepsilon = \nu = 1$ and the Kolmogorov shell number is set to $n = 0$. We wanted dimensionless parameters in correspondence with the atmospheric boundary layer (ABL), and thus the dimensionless temperature was taken to have the value $\theta_\eta = 2.83 \times 10^{-8}$ in Eq. (2.12). The range of shell numbers in our simulation was chosen as $n = M, M + 1, \ldots, R$ with $M = -15$ and $R = 7$ and with constant stirring forces applied at the first two shells, M and $M + 1$. We aimed to achieve a Reynolds number $\mathrm{Re} = u_{\mathrm{rms}} 2^M$ comparable to the value $\mathrm{Re} \sim 10^7$ cited as typical in the ABL [67]. However, with our choice of forcing, neither of the statistical quantities

$$u_{rms}^2 = \sum_{n=M}^{R} \langle |u_n|^2 \rangle, \qquad \varepsilon = \sum_{n=M}^{R} k_n^2 \langle |u_n|^2 \rangle \tag{4.1}$$

was under our precise control. We therefore adjusted the forcing until we obtained $u_{\mathrm{rms}} \sim O(10^2)$ and $\varepsilon \sim O(1)$, which

was satisfied with the stirring forces

$$f_M = -0.008900918232183095 - 0.0305497603210104\,i,$$
$$f_{M+1} = 0.005116337459331228 - 0.018175040700335127\,i, \tag{4.2}$$

which gave the precise value $\varepsilon \doteq 1.478$, close to our target value of unity. We then rescaled all quantities to correct dissipation-scale units by taking

$$u_n \to u_n/\varepsilon^{1/4}, \quad k_n \to k_n/\varepsilon^{1/4}, \quad f_n \to f_n/\varepsilon^{3/4}, \tag{4.3}$$

which yielded $u_{\rm rms} = 56.48$, $\mathrm{Re} = 2.04 \times 10^6$ and $\theta_\eta = 2.328 \times 10^{-8}$. All results presented below are in these Kolmogorov units.

The time step of our simulation was chosen (in original units) to be equal to $\Delta t = 10^{-5}$ which was about an order of magnitude smaller than the viscous time at the highest wave number, $t_{\rm vis} = 1/k_R^2 \doteq 6.1 \times 10^{-5}$. Since one large-eddy turnover-time of the simulation was $T = 1/k_M u_{\rm rms} \doteq 640$ dimensionless time units, it was too time-consuming to calculate time-averages over many such times T in a single run of the model on one computer. We therefore took advantage of parallel computing by using a strategy rst computing a long run of the model for $N_{\rm samp} = 300$ large-eddy turnover times with increased time step $\Delta t = 10^{-3}$ and then creating $N_{\rm samp}$ independent initial-data by sampling that under-resolved solution in intervals of one turnover time. These 300 independent initial data were then distributed over the nodes of a computer cluster and each integrated again for time T with the time step $\Delta t = 10^{-5}$. To avoid possible early time artefacts from under-resolution, we discarded the first 100 steps of these well-resolved simulations in calculating all long-time averages (and, in fact, the statistics were checked to change negligibly also by including those initial time steps).

Both the noisy model Eq. (3.8) and the deterministic model Eq. (3.1) were solved with the same numerical Taylor-Itō scheme Eq. (3.18), the latter simply by setting $\theta_\eta = 0$. The calculations were performed in double-precision arithmetic and only for the deterministic model at the highest wave numbers did we approach the underflow level of double precision. In fact, it is one of the numerical advantages of stochastic models that the requirements on arithmetic precision are considerably reduced, a fact which has been previously stressed for climate modeling [109]. The time step Δt and the total number $N_{\rm samp}$ of large-eddy times used to calculate averages were the same for both noisy and deterministic cases. We discuss in Appendix C the various tests that we have made that those parameter choices were adequate to yield well-converged statistics.

B. Energy spectra with thermal noise

We first present numerical results on the simplest statistical quantity of interest, the energy spectrum. To make thermal energy equipartition as evident as possible, we shall show the average $\bar{\epsilon}_n$ of the kinetic energy per mass in the mode with shell number n

$$\epsilon_n = \tfrac{1}{2}|u_n|^2, \tag{4.4}$$

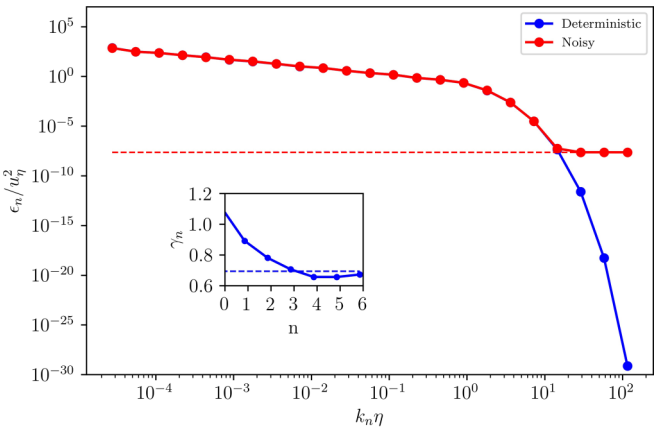

FIG. 5. The energy spectrum of the deterministic model (heavy blue line, ——) and noisy model (heavy red line, ——). The dashed red line (– – –) shows the thermal equipartition value in Eq. (4.5). *Inset:* The local stretching exponents Eq. (4.6) for the deterministic model spectrum (blue solid circles, ●) and theoretical value in Eq. (3.14) (dashed blue line, – – –).

plotted versus wave number k_n. This differs slightly from the standard energy spectrum for the shell model which is conventionally defined by $E_n = \bar{\epsilon}_n/k_n$, as in Eq. (3.15). The quantity Eq. (4.4) is more convenient because thermal equipartition gives a constant value independent of n,

$$e_n^{eq} = \theta_\eta, \tag{4.5}$$

in Kolmogorov dissipation units. In Fig. 5 we plot the energy in mode n given by Eq. (4.4) for both the deterministic and noisy Sabra models.

The two spectra are indistinguishable in the inertial range, where both exhibit a power-law decay $\propto k_n^{-\alpha}$ with exponent a bit larger than the K41 value $\alpha = 2/3$. The increase of α above the K41 value is due to standard inertial-range intermittency effects, which do not differ for the deterministic and noisy models. The behavior of the spectrum in the dissipation range is, however, drastically different for the two models, with the spectrum of the deterministic model exhibiting a very rapid exponential-type decay and the spectrum of the noisy model saturating at the equipartition value Eq. (4.5). Altogether, the results are very close to our predicted spectrum for 3D incompressible fluid turbulence pictured in Fig. 1, except that the equipartition wave number is slightly larger, $k_{\rm eq}\eta \doteq 15$, rather than $k_{\rm eq}\eta \doteq 10$ for 3D. The somewhat smaller equipartition wave number in 3D is due in part to the rising equipartition spectrum there and also to the faster exponential decay in the absence of thermal noise. By contrast, the energy spectrum Eq. (4.4) of the shell model becomes flat in thermal equipartition and exhibits the stretched-exponential decay Eq. (3.14) without thermal noise. We have verified this stretched-exponential form of the spectrum from our numerical results, by calculating a local stretching exponent

$$\gamma_n = \log_2 \left|\ln\langle|u_{n+1}|^2\rangle\right| - \log_2 \left|\ln\langle|u_n|^2\rangle\right| \tag{4.6}$$

at dissipation-range shell numbers $n > 0$ in the deterministic model, with the results plotted in the inset of Fig. 5. The local exponents indeed agree well with the theoretically expected value $\gamma = \log_2(\frac{1+\sqrt{5}}{2})$ at $n \geqslant 4$.

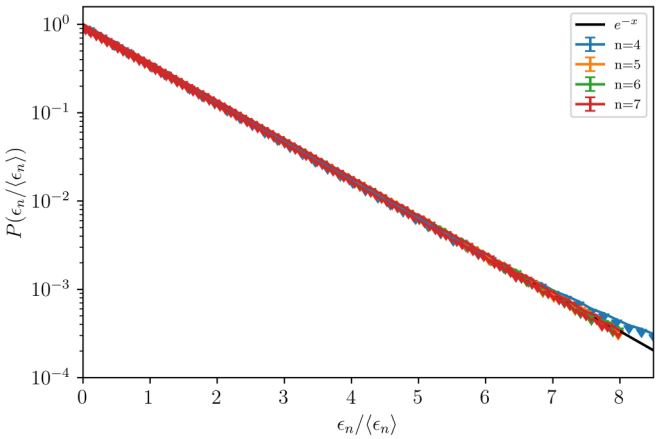

FIG. 6. PDFs of the normalized modal energy $\epsilon_n/\langle\epsilon_n\rangle$ for shells $n = 4, 5, 6, 7$ and an exponential distribution with rate parameter 1. The error bars depict standard error of the mean from the long-time average.

With thermal noise present, the modes at the highest wave number not only have energy spectrum in thermal equilibrium, but in fact have all statistics quite accurately described by the Gaussian Gibbs measure Eq. (3.10). Plotted in Fig. 6 are the PDF's of the modal energies $\epsilon_n = \frac{1}{2}|u_n|^2$ for the four highest shells $n = 4, 5, 6, 7$ compared with the exponential PDF $p(\epsilon) = \beta e^{-\beta\epsilon}$ that follows from Eq. (3.10). The energy for the lowest of these modes, $n = 4$, agrees well with the exponential PDF out to about 7 standard deviations, but has a distinctly broader tail past this point. The three highest modes with $n = 5, 6, 7$ have energy PDF's that are indistinguishable from the thermal-equilibrium exponential PDF to within numerical errors (which arise mostly from the finite number of samples).

C. Dissipation-range intermittency

The dissipation range of 3D incompressible fluid turbulence is widely expected to exhibit extreme spatiotemporal intermittency because of the super-algebraic decay of the energy spectrum at high wave numbers k. This was first predicted by Kraichnan [39], who argued heuristically that most of the contributions to moments of velocity-gradients at high-k would come "from the few exceptional regions," where a large but still modest fluctuation around the Kolmogorov scale had been exponentially magnified in relative magnitude by the rapid fall-off in the spectrum. This argument was later given in a more mathematically precise form related to singular solutions of the dynamics in the complex time plane and extended also to temporal intermittency of simple nonlinear dynamics without spatial structure [36]. This type of intermittency in the "far dissipation range" is expected to occur even in relatively low Reynolds number turbulent flows and has been observed in numerical simulations of the Navier-Stokes equation [110,111].

The deterministic Sabra model Eq. (3.1) possesses all of the ingredients for such extreme intermittency in its far dissipation range and our numerics give vivid confirmation of the expected effects. For example, plotted in Fig. 7(a) are the modal energies $\epsilon_n(t)$ as a function of time t for the dissipation-range shells $n = -1, \ldots, R$ in a simulation with $M = -15$ and $R = 7$. It can be seen there that mild fluctuations for $n = -1, 0$ appear with a slight time delay at larger n but also hugely enhanced, so that the energies at distinct instants differ by hundreds of orders of magnitude. The fluctuations are so severe that our computations are brought near to the underflow level of the double-precision arithmetic. An average of $\epsilon_n(t)$ over the pictured time interval for a dissipation-range mode with $n > 0$ would thus be completely dominated by the single exceptional event around $t \simeq 50$. However, the same quantities plotted in Fig. 7(b) for the noisy Sabra model Eq. (3.8), which includes physically realistic thermal noise, has these extreme fluctuations replaced by Gaussian velocity fluctuations at the level of energy equipartition. This thermal velocity $u_{\rm th}$ is small compared with the Kolmogorov-scale velocity u_η (by a factor of $\theta_\eta^{1/2}$) but much larger than the extremely tiny velocities attained in the deterministic theory. We expect likewise for incompressible fluid turbulence occurring in the laboratory or in Nature that the type of strong intermittency predicted by Kraichnan [39] to appear in the far dissipation range is, in fact, thoroughly erased by thermal noise.

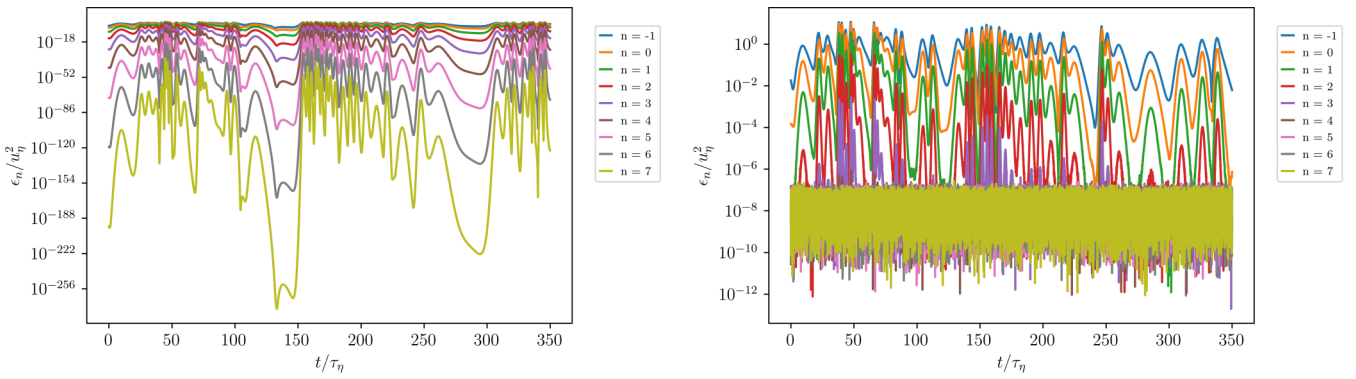

(a) Deterministic Sabra **(b)** Noisy Sabra.

FIG. 7. Plots of modal energies $\epsilon_n(t)$ versus time t for shells in the dissipation range with $n = -1$ to $n = 7$. (a) The deterministic Sabra model results, exhibiting the extreme intermittency predicted by Kraichnan [39], and (b) the stochastic model results, with the large intermittent fluctuations completely washed out by Gaussian thermal fluctuations.

Sizable dissipation-range intermittency remains in the stochastic shell model, as made clear by the results in Fig. 7(b), but we argue that it is a high-Re effect of inertial-range intermittency propagating into the dissipation range. This "near-dissipation-range intermittency" is present also in the deterministic Sabra model and, in a spatiotemporal form, in turbulence modelled by the deterministic Navier-Stokes equation. This is the type of near-singularity due to extreme events intensively studied in recent works [44–50]. In fluid turbulence such intermittency is known to lead to strong fluctuations in the "local viscous/cutoff length" $\eta(\mathbf{x}, t)$, which is conventionally defined [32,112] by the condition that the local Reynolds number at that scale be order unity:

$$\frac{\eta \delta_\eta u(\mathbf{x}, t)}{\nu} \simeq 1, \tag{4.7}$$

where $\delta_\eta u(\mathbf{x}, t) = |\mathbf{u}(\mathbf{x} + \eta, t) - \mathbf{u}(\mathbf{x}, t)|$. While typically $\eta(\mathbf{x}, t) \simeq \eta$, much larger and much smaller cutoff lengths appear. As already discussed in Sec. II D, this fluctuating viscous length has been represented phenomenologically [32] by $\eta_h \sim L\mathrm{Re}^{-1/(1+h)}$, where $h = h(\mathbf{x}, t)$ is the local Hölder exponent of the velocity in the Parisi-Frisch multifractal model [9,83]. Below the length scale $\eta(\mathbf{x}, t)$ the velocity field is expected to be smooth, with a local energy spectrum defined by a suitable band-pass filter that is exponentially decaying. These are the considerations that led Frisch and Vergassola to predict for velocity structure functions an "intermediate dissipation range" [40], bridging the inertial-range and the far dissipation range. A definition of a "local viscous shell number" analogous to Eq. (4.7) may be made also in shell models, both deterministic and noisy, by setting

$$N_{\mathrm{vis}}(u) := \min\left\{ n : \frac{|u_n|}{\nu k_n} \leqslant 1 \right\}. \tag{4.8}$$

and the predictions of Ref. [40] concerning the intermediate dissipation range were previously verified in a numerical simulation of the GOY shell model [84].

We expect that a similar physics lies behind the intermittency displayed in Fig. 7(b) for our noisy shell model, but with the rapid exponential decay of amplitudes below the viscous cutoff replaced in the noisy model by a thermal equipartition, like that exhibited by the average energy spectrum for shell numbers $n \geqslant 5$ in Fig. 5. As a consequence of the inertial-range intermittency, however, the shell number at which this equipartition first sets in must fluctuate greatly from realization to realization. It is actually a somewhat subtle issue how to define precisely "energy equipartition" for an individual realization, because equipartition is a statistical concept. Even realizations selected from the thermal Gibbs state Eq. (3.10) show considerable fluctuations in energy from the equipartition value and some averaging in time is typically required to bring the modal energy close to the ensemble mean value even for such an equilibrium realization. As one possible measure of the "equilibration shell number" $N_e(u)$ for an individual realization u from our turbulent simulation, we can average the modal energy $\epsilon_n = (1/2)|u_n|^2$ over one Kolmogorov time $t_\eta = \eta/u_\eta$ and we then identify $N_e(u)$ as the smallest integer such that this local time-average $(1/2)\langle |u_n|^2 \rangle_\eta$ is below $2\theta_\eta$ for all $n \geqslant N_e(u)$. For examples of such locally time averaged realizations, see Figure 3 in Ref. [58]. We have plotted in Fig. 8 the PDF of the local equipartition shell number $N_e(u)$ obtained from our DNS with the above definition, together with the PDF of the viscous cutoff shell number $N_{\mathrm{vis}}(u)$ defined in Eq. (4.8).

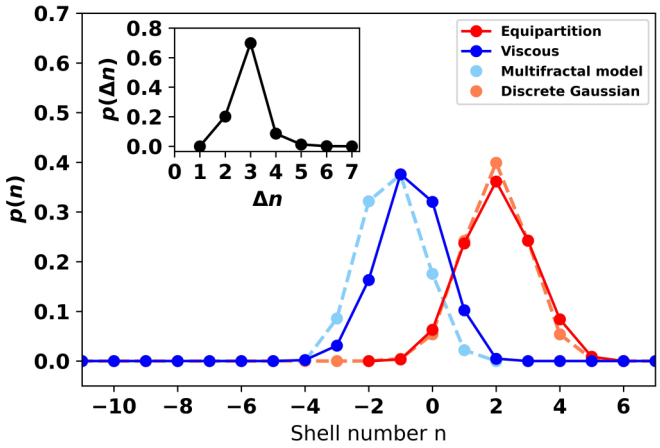

FIG. 8. PDF's of $N_{\mathrm{vis}}(u)$ (**blue**) and $N_e(u)$ (**red**), along with a simple multifractal model for the PDF of $N_{\mathrm{vis}}(u)$ (**pale blue**) and a fit by a discrete Gaussian distribution for the PDF of $N_e(u)$ (**pale red**). *Inset:* The PDF of the shift $\Delta N(u)$ in each realization. Standard errors of the mean for $N_{\mathrm{vis}}(u)$ and $N_e(u)$ are smaller than the marker size.

Before examining the simulation results, we must first acknowledge that our definition of the "equilibration shell number" $N_e(u)$ suffers from a good bit of arbitrariness. We have therefore explored as well alternative definitions. For example, if averaging over time t_{avg} produces an equipartition spectrum down to shell $N(t_{\mathrm{avg}})$, then averaging over a longer time might extend that range. Since the natural viscous timescale of the stochastic dynamics at one lower shell increases by 4, we have considered another possible definition by successively increasing the averaging time t_{avg} from t_η by factors of 4 and by redefining $N_e(u) = N(4t_{\mathrm{avg}})$ as long as $N(4t_{\mathrm{avg}}) < N(t_{\mathrm{avg}})$ [113]. This alternative definition yielded slightly lower estimates of $N_e(u)$ for some realizations u, but with the same qualitative features. A completely different approach to defining $N_e(u)$ would be to apply standard distribution tests from mathematical statistics, such as p values [114], to the hypothesis that the shell variables $u_\eta, u_{K+1}, \ldots, u_N$ are drawn from the multivariate distribution Eq. (3.10) and then define $N_e(u)$ to be the smallest $K \leqslant N$ for which that hypothesis is accepted. However, since any definition of the "equilibration shell number" seems to involve various subjective choices and since all definitions that we have considered exhibit qualitatively similar intermittency, we shall only discuss here the quantity $N_e(u)$ defined in the previous paragraph.

We first observe in Fig. 8 that the equilibration shell number $N_e(u)$ does fluctuate substantially from realization to realization, with nonvanishing probability to take values from -2 to 6 in our ensemble of events gathered from a simulation of 300 large-eddy turnover times. We have no theoretical prediction for the PDF of $N_{\mathrm{eq}}(u)$, but we observe that it is fit fairly well in this core range by a standard discrete Gaussian PDF [115] of the form $p(n) = e^{-(n-2)^2/2}/\Theta$, plotted as well

in Fig. 8. Most interestingly, the PDF's of $N_{\rm vis}(u)$ and $N_e(u)$ are roughly similar in form, but that for $N_e(u)$ is shifted to the right by $2-3$ shells. This observation suggests that the same dynamics is responsible for the fluctuations in both $N_{\rm vis}(u)$ and $N_e(u)$. This supports the picture we have proposed that inertial-range intermittency leads to a fluctuating viscous cutoff shell number, above which the amplitude of u_n drops drastically in n with the stretched-exponential decay (3.14) which is the same for all realizations. In that case, within a small number of shells which is nearly independent of u the amplitude of the shell velocity drops to the level u_{th} where thermal equipartition is achieved. As a further test of this explanation, we have also calculated with our DNS the PDF of the shift $\Delta N(u) = N_e(u) - N_{th}(u)$ in each realization, with the result plotted in the inset of Fig. 8. This data shows a probability of about $2/3$ for $\Delta N = 3$, and considerably smaller probabilities $\doteq 2/9$ for $\Delta N = 2$ and $\doteq 1/9$ for $\Delta N = 4$. We conclude that the shell velocity amplitude indeed drops to the equipartition level u_{th} about 3 shells above the viscous cutoff shell number $N_e(u)$ in every realization. The intermittency that appears in the dissipation range of the noisy model thus appears to be imprinted by small- and large-amplitude events that propagate down from the inertial range. The few events observed with $N_e(u) = -2$ may be described as very low-intensity "lulls" and the handful of events with $N_e(u) = 6$ as extreme amplitude "bursts."

The burst event u that we considered in our convergence studies in Secs. III B 2 and III B 3 is the only realization with $N_e(u) = 6$ that we encountered in our long numerical simulation over 300 large-eddy turnover times. As discussed there, even this largest value $N_e(u) = 6$ would correspond in the ABL to an "equilibration length" about 124 times larger than the mean free path of air. Such a significant separation in scales suffices to justify the validity of a hydrodynamic description even for such extreme events. Of course, we cannot rule out that running our shell model dynamics for much longer times would produce much more intense events still, with $N_e(u) > 6$. To properly identify the most extreme event at our given Reynolds number Re and dimensionless temperature θ_η which achieves the largest value $N_e^\star$ (possibly $=\infty$) would require specialized tools of rare-event sampling beyond the scope of the current work. However, more systematic investigation of such extreme behaviors is important work for the future.

The results of the present section demonstrate that sizable intermittency remains in the dissipation range of our stochastic shell model with thermal noise. Our numerical results are consistent with the hypothesis that these strong fluctuations are due to intermittent events, ranging from "lulls" to "bursts," that propagate in from the inertial-range. However, a quantitative relationship remains to be established with inertial-range scaling. Furthermore, it remains to be understood how such intermittency manifests in standard statistical averages and at what wave-number scale. All of these issues are addressed in the following section.

D. Structure functions

To study intermittency effects across both inertial and dissipation ranges in our simulations, we use p-th-order structure functions, which we define here as statistical "p norms"

$$\|u_n\|_p = \langle |u_n|^p \rangle^{1/p} \tag{4.9}$$

of the shell node u_n. The additional pth root in Eq. (4.9) compared with the standard definition makes comparing results for different choices of p more transparent. Although these are norms literally only for $p \geqslant 1$, we consider all real values of $p > -1$, because negative p values give information about rare events which are smoother or more regular than typical. Similar information could be obtained also from so-called "inverse structure functions" [116] but we confine ourselves here to the more traditional direct structure functions. Note that the shell-model quantities Eq. (4.9) correspond only in the inertial-range to the standard structure functions defined by moments of velocity-increments in Navier-Stokes turbulence, but more generally they correspond to structure functions of a suitably band-passed velocity field $\mathbf{u}_n(\mathbf{x}, t)$ at wave-number magnitudes $k_n \sim 2^n k_0$. This distinction is crucial in the turbulent dissipation range, where first-order velocity-increments are completely dominated by the linear term in their Taylor series and are an inadequate tool to probe the energy spectrum and intermittency effects. An empirical study of incompressible fluid turbulence which aimed to investigate the same physics issues that we do here for shell models would need to employ a band-pass filter kernel $f_n(\mathbf{k})$ with very rapid decay for $|\mathbf{k}| < k_n$, optimally vanishing identically for $|\mathbf{k}| < ck_n$ with some constant $c > 0$.

In Fig. 9 we plot the structure functions $\|u_n\|_p/u_{\rm th}$ versus n for the deterministic and noisy models, both normalized by the thermal velocity $u_{\rm th} = (2\theta_\eta)^{1/2}$ in Kolmogorov units. With this normalization, the thermal equipartition value of the pth-order function is $[\Gamma(1+\frac{p}{2})]^{1/p}$ in terms of the Euler Γ function. We plot the structure functions for six representative values of p, both positive and negative, over the entire range of n. The first important observation is that the structure functions for the deterministic and noisy models are identical in the inertial-range, within numerical accuracy. This is not unexpected, because the thermal noise is extremely weak in the inertial range and the direct effect on the dynamics should be negligible. The pth-order functions here exhibit power-law scaling $\propto k_n^{-\sigma_p}$, which is indicated by the straight-line fits in the log-log plots in Fig. 9. These exponents are related by $\sigma_p = \zeta_p/p$ to the standard structure-function scaling exponents ζ_p, and the values obtained from our linear fits agree for $p > 0$ with those previously appearing in the literature; see Fig. 10, where we plot our values together with those reported in Ref. [56], showing agreement within our error bars [117]. The decrease of σ_p with the order p is a reflection of temporal intermittency in the shell model dynamics, which has been long understood to be associated with strong "bursts" that propagate from low to high wave numbers [104,118,119]. This inertial-range dynamics is essentially unaltered by the presence of weak thermal noise.

In the dissipation range, however, the pth-order structure functions of the deterministic and noisy models are entirely different. Analogous to what is observed in the pair of energy spectra ($p = 2$) plotted in Fig. 5, the structure functions for the noisy model approach thermal equipartition at high wave numbers, whereas the same functions for the deterministic

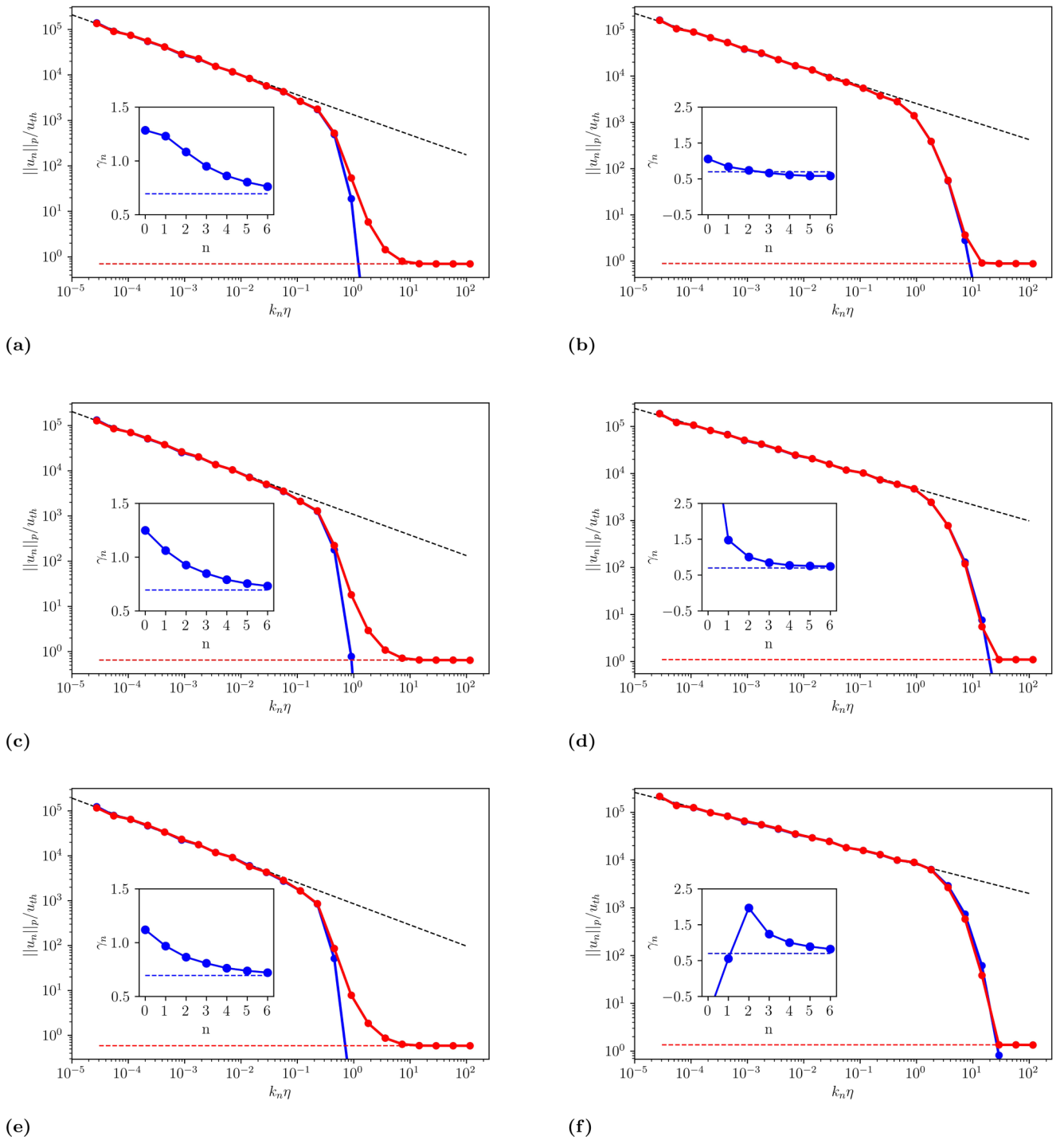

FIG. 9. Structure functions Eq. (4.9) for the deterministic model (heavy blue lines, ——) and for the noisy model (heavy red lines, ——). The predicted equipartition levels $[\Gamma(1+p/2)]^{1/p}$ are indicated by the horizontal dashed red lines (– – –) and power-law fits in the inertial range are plotted as black dashed lines (– – –). The left panels show negative values (a) $p=-0.3$, (c) $p=-0.6$, (e) $p=-0.9$, and the right panels show positive values (b) $p=1$, (d) $p=3$, (f) $p=6$. Standard errors of the mean for structure functions are smaller than the marker size. The insets show with heavy blue line (——) the local stretching exponent Eq. (4.10) and with horizontal dashed blue line (– – –) theoretical prediction $\gamma=\log_2(\frac{1+\sqrt{5}}{2})$.

model exhibit a super-algebraic decay. In fact, the pth-order structure functions of the deterministic model for all p values exhibit the same stretched-exponential decay Eq. (3.14) as does the energy spectrum. This is verified in the insets of Fig. 9, which plot the local stretching exponents:

$$\gamma_n^{(p)}=\log_2|\ln\|u_{n+1}\|_p|-\log_2|\ln\|u_n\|_p| \tag{4.10}$$

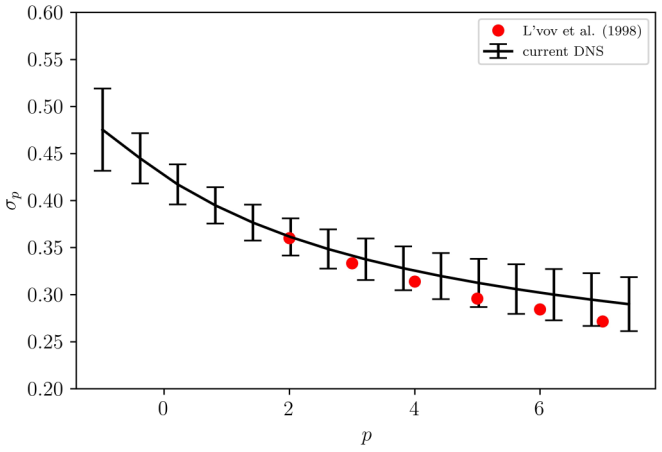

FIG. 10. The scaling exponents $\sigma_p = \zeta_p/p$ of structure functions $\|u_n\|_p$ for 210 values of p between $p = -1$ and $p = 8$, from our DNS (solid black line, ——). The values for σ_p from Ref. [56] for $p = 1$–7 are plotted as solid red circles (●). The errors are calculated as a sum of two sources, presumed independent. The first source of error is calculated by restricting the range of the linear fit from 10 to 6 shells, shifting it within the original 10 shells, and taking the standard deviation of all the obtained slope values as the dominant source of the error. The second source of error is calculated by sub-sampling the data set into 10 parts, calculating the scaling exponents separately for each, and finding the standard deviation of the obtained exponents. The systematically smaller results obtained in Ref. [56] compared with our mean values are presumably due to extremely rare, intense events missed in our sample of 300 large-eddy turnover times but encountered in the longer runs of Ref. [56].

and the theoretical prediction $\gamma = \log_2(\frac{1+\sqrt{5}}{2})$. Especially the negative p values and $p = 1$ exhibit the predicted stretched exponential, whereas $p = 3$ and $p = 6$ only approach this behavior for large n. The plausible explanation is that the intense "bursts" which dominate the structure functions for $p = 3$ and 6 penetrate to very high wave numbers, so that for our deterministic simulation the cutoff $R = 7$ is too small to capture well the stretched-exponential. For $-0.9 < p < 1$, however, the "lulls" or low-intensity events which dominate those p values end at relatively low wave numbers, so that the stretched-exponential above that wave number is well-resolved. The wave numbers where the asymptotic behaviors first appear, equipartition or stretched-exponential, likewise strongly depend on the order p and, from Fig. 9, clearly increase with p. This is directly associated with the strong fluctuations in the equipartition shell number $N_e(u)$, observed in the statistics in Fig. 8. In consequence, the negative-order structure functions which get dominant contributions from "lulls" with $N_e(u) \leqslant 0$ show direct effects of thermal noise at the Kolmogorov wave number and even lower wave numbers. This should be true also for three-dimensional hydrodynamic turbulence, but obtaining those structure functions from a laboratory experiment would require extremely accurate velocity measurements, since the thermal velocity u_{th} which sets the floor will be 3–4 orders of magnitude smaller than the Kolmogorov velocity.

To establish a quantitative connection with inertial-range scaling, we have made also a very simple multifractal model of the PDF of the viscous cutoff shell number $N_{\rm vis}(h)$, with the ansatz (in Kolmogorov units)

$$N_{\rm vis}(h) = \text{Round}\left[\log_2(\text{Re})\left(\frac{1}{1+h} - \frac{3}{4}\right)\right], \qquad (4.11)$$

where "Round" denotes rounding to the nearest integer, and where the PDF of the Hölder exponent h is taken to be $P(h) \propto \text{Re}^{D(h)/(1+h)}$ for multifractal dimension spectrum $D(h)$. Using the Legendre transform relation $D(h) = \inf_p\{ph - \zeta_p\}$, we have determined the dimension spectrum from our numerical results for ζ_p, with the resulting model PDF of $N_{\rm vis}$ also plotted in Fig. 8. Although our model is less sophisticated than the corresponding multifractal model developed for the PDF of $\eta(\mathbf{x}, t)$ in 3D fluid turbulence [120], it matches reasonably well the PDF of $N_{\rm vis}(u)$ from our DNS. This is consistent with an earlier study [84] verifying in the GOY shell model the predictions of the multifractal model for an "intermediate dissipation range" [40], since those predictions are based on the same assumption Eq. (4.11). We conclude that the fluctuating viscous cutoff $N_{\rm vis}(u)$ in our noisy Sabra model has statistics plausibly associated to inertial-range intermittency of "lulls" and "bursts," and the equipartition shell number $N_{\rm eq}(u)$ follows suit, occurring generally about just three shells higher.

V. DISCUSSION AND CONCLUSIONS

The main claim of this paper is that thermal noise fundamentally modifies the far dissipation range of turbulent flow, leading to a thermal equipartition range in the turbulent energy spectrum at length scales about $\eta/10$, one-tenth of the Kolmogorov length η, or even larger. If so, then the correct equation to describe low-Mach-number fluid turbulence down to sub-Kolmogorov scales is not incompressible Navier-Stokes, but is instead the fluctuating hydrodynamics of Landau-Lifschitz [15] in its incompressible limiting form [16–20]. This conclusion was already anticipated in the pioneering papers by Betchov [53,54]. We have further explained why standard scaling arguments [5–7] for validity of the deterministic Navier-Stokes equation at arbitrarily high Reynolds numbers do not contradict our conclusions. We have also discussed interactions of turbulent intermittency with thermal noise effects that should lead to large spatiotemporal fluctuations in the length scale at which thermal equipartition occurs in individual realizations. Finally, we have verified our various theoretical conclusions by simulations with a Sabra shell model of fluctuating hydrodynamics.

More questions are certainly raised by our results in this paper than can be currently answered definitively, and there is an urgent need for new computations, laboratory experiments, physical theory, and rigorous mathematical analysis to address them. Many of these questions were raised already by Betchov in his early works [53–55], as we discuss further below, and remain completely open to the present day.

A. Relations to prior theory

First, however, it is important to discuss relations of our work to earlier studies. There is a large body of work attempting to define fluctuating hydrodynamics equations of

the form Eq. (1.2) as continuum stochastic partial-differential equations (SPDE's), with the view that this is necessary for the understanding of turbulence. For example, the excellent book on SPDE's in hydrodynamics [22] states in its preface that

> "In a sentence, one of the purposes of the course was to understand the link between the Euler and Navier-Stokes equations or their stochastic versions and the phenomenological laws of turbulence."

and the chapters of this book attempt to make mathematical sense of equations like Eq. (1.2) as continuum SPDE's. This was also the point of view of the earlier paper on the stochastic shell model [98] which showed how to make sense of Eqs. (3.8) in the limit $N \to \infty$ (for thermal equilibrium). An exact mathematical solution of this problem for fluctuating hydrodynamics would allow the limit $\Lambda \to \infty$ formally to be taken so that the Eq. (1.2) would make sense as an SPDE with the invariant measure Eq. (1.4). This is a problem of the same nature as the nonperturbative construction of a renormalized quantum field theory and it has only been solved for simpler models such as the KPZ equation [99], where it is already extremely difficult [121]. We have argued that this point of view is, in fact, physically incorrect for fluctuating hydrodynamics and that at any finite Reynolds number, however large, the Eqs. (1.2) must be regarded as low-wave-number "effective field theories" with an explicit UV cutoff Λ, somewhat arbitrary, but chosen to satisfy the constraints $1/\ell_\nabla \ll \Lambda \ll 1/\lambda_{\rm micr}$. This point of view is not novel, of course, but is standard in the field of fluctuating hydrodynamics [16–19,25–27].

There have also been renormalization group analyses of stochastically forced Navier-Stokes fluids to study systematically the effect of changing Λ, notably by Forster *et al.* [16,17], who included the case with stochastic force representing thermal noise as their "Model A." This paper carried out a Wilson Fourier-slicing RG analysis of the thermal fluid at equilibrium obtaining scale-dependent viscosity ν_ℓ and temperature T_ℓ with effective dimensionless nonlinear coupling constant of the velocity fluctuations at scale ℓ given in space dimension d by

$$g_\ell := \left(\frac{k_B T_\ell}{\rho \nu_\ell^2 \ell^{d-2}}\right)^{1/2}. \tag{5.1}$$

These authors reached the conclusion that the thermal fluid is IR asymptotically free for $d > 2$, with coupling $g_\ell \to 0$ for $\ell \to \infty$, corresponding to a linear Langevin model for relaxation of long-wavelength fluctuations (Onsager regression hypothesis). Conversely, they concluded that the thermal fluid is UV strongly coupled, with the constant g_ℓ becoming large for $\ell \to \infty$, and they equated this strong-coupling regime with turbulence:

> "We will not attempt to treat the formidable and probably more interesting problem of the ultraviolet (short-distance, short-time) correlations described by (2.1), i.e., of fully developed turbulence\dots " [17]

Exactly the opposite situation was shown to hold for $d < 2$ by Refs. [16,17], with now thermal velocity fluctuations UV asymptotically free and IR strongly coupled. As discussed in Sec. III A, the shell model that we study numerically in this work is effectively a model in 0 space dimension and, according to the RG analysis of Forster *et al.*, it is UV asymptotically free, so that the shell variables u_n are described by independent linear Langevin models for very large n. Because 3D FNS is instead UV strongly coupled, it might be argued that thermal fluctuations in our shell model are qualitatively different at high wave numbers than those for 3D fluids and that our shell model is thus unsuitable to test the effects of thermal noise in the turbulent dissipation range.

In fact, it is not hard to see that thermal velocity fluctuations both in 3D fluids and in our stochastic shell model are weakly coupled at the Kolmogorov dissipation length and down to much smaller scales. Note that the coupling constant g_ℓ of Forster *et al.* in Eq. (5.1) coincides for $\ell = \eta$ with the thermal Reynolds number $\mathrm{Re}_\eta^{\rm th}$ which we defined in Eq. (2.4) and thus $g_\eta = \theta_\eta^{1/2}$ by Eq. (2.17). It follows that the coupling constant g_η at the Kolmogorov scale is tiny for realistic magnitudes of θ_η. The naïve belief expressed in Ref. [17] that turbulent flows must correspond to large coupling constant g_ℓ is not necessarily true.

It is true that this coupling will increase as ℓ is further decreased, both in turbulent flows and even in a thermal equilibrium fluid at rest. One can estimate the wave number $k_{\rm coup}$ where coupling becomes strong by setting $g_\ell \sim 1$ in Eq. (5.1) and solving for $k \sim 1/\ell$, yielding [122]

$$k_{\rm coup} = \left(\frac{k_B T}{\rho \nu^2}\right)^{\frac{1}{d-2}}. \tag{5.2}$$

Simple estimates then imply that $k_{\rm coup}$ in Eq. (5.2) is so large that it is strictly outside the regime of validity of a hydrodynamic description! To see this, we can substitute the standard kinetic theory estimate for kinematic viscosity $\nu \sim \lambda_{\rm micr} c_{\rm th}$, with $c_{\rm th}$ the thermal velocity and sound speed, into Eq. (5.2), which yields

$$k_{\rm coup} \sim \left(n\lambda_{\rm micr}^2\right)^{\frac{1}{d-2}} \sim \left(\frac{\lambda_{\rm micr}^2}{\ell_{\rm intp}^d}\right)^{\frac{1}{d-2}}, \tag{5.3}$$

where n is the particle number density of the fluid and $\ell_{\rm intp} := n^{-1/d}$ is the mean interparticle distance. In a liquid, $\lambda_{\rm micr} \sim \ell_{\rm intp} \sim R$, where R is the radius of the molecule, and we see that $k_{\rm coup} R \sim 1$. In a gas described by the Boltzmann kinetic equation, $k_{\rm coup}$ is even larger. The low-density limit for validity of the Boltzmann equation first identified by Bogolyubov [123] and Grad [124] is that in which $\lambda_{\rm mfp}/\ell_{\rm intp} \gg 1$ and $\ell_{\rm intp}/R \gg 1$ with $\lambda_{\rm mfp} \sim 1/nR^{d-1}$ held fixed. It is then easy to see that for such a Boltzmann gas $k_{\rm coup} R \sim (\ell_{\rm intp}/R)^{\frac{d}{d-2}} \gg 1$. These considerations suggest that the strong-coupling problem encountered in the limit $\Lambda \to \infty$ is of only academic mathematical interest and is not relevant to the physical description of molecular fluids in thermal equilibrium.

It is worth pointing out that the limit $\Lambda \to \infty$ reappears in a different guise when taking the infinite Reynolds-number limit, $\mathrm{Re} = UL/\nu \to \infty$ with mean dissipation $\varepsilon = U^3/L$ and fluid parameters ρ, T all held fixed. In that case, $\widehat{\Lambda} := L\Lambda > L/\eta \to \infty$ so that the UV cutoff diverges to infinity when the fluctuating hydrodynamic equations are nondimensionalized with the integral-scale quantities L and U. This limit will be the subject of our following work [125]. Here we just note

that, assuming the validity of the Landau-Lifschitz Eqs. (1.2) for arbitrarily large values of Re, we find in Ref. [125] that the limiting velocity fields are singular (weak) solutions of the *deterministic* Euler equation. Thus, both the molecular noise and the molecular viscosity vanish in this limit. It is not entirely clear, however, that the fluctuating hydrodynamic Eqs. (1.2) do remain valid for very large Re, because increasing intermittency could allow extreme turbulent singularities to reach down to the microscopic length scale $\lambda_{\rm micr}$. This possibility will be discussed more in Sec. V C below.

Finally, there has been much work on thermalization and equipartition spectra in various mathematical model fluid problems, especially truncated Euler [77,78,126–128], but also truncated Burgers [129–132], hyperviscous Navier-Stokes and Burgers [133–136], and shell models [137–140]. For a good overview of this large literature, see Ref. [141]. In these various deterministic models, equipartition energy spectra ($\sim k^{d-1}$ for dimension d) and Gaussian thermal statistics have been observed over certain ranges of wave number, rather similar to our observations. None of these works, however, have included stochastic terms to model the effects of thermal noise. There have been a few prior works on stochastic shell models, such as Refs. [98,142], but with different noise than ours and with very different goals. Our aim in this work has been to use our stochastic shell model as a surrogate for 3D fluctuating Navier-Stokes equation, to assess the effects of thermal noise in the turbulent dissipation range of molecular fluids and to understand the interactions between thermal noise and turbulent intermittency. As we have argued in depth, the shell model is suitable for this purpose. It is theoretically interesting that truncated 3D Euler can mimic many of the features of 3D FNS. Not only does the bath of thermalized hydrodynamic modes at high wave numbers create an "efffective viscosity" [77,78,126] but also, following ideas of Kraichnan [77,143], it should create an "effective noise" satisfying a fluctuation-dissipation relation. Nevertheless, the predictions of 3D truncated Euler differ in several ways from those of 3D FNS, in particular lacking a viscous dissipation range at intermediate scales. Most significantly, 3D truncated Euler has never been proposed as a realistic model of the dissipation range of a molecular fluid, whereas 3D FNS is expected to be an accurate mesoscopic model down to almost microscopic length scales.

B. Prospects for empirical verification

The most important question raised by our work is the existence of the predicted thermal equipartition range in the sub-Kolmogorov scales, which we argued supplants the traditional "far dissipation range" of deterministic Navier-Stokes. We thus find that deterministic Navier-Stokes Eq. (1.1) and fluctuating Navier-Stokes Eq. (1.2) make two radically different sets of predictions for the turbulent dissipation range, and it must now be determined which is correct. Current numerical codes for solving the incompressible fluctuating hydrodynamic equations [18,19] are adequate to investigate turbulent flows at Taylor-scale Reynolds numbers up to 100 or so and such simulations should provide additional confirmation of our predictions. In fact, since the original submission of this paper, a preprint [144] has appeared which reports on such a simulation, directly motivated by our work. Although those simulations reached only $\mathrm{Re}_\lambda = 143$, that suffices to test our prediction of an equipartition k^2 energy spectrum appearing at the Kolmogorov scale and Gaussian velocity statistics rather than strong intermittency in the far dissipation range. Both of these predictions were fully verified; see Ref. [144] for details. This numerical confirmation gives strong *a posteriori* validation to our methodology of using the stochastic shell model Eq. (3.8) as a surrogate for 3D FNS Eq. (1.2). Our predictions for effects of inertial-range intermittency cannot yet be corroborated, because 3D FNS cannot currently be solved numerically at the high Reynolds numbers required. Nevertheless, our work and that of Ref. [144] set the stage for a clash of two competing physical theories.

Ultimately, of course, the matter must be resolved by experiment. While the predictions of fluctuating hydrodynamics have been verified in many globally far-from-equilibrium flows [13] and there is little doubt at all that thermal noise effects must be present at sub-Kolmogorov scales, the detailed predictions of fluctuating hydrodynamics can be legitimately questioned in turbulent flows where they have not yet been measured. The possibility exists that the local equilibrium assumption underlying the fluctuation-dissipation relation Eq. (1.3) could break down, as already noted by Betchov [54] (see Sec. II.D). This is especially true since extreme turbulent intermittency could threaten the validity of any hydrodynamic description at all, at least locally.

More than 60 years after the early experimental attempt of Betchov [53], it remains a grand challenge to develop techniques which can measure the coarse-grained fluid velocities in Eq. (2.29) at the relevant length scales $\ell < \eta$. All traditional fluid-velocity measurement techniques have well-known limitations in achieving such fine spatial resolution. Betchov himself in his study [53] used a standard technique of hot-wire anemometry [145] to measure turbulent velocity fields. He made special efforts to minimize the high-frequency noise in the wires to increase their resolution and sensitivity. Furthermore, he investigated a novel multi-jet configuration in a "porcupine" box designed to create a nearly isotropic flow of high turbulence intensity, avoiding the weak electrical signal due to low turbulence intensity in grid-turbulence. Despite these efforts, the thermal noise spectrum of the fluid velocity predicted by Betchov remained about four orders of magnitude below the sensitivity of his measurements; see his Fig. 6, where the highest wave numbers of his measured spectrum are also clearly contaminated by electrical noise in the wire. These limitations of hot-wire technology remain to the present day. Here we may note that a recent study of grid turbulence in the Modane wind tunnel by hot-wires [42] has remarked concerning the measured energy spectra that "all of them appear to increase as functions of k beyond a wave number k_M" and that "the value of k_M depends on the spectra, but is found to be typically $k_M\eta \simeq 3$." This behavior, of course, naïvely accords with our predictions. The authors explain these observations however "as a contamination by the small-scale response of the hot wires" and we have no reason to doubt this conclusion, but it underlines the essential limitations of the hot-wire technology.

Another popular set of methods to determine fluid velocity vectors are those under the rubric of "particle-image

velocimetry" or PIV, which do so by measuring the displacements of small, neutrally bouyant solid beads that seed the flow [146]. It has been argued that such particles are advected by a fluctuating fluid velocity coarse-grained over scales comparable to their radius [19], although the bead obviously displaces and distorts the flow in its near vicinity. We may note that a new "Giant von Kármán" (GVK) experiment is currently underway at CEA in France which will attempt to measure turbulent velocities down to scales $\sim\eta/5$ using PIV with monodisperse polystyrene beads of diameter 5 μm (B. Dubrulle, private communication) [147]. It is not entirely clear that the velocity of even a single such particle will correspond to the velocity relevant for fluctuating hydrodynamics, which corresponds to the local coarse-graining Eq. (2.29) over individual molecules. The motion of such submerged beads is known to be sensitive to the local thermal fluctuations of the velocity, but the effects appear only in the long-time tails of the particle velocity auto-correlation [148]. Furthermore, while the instantaneous velocities of micronscale Brownian particles have been successfully measured in quiescent flows when confined by optical traps [149,150], it will be very difficult to measure the velocity of even one such freely advected particle, let alone many. The large number of particles that must seed the flow in PIV introduce "ghost particles" that must be disambiguated by sophisticated post-processing techniques that introduce additional numerical noise in the inferred velocities [151]. Another velocity measurement technique exploiting tracer particles is "laser doppler velocimetry" or LDV, which has achieved micronscale spatial resolution in turbulent boundary layers [152], but similar difficulties of interpretation and sensitivity appear. The sub-Kolmogorov scales of turbulent fluid flows remain a vast *terra incognita* of experimental science.

It may be more reasonable to hope first for indirect evidence of the effects of thermal noise. There are, in fact, many physical processes in turbulent flows which are recognized to involve sub-Kolmogorov scales in a fundamental way but which in a stationary, laminar fluid are known to be strongly influenced by thermal noise. These include high Schmidt/Prandtl-number scalar mixing [153], droplet and bubble formation [154,155], chemical reactions (combustion) [156,157], and locomotion of micro-organisms [158], among others. Current theory and numerical modeling of all these processes in turbulent flows omit thermal noise completely, e.g., in the case of high Schmidt/Prandtl-number scalar mixing [159–161], dynamics of droplets and bubbles [162–164], chemical combustion [165–167], and locomotion in turbulent flows [168,169]. The possibility exists in all of these cases of interesting interplay between turbulence and thermal effects, which might yield clear experimental signatures. These problems are all ripe also for numerical investigation by fluctuating hydrodynamics, which should spur development of novel schemes which are more efficient at the high Reynolds numbers required.

C. Validity of a hydrodynamic description

A key question underlying the current intense interest in extreme events and smallest scales in a turbulent flow [44–50] is whether such near-singular events may lead to a breakdown in the hydrodynamic approximation. In our shell model simulation with parameters appropriate to the ABL, the most singular event that we observed in 300 large-eddy turnover times penetrated down to a length scale 8.4 μm, which is still 124 times greater than the mean-free-path length of air. The 3D FNS model should remain valid for such a singular event in the atmosphere. However, we cannot rule out that even more extreme events will occur if much longer times are considered or if the Reynolds number is further increased. As discussed in Sec. II D, the Parisi-Frisch multifractal model predicts that the smallest length scale η_h for a zero Hölder singularity $h = 0$ will reach down to a length scale $\lambda_{\rm micr}/{\rm Ma}$ just marginally greater than $\lambda_{\rm micr}$ for ${\rm Ma} \ll 1$, and there is some weak evidence that the smallest Hölder exponent in incompressible fluid turbulence is $h_{\rm min} = 0$ [87]. However, if negative Hölder singularities arise, then scales of order $\lambda_{\rm micr}$ or even smaller could be excited. This possibility seems to us quite realistic and, if it should occur, the hydrodynamic description would break down in the vicinity of such an extreme singularity.

Nevertheless, we argue that Landau-Lifschitz fluctuating hydrodynamics can still be employed, if supplemented with some finer-scale description near the singular set. An important point, often not appreciated in discussions of the dynamical equations of turbulent flow, is that a hydrodynamic description can be valid even when the conditions of its applicability are not valid globally. A relevant example, discussed previously in Ref. [86], Sec. III(e), is the singularities speculated by Leray (Ref. [10], Sec. 3) to develop starting from smooth initial data for the incompressible Navier-Stokes dynamics above some critical Reynolds number ${\rm Re}_c$. It is known that the positions of such hypothetical singularities, if they exist, must be a set of space-time points $(\mathbf{x}_*, t_*)$ of Hausdorff dimension $\leqslant 1$ where the fluid velocity itself blows up as $|\mathbf{u}(x,t)| \geqslant C/r$ for $r \to 0$ as one approaches the singularity, with $r^2 = |\mathbf{x} - \mathbf{x}_*|^2 + \nu|t - t_*|$; see Ref. [170], Corollary 1. In fact, this conclusion can be deduced heuristically from the multifractal result Eq. (2.25) for the viscous cutoff length η_h, if one takes into account a constant prefactor by replacing ${\rm Re} \mapsto {\rm Re}/{\rm Re}_c$. In that case one can see that $\eta_h > 0$ for any finite value of Re, except that $\eta_h \to 0$ when ${\rm Re} > {\rm Re}_c$ and $h \to -1$; see Ref. [86], Sec. III(e).

We therefore conclude (in disagreement with Ref. [9], Sec. 8.3) that negative Hölder singularities and locally infinite fluid velocities are consistent with the incompressible fluid approximation, as long as those equations are interpreted in the integral or "weak" sense, i.e., as balances of momentum integrated over intervals of time and over control volumes in space. The local breakdown of the conditions of validity of the hydrodynamic approximation need not violate those equations, at least if the points of breakdown occur in a sufficiently low-dimensional subset of space-time. In that case, a hybrid description should be possible with the incompressible fluid equations coupled to a more microscopic model (kinetic theory, molecular dynamics) in the region of singularity. For these same reasons, we believe that the fluctuating hydrodynamic description invoked in this work can be valid, even if negative Hölder singularities develop in the infinite-Re limit or perhaps already for finite ${\rm Re} > {\rm Re}_c$. Indeed, the rigorous Onsager-Machlup large-deviations theory derived in Ref. [7]

for a stochastic lattice gas in the limit of (global) Kn $\ll 1$ and Ma $\ll 1$ is valid at any fixed value of Re even if Leray singularities appear in the solutions of incompressible Navier-Stokes equation. It is worth observing that the fluctuating hydrodynamic equations can be derived microscopically with nonuniform spatial grids [27] so that a global wave-number cutoff Λ need not be imposed and instead local cutoff lengths can be adapted to the particular solution.

We may note that the strong subsonic flow condition, Ma $\ll 1$, does set some upper limit on the Reynolds numbers that are achievable within an incompressible fluid approximation. In both nature and in the laboratory, $\mathrm{Re} = UL/\nu$ is generally made larger by increasing L and/or $U = (\varepsilon L)^{1/3}$, so that achieving very high Re at fixed ε requires Ma $\simeq 1$ or even $\gg 1$, as in astrophysical turbulence environments such as the molecular gas of the interstellar medium. In such compressible fluid turbulence strong shock discontinuities develop with $h = 0$ and a shock-width of order $\sim\lambda_{\mathrm{mfp}}$, so that the fluid approximation breaks down locally and a Boltzmann kinetic equation is required to describe the internal structure of the shock [171–173]. For compressible fluid turbulence, the thermal effects will be described by the fluctuating hydrodynamics of the compressible Navier-Stokes equation [13,14,24–26] or for large-Ma flows with strong shocks, by the nonlinear fluctuating Boltzmann equation [174]. It should be noted that even in the latter case, a hydrodynamic description is still valid at length scales $\ell \gg \lambda_{\mathrm{mfp}}$, because at scales much larger than the shock width the dynamics is accurately described by a (weak) Euler solution with an idealized discontinuity [175]. As we shall discuss in our following paper, the general description of turbulent inertial ranges by suitable (weak) solutions of the Euler equations [176–178] is unchanged by thermal noise effects in the dissipation range.

New physical theory and new mathematical analysis are however demanded by our results. Existing derivations of the nonlinear fluctuating hydrodynamic equations [25–27] are based upon the projection-operator methods of Zwanzig-Mori [179,180]. Although these methods are formally exact and have seen recent mathematical and computational development [181,182], they have not been fully justified from the point of view of rigorous statistical mechanics. In fact, important questions exist regarding the ultimate limits of validity of the fluctuating hydrodynamic equations, since those equations often work quite well for micro- and nanoscale fluid systems without a clear separation of scales. This suggests that the existing rigorous framework of hydrodynamic scaling limits [7,183] may be too restrictive. The resulting stochastic hydrodynamic equations present also some very challenging questions regarding their mathematical formulation. As the existing formal microscopic derivations [25–27] make clear, the fluctuating hydrodynamics equations are *not* stochastic PDE's because they contain an explicit UV cutoff Λ. Current mathematical theory (e.g., [22]) suffices to show that such cutoff models specify a well-posed dynamics for each finite value of Λ, but the fundamental issue remains to be addressed that physical predictions should be Λ-independent. The reflexive response might be to attempt to show that a well-defined SPDE exists in the limit $\Lambda \to \infty$, with a suitable choice of "bare" parameters, so that finite-Λ models can be regarded as "approximations" to this idealized continuum limit. Based on our arguments in Sec. II A, this point of view seems rather unphysical. It seems to us that a more natural goal is to establish some exact "renormalization group invariance" of the finite-Λ effective field-theories which expresses invariance of their predictions to changes of UV cutoff Λ and of other arbitrary features of the models, such as the numerical discretization.

D. Future directions

In this paper we have focused on the dissipation range of fully developed, homogeneous turbulence, but there should be influences of thermal noise also on other turbulent flows and processes. Several of these novel effects and new directions of research were suggested already by Betchov. For example, he argued that thermal noise could play an important role in triggering transition to turbulence (Ref. [54], Secs. IIE and IIG), a possibility currently being actively explored [184,185], and that thermal noise could generate unpredictability in fully developed turbulence (Ref. [54], Sec. IIH), anticipating modern ideas on spontaneous stochasticity [101,186]. In Ref. [55], Betchov suggested information-theoretic approaches as a possible means to distinguish Gaussian thermal fluctuations from turbulent fluctuations, in line with recent research [187,188]. Betchov recognized as well that thermal noise effects must occur not only in incompressible fluid turbulence but also in other turbulent systems, e.g., in magnetized plasmas, where he extended magnetohydrodynamic equations to include stochastic electric fields from thermal fluctuations (Ref. [54], Sec. III). Such molecular noise characteristics have recently been derived for homogeneous plasma kinetics even at the level of large deviations [189] and at the linear level in the collisional two-fluid regime of magnetized plasmas [190,191]. We expect that there will be signatures of thermal noise in astrophysical plasma turbulence at high magnetic Prandtl numbers, such as the partially ionized interstellar medium [192]. In fact, thermal noise must be expected to act upon any fluid modes which are strongly affected by molecular dissipation. Another example is the viscous sublayer eddies of wall-bounded turbulence, where additional fluctuating forces are predicted to appear in the vicinity of solid walls associated with dissipative, microscopic slip coefficients [14,193].

In consequence of these many important directions of research, this paper which focuses on the dissipation range is just the first in a series to study the influence of thermal noise on turbulent flows. In Ref. [125] we shall discuss its more subtle effects on the turbulent inertial-range in the limit $\mathrm{Re} \gg 1$, in particular the role of thermal noise in triggering Eulerian spontaneous stochasticity [101,186]. We plan to make also a parametric study of the Reynolds-number dependence of the dissipation-range intermittency discussed in this work, to explore possible limitations to the hydrodynamic description of small-scale fluid turbulence. In a work in preparation [194], we study high Schmidt-number turbulent mixing and we show that the exponentially decaying scalar spectrum theoretically predicted for the viscous-diffusive range [195] and verified numerically by deterministic Navier-Stokes simulations [196,197] is erased by thermal noise and replaced by a k^{-2} power-law spectrum associated to giant concentration

fluctuations [198,199]. Similar effects should be present also in the high magnetic Prandtl-number kinematic dynamo. Because of the universality of the fluctuation-dissipation relation, thermal noise is inextricably linked to dissipation and the two effects must always appear together.

ACKNOWLEDGMENTS

We acknowledge the Simons Foundation for support of this work through Targeted Grant in MPS-663054 at JHU and MPS-662985 at UIUC, "Revisiting the Turbulence Problem Using Statistical Mechanics." We also thank many colleagues for fruitful discussions of the science, especially Frank Alexander, John Bell, Freddy Bouchet, Léonie Canet, Bérengère Dubrulle, Alej Garcia, Rui Ni, and Tamer Zaki.

APPENDIX A: PROOF OF THE FLUCTUATION-DISSIPATION RELATIONS

We here derive the fluctuation-dissipation relation Eq. (1.3) for the incompressible Navier-Stokes equation and the corresponding result for the noisy Sabra model Eq. (3.8). The former result is well-known [13,14,16,17,25,26] but we give the proof here for completeness and, also, to stress the close parallels to the same result for the Sabra model. A good general reference is Ref. [200].

1. FDR for Navier-Stokes

We begin with the truncated fluctuating Navier-Stokes system Eq. (2.1) which can be written as a system of SDE's for the Fourier modes

$$\hat{\mathbf{u}}_{\mathbf{k}} = \int_{\Omega} d^3x\, e^{-i\mathbf{k}\cdot\mathbf{x}}\mathbf{u}(\mathbf{x}) \tag{A1}$$

of the velocity field satisfying $|\mathbf{k}| < \Lambda$. Because of the reality condition

$$\hat{\mathbf{u}}^*_{\mathbf{k}} = \hat{\mathbf{u}}_{-\mathbf{k}} \tag{A2}$$

not all of these modes are independent. We take the modes whose wave vector lies in the half-set

$$K^+ = \left\{ \begin{array}{ll} k_x > 0, & \text{or} \\ \mathbf{k} : k_y > 0 & \text{if } k_x = 0, \text{ or} \\ k_z \geqslant 0 & \text{if } k_x = k_y = 0 \end{array} \right\}, \tag{A3}$$

as the independent complex modes. The fluctuating Navier-Stokes equation can then be written as

$$\partial_t \hat{u}_{\mathbf{k},m} + ik_n\left(\delta_{mp} - \frac{k_m k_p}{k^2}\right)\sum_{\mathbf{p}+\mathbf{q}=\mathbf{k}} \hat{u}_{\mathbf{p},n}\hat{u}_{\mathbf{q},p} + \nu k^2 \hat{u}_{\mathbf{k},m} = \hat{q}_{\mathbf{k},m} \tag{A4}$$

for $\mathbf{k} \in K^+$ with $|\mathbf{k}| < \Lambda$, and where $\hat{\mathbf{q}}_{\mathbf{k}}$ is a suitable random force, further specified below, that represents the thermal noise. Here we note that the wave numbers $\mathbf{p}$, $\mathbf{q}$ which are summed over in the expression

$$B_{\mathbf{k},m}(\hat{\mathbf{u}}, \hat{\mathbf{u}}^*) = -ik_n\left(\delta_{mp} - \frac{k_m k_p}{k^2}\right)\sum_{\mathbf{p}+\mathbf{q}=\mathbf{k}} \hat{u}_{\mathbf{p},n}\hat{u}_{\mathbf{q},p}, \tag{A5}$$

may lie in the complementary set $K^- = -K^+$ and in the case that $\mathbf{p} \in K^-$, then $\hat{\mathbf{u}}_{\mathbf{p}}$ should be interpreted instead as $\hat{\mathbf{u}}^*_{-\mathbf{p}}$. There is a corresponding equation of motion for the complex-conjugate variables

$$\partial_t \hat{u}^*_{\mathbf{k},m} = B^*_{\mathbf{k},m}[\hat{\mathbf{u}}, \hat{\mathbf{u}}^*] - \nu k^2 \hat{u}^*_{\mathbf{k},m} + \hat{\mathbf{q}}^*_{\mathbf{k},m}, \tag{A6}$$

with $B^*_{\mathbf{k},m}[\hat{\mathbf{u}}, \hat{\mathbf{u}}^*] := B_{\mathbf{k},m}[\hat{\mathbf{u}}, \hat{\mathbf{u}}^*]^*$ when $\mathbf{k} \in K^+$ and $|\mathbf{k}| < \Lambda$. Finally, we note that the random force $\hat{\mathbf{q}}_{\mathbf{k}}(t)$ is Gaussian with mean zero and covariance

$$\langle \hat{\mathrm{q}}_{\mathbf{k},m}(t)\hat{\mathrm{q}}^*_{\mathbf{k}',n}(t')\rangle = \frac{2\nu k_B T}{\rho} V \delta_{\mathbf{k},\mathbf{k}'}\delta(t-t')\big(k^2\delta_{mn} - k_m k_n\big), \tag{A7}$$

with $\hat{\mathbf{q}}^*_{\mathbf{k}} = \hat{\mathbf{q}}_{-\mathbf{k}}$ and $\mathbf{k}\cdot\hat{\mathbf{q}}_{\mathbf{k}} = 0$. To see the equivalence with Eq. (1.3), we note $\boldsymbol{\nabla}\cdot\tilde{\boldsymbol{\tau}}$ in Eq. (1.2) can be written as

$$\boldsymbol{\nabla}\cdot\tilde{\boldsymbol{\tau}} = \tilde{\mathbf{q}} + \boldsymbol{\nabla}\tilde{\pi}, \tag{A8}$$

with the random scalar field $\tilde{\pi}$ chosen so that $\boldsymbol{\nabla}\cdot\tilde{\mathbf{q}} = 0$, and in that case $\tilde{\pi}$ can be absorbed into the pressure and $\tilde{\mathbf{q}}$ is Gaussian with covariance

$$\langle \tilde{\mathrm{q}}_m(\mathbf{x},t)\tilde{\mathrm{q}}_n(\mathbf{x}',t')\rangle = \frac{2\nu k_B T}{\rho}(-\triangle_x\delta_{m,n} + \boldsymbol{\nabla}_{x,m}\boldsymbol{\nabla}_{x,n}) \times \delta^3(\mathbf{x}-\mathbf{x}')\delta(t-t'). \tag{A9}$$

The Fourier coefficient $\hat{\mathbf{q}}_{\mathbf{k}}(t)$ of $\tilde{\mathbf{q}}(\mathbf{x},t)$ then satisfies Eq. (A7).

We now wish to show that the noise covariance Eq. (A7) is correctly chosen so that the Gibbs measure

$$P_G[\hat{\mathbf{u}}, \hat{\mathbf{u}}^*] = \frac{1}{Z}\exp\left[-\mathcal{E}/k_B T\right] \tag{A10}$$

for kinetic energy

$$\mathcal{E} = \int_{\Omega} d^3x\, \frac{\rho}{2}|\mathbf{u}(\mathbf{x})|^2 = \frac{\rho}{2V}\sum_{|\mathbf{k}|<\Lambda}|\hat{\mathbf{u}}_{\mathbf{k}}|^2 = \frac{\rho}{V}\sum_{\mathbf{k}\in K^+,|\mathbf{k}|<\Lambda}|\hat{\mathbf{u}}_{\mathbf{k}}|^2 \tag{A11}$$

is invariant under the stochastic dynamics Eq. (A4) with no large-scale forcing. The proof is based on the Fokker-Planck equation for the probability distribution $P[\hat{\mathbf{u}}, \hat{\mathbf{u}}^*]$ of the Fourier modes. We employ the standard device of treating $\hat{\mathbf{u}}_{\mathbf{k}}$ and its complex conjugate $\hat{\mathbf{u}}^*_{\mathbf{k}}$ as independent variables in complex differential calculus (Wirtinger derivatives). The Fokker-Planck equation equivalent to the coupled Langevin Eqs. (A4) is easily checked to be

$$\partial_t P = \sum_{\mathbf{k}\in K^+}\left[-\frac{\partial}{\partial\hat{\mathbf{u}}_{\mathbf{k}}}\cdot\Big(\mathbf{V}_{\mathbf{k}}[\hat{\mathbf{u}}, \hat{\mathbf{u}}^*]P\Big) - \frac{\partial}{\partial\hat{\mathbf{u}}^*_{\mathbf{k}}}\cdot\Big(\mathbf{V}^*_{\mathbf{k}}[\hat{\mathbf{u}}, \hat{\mathbf{u}}^*]P\Big) + \frac{2\nu k_B T}{\rho}V(k^2\mathbf{I} - \mathbf{k}\mathbf{k}) : \frac{\partial^2}{\partial\hat{\mathbf{u}}_{\mathbf{k}}\partial\hat{\mathbf{u}}^*_{\mathbf{k}}}P\right] := \mathcal{L}^*P, \tag{A12}$$

where

$$\mathbf{V}_{\mathbf{k}}[\hat{\mathbf{u}}, \hat{\mathbf{u}}^*] = \mathbf{B}_{\mathbf{k}}[\hat{\mathbf{u}}, \hat{\mathbf{u}}^*] - \nu k^2\hat{\mathbf{u}}_{\mathbf{k}} \tag{A13}$$

and $\mathbf{V}^*_{\mathbf{k}}[\hat{\mathbf{u}}, \hat{\mathbf{u}}^*] := \mathbf{V}_{\mathbf{k}}[\hat{\mathbf{u}}, \hat{\mathbf{u}}^*]^*$ are the components of the drift velocity in the phase-space.

The proof further uses two fundamental properties of the truncated Euler dynamics: the *Liouville theorem* on

conservation of phase-volume,

$$\sum_{\mathbf{k}\in K^+}\left(\frac{\partial}{\partial\hat{\mathbf{u}}_\mathbf{k}}\cdot\mathbf{B}_\mathbf{k}[\hat{\mathbf{u}},\hat{\mathbf{u}}^*]+\frac{\partial}{\partial\hat{\mathbf{u}}^*_\mathbf{k}}\cdot\mathbf{B}^*_\mathbf{k}[\hat{\mathbf{u}},\hat{\mathbf{u}}^*]\right)=0, \tag{A14}$$

and the *conservation of kinetic energy*,

$$\sum_{\mathbf{k}\in K^+}\left(\mathbf{B}_\mathbf{k}[\hat{\mathbf{u}},\hat{\mathbf{u}}^*]\cdot\frac{\partial\mathcal{E}}{\partial\hat{\mathbf{u}}_\mathbf{k}}+\mathbf{B}^*_\mathbf{k}[\hat{\mathbf{u}},\hat{\mathbf{u}}^*]\cdot\frac{\partial\mathcal{E}}{\partial\hat{\mathbf{u}}^*_\mathbf{k}}\right)=0. \tag{A15}$$

The Liouville theorem for truncated Euler has been well-known since the work of Lee [62] and, in fact, follows easily from definition Eq. (A5) by the observation that

$$\begin{aligned}\frac{\partial}{\partial\hat{\mathbf{u}}_\mathbf{k}}\cdot\mathbf{B}_\mathbf{k}[\hat{\mathbf{u}},\hat{\mathbf{u}}^*]&=-2i\mathbf{k}\cdot\hat{\mathbf{u}}(\{\mathbf{0}\}),\\ \frac{\partial}{\partial\hat{\mathbf{u}}^*_\mathbf{k}}\cdot\mathbf{B}^*_\mathbf{k}[\hat{\mathbf{u}},\hat{\mathbf{u}}^*]&=2i\mathbf{k}\cdot\hat{\mathbf{u}}(\mathbf{0}).\end{aligned} \tag{A16}$$

The conservation of kinetic energy Eq. (A15) follows from the detailed conservation for wave-vector triads first noted by Onsager [63]. The consequence of Eqs. (A14) and (A15) is that

$$\sum_{\mathbf{k}\in K^+}\left[-\frac{\partial}{\partial\hat{\mathbf{u}}_\mathbf{k}}\cdot(\mathbf{B}_\mathbf{k}[\hat{\mathbf{u}},\hat{\mathbf{u}}^*]P_G)-\frac{\partial}{\partial\hat{\mathbf{u}}^*_\mathbf{k}}\cdot(\mathbf{B}^*_\mathbf{k}[\hat{\mathbf{u}},\hat{\mathbf{u}}^*]P_G)\right]=0, \tag{A17}$$

so that $P_G[\hat{\mathbf{u}},\hat{\mathbf{u}}^*]$ is an invariant measure for the truncated Euler system.

The full stationarity condition $\partial_t P_G=0$ therefore simplifies to

$$\begin{aligned}&\sum_{\mathbf{k}\in K^+}\nu k^2\left[\frac{\partial}{\partial\hat{\mathbf{u}}_\mathbf{k}}\cdot(\hat{\mathbf{u}}_\mathbf{k}P_G)+\frac{\partial}{\partial\hat{\mathbf{u}}^*_\mathbf{k}}\cdot(\hat{\mathbf{u}}^*_\mathbf{k}P_G)\right]\\ &\quad=-\frac{2\nu k_BT}{\rho}V\sum_{\mathbf{k}\in K^+}(k^2\mathbf{I}-\mathbf{kk}):\frac{\partial^2}{\partial\hat{\mathbf{u}}_\mathbf{k}\partial\hat{\mathbf{u}}^*_\mathbf{k}}P_G.\end{aligned} \tag{A18}$$

It is worth observing that this is exactly the stationarity condition for the Gibbs measure under the linear Ornstein-Uhlenbeck dynamics

$$\partial_t\hat{\mathbf{u}}_\mathbf{k}=-\nu k^2\hat{\mathbf{u}}_\mathbf{k}+\hat{\mathbf{q}}_\mathbf{k},\quad \partial_t\hat{\mathbf{u}}^*_\mathbf{k}=-\nu k^2\hat{\mathbf{u}}^*_\mathbf{k}+\hat{\mathbf{q}}^*_\mathbf{k}, \tag{A19}$$

corresponding to the fluctuating Stokes equation. However, the elementary derivatives

$$\begin{aligned}\frac{\partial P_G}{\partial\hat{\mathbf{u}}_\mathbf{k}}&=-\frac{\rho\hat{\mathbf{u}}^*_\mathbf{k}}{Vk_BT}P_G,\quad \frac{\partial P_G}{\partial\hat{\mathbf{u}}^*_\mathbf{k}}=-\frac{\rho\hat{\mathbf{u}}_\mathbf{k}}{Vk_BT}P_G,\\ \frac{\partial^2P_G}{\partial\hat{\mathbf{u}}_\mathbf{k}\partial\hat{\mathbf{u}}^*_\mathbf{k}}&=-\left[\frac{\rho}{Vk_BT}(\mathbf{I}-\hat{\mathbf{k}}\hat{\mathbf{k}})-\frac{\rho^2\hat{\mathbf{u}}^*_\mathbf{k}\hat{\mathbf{u}}_\mathbf{k}}{(Vk_BT)^2}\right]P_G\end{aligned} \tag{A20}$$

imply that both sides of Eq. (A18) are indeed equal to the same quantity

$$\sum_{\mathbf{k}\in K^+}\nu k^2\left(4-\frac{2\rho|\hat{\mathbf{u}}_\mathbf{k}|^2}{Vk_BT}\right)P_G. \tag{A21}$$

Thus, P_G is an invariant measure, as claimed. Because of the nondegeneracy of the noise and the boundedness of the drift, this is in fact the unique invariant measure.

It is furthermore easy to show by the same arguments that the backward Fokker-Planck operator

$$\begin{aligned}\mathcal{L}F=\sum_{\mathbf{k}\in K^+}\Bigg[&\mathbf{V}_\mathbf{k}[\hat{\mathbf{u}},\hat{\mathbf{u}}^*]\cdot\frac{\partial F}{\partial\hat{\mathbf{u}}_\mathbf{k}}+\mathbf{V}^*_\mathbf{k}[\hat{\mathbf{u}},\hat{\mathbf{u}}^*]\cdot\frac{\partial F}{\partial\hat{\mathbf{u}}^*_\mathbf{k}}\\ &+\frac{2\nu k_BT}{\rho}V(k^2\mathbf{I}-\mathbf{kk}):\frac{\partial^2}{\partial\hat{\mathbf{u}}_\mathbf{k}\partial\hat{\mathbf{u}}^*_\mathbf{k}}F\Bigg]\end{aligned} \tag{A22}$$

for any real functions $F[\hat{\mathbf{u}},\hat{\mathbf{u}}^*]$, $G[\hat{\mathbf{u}},\hat{\mathbf{u}}^*]$ satisfies the following adjoint property with respect to the equilibrium Gibbs measure P_G :

$$\int G(\mathcal{L}F)\,P_G\,d\hat{\mathbf{u}}\,d\hat{\mathbf{u}}^*=\int(\tilde{\mathcal{L}}G)F\,P_G\,d\hat{\mathbf{u}}\,d\hat{\mathbf{u}}^*, \tag{A23}$$

where $d\hat{\mathbf{u}}\,d\hat{\mathbf{u}}^*=\prod_{\mathbf{k}\in K^+}d\hat{\mathbf{u}}_\mathbf{k}\,d\hat{\mathbf{u}}^*_\mathbf{k}$, and where

$$\begin{aligned}\tilde{\mathcal{L}}F=\sum_{\mathbf{k}\in K^+}\Bigg[&\tilde{\mathbf{V}}_\mathbf{k}[\hat{\mathbf{u}},\hat{\mathbf{u}}^*]\cdot\frac{\partial F}{\partial\hat{\mathbf{u}}_\mathbf{k}}+\tilde{\mathbf{V}}^*_\mathbf{k}[\hat{\mathbf{u}},\hat{\mathbf{u}}^*]\cdot\frac{\partial F}{\partial\hat{\mathbf{u}}^*_\mathbf{k}}\\ &+\frac{2\nu k_BT}{\rho}V(k^2\mathbf{I}-\mathbf{kk}):\frac{\partial^2}{\partial\hat{\mathbf{u}}_\mathbf{k}\partial\hat{\mathbf{u}}^*_\mathbf{k}}F\Bigg],\end{aligned} \tag{A24}$$

with

$$\tilde{\mathbf{V}}_\mathbf{k}[\hat{\mathbf{u}},\hat{\mathbf{u}}^*]=-\mathbf{B}_\mathbf{k}[\hat{\mathbf{u}},\hat{\mathbf{u}}^*]-\nu k^2\hat{\mathbf{u}}_\mathbf{k}, \tag{A25}$$

is the time-reversal $\tilde{\mathcal{L}}$ of the operator $\mathcal{L}$ under $\mathbf{u}\to-\mathbf{u}$. The adjoint property Eq. (A23) is equivalent to the *detailed balance condition*

$$P[\mathbf{u},t|\mathbf{u}_0,0]P_G[\mathbf{u}_0]=P[-\mathbf{u}_0,t|-\mathbf{u},0]P_G[-\mathbf{u}] \tag{A26}$$

for the transition probability densities of the nonlinear diffusion Eq. (A12). Thus, the fluctuating Navier-Stokes dynamics is time-reversible in thermal equilibrium.

Finally, we derive for the Gibbs distribution P_G the spectrum of the mean energy per unit mass

$$E=\frac{\langle\mathcal{E}\rangle}{\rho V}=\frac{1}{2V^2}\sum_{|\mathbf{k}|<\Lambda}\langle|\hat{\mathbf{u}}_\mathbf{k}|^2\rangle, \tag{A27}$$

which is conventionally considered for turbulence of an incompressible fluid. The variance of the Gaussian measure is given by

$$\langle|\hat{\mathbf{u}}_\mathbf{k}|^2\rangle=\frac{2Vk_BT}{\rho}, \tag{A28}$$

which expresses energy equipartition, taking into account the two "spin" degrees of freedom for the solenoidal Fourier modes. Then taking the infinite-volume limit

$$\frac{1}{V}\sum_\mathbf{k}\to\frac{1}{(2\pi)^3}\int d^3k\quad\text{for } V\to\infty \tag{A29}$$

and we see that $E=\int_0^\Lambda dk\,E(k)$ with

$$E(k)\sim\frac{k_BT}{\rho}\frac{4\pi k^2}{(2\pi)^3}. \tag{A30}$$

This is the k^2 equipartition spectrum first derived by Lee [62] and Hopf [64] for truncated Euler dynamics.

2. FDR for Sabra model

Corresponding results for the Sabra shell model are obtained by identical arguments. The Fokker-Planck equation for the probability distribution $P[u, u^*]$ of the vector $u = (u_0, u_1, \ldots, u_N)$ of shell-variables is easily derived from the coupled Langevin Eqs. (3.8) as

$$\partial_t P = \sum_{n=0}^{N} \Bigg[-\frac{\partial}{\partial u_n}(V_n[u,u^*]P) - \frac{\partial}{\partial u_n^*}(V_n^*[u,u^*]P) + \frac{4\nu k_B T}{\varrho} k_n^2 \frac{\partial^2}{\partial u_n \partial u_n^*} P \Bigg] := \mathcal{L}^* P, \tag{A31}$$

where (now writing $B_n[u]$ as $B_n[u, u^*]$)

$$V_n[u,u^*] = B_n[u,u^*] - \nu k_n^2 u_n \tag{A32}$$

and $V_n^*[u, u^*] = V_n[u, u^*]^*$. The inviscid Sabra model dynamics also satisfies a Liouville theorem

$$\sum_{n=0}^{N} \left(\frac{\partial}{\partial u_n} B_n[u,u^*] + \frac{\partial}{\partial u_n^*} B_n^*[u,u^*] \right) = 0, \tag{A33}$$

which is direct by inspection of Eq. (3.2), and conserves kinetic energy:

$$\sum_{n=0}^{N} \left(B_n[u,u^*] \frac{\partial \mathcal{E}}{\partial u_n} + B_n^*[u,u^*] \frac{\partial \mathcal{E}}{\partial u_n^*} \right) = 0. \tag{A34}$$

Consequently, the stationarity condition $\partial_t P_G = 0$ for the measure $P_G[u, u^*]$ defined in Eq. (3.10) simplifies to

$$\sum_{n=0}^{N} \nu k_n^2 \left[\frac{\partial}{\partial u_n}(u_n P_G) + \frac{\partial}{\partial u_n^*}(u_n^* P_G) \right] = -\left(\frac{4\nu k_B T}{\varrho} \right) \sum_{n=0}^{N} k_n^2 \frac{\partial^2}{\partial u_n \partial u_n^*} P_G. \tag{A35}$$

However, the elementary derivatives

$$\frac{\partial P_G}{\partial u_n} = -\frac{\varrho u_n^*}{2k_B T} P_G, \quad \frac{\partial P_G}{\partial u_n^*} = -\frac{\varrho u_n}{2k_B T} P_G,$$
$$\frac{\partial^2 P_G}{\partial u_n \partial u_n^*} = -\left[\frac{\varrho}{2k_B T} - \frac{\varrho^2 |u_n|^2}{(2k_B T)^2} \right] P_G \tag{A36}$$

imply that both sides of Eq. (A35) are equal to the same quantity

$$\sum_{n=0}^{N} \nu k_n^2 \left(2 - \frac{\varrho |u_n|^2}{k_B T} \right) P_G. \tag{A37}$$

Thus, the Gibbs distribution P_G is the unique invariant measure of the noisy Sabra model dynamics Eq. (3.8) when the external driving force is set to zero, $f_n = 0$. Furthermore, the analogue of the adjoint property Eq. (A23) for fluctuating Navier-Stokes holds also for the noisy shell model, so that the dynamics is time-reversible under the transformation $u_n \to -u_n$ in thermal equilibrium.

APPENDIX B: DERIVATION OF THE SLAVED TAYLOR-ITŌ SCHEME

For completeness we sketch here the derivation of the Taylor-Itō scheme from Ref. [103] for our noisy Sabra model Eq. (3.8), written as

$$du_n = a_n dt + b_n dW_n, \tag{B1}$$

with

$$a_n = B_n[u] - \nu k_n^2 u_n + f_n, \quad b_n = \left(\frac{2k_B T}{\varrho} \right)^{1/2} k_n. \tag{B2}$$

Explicit integration of the linear viscous term gives

$$u_n(t_{k+1}) = e^{-\nu k_n^2 \Delta t} \Bigg[u_n(t_k) + \int_{t_k}^{t_{k+1}} c_n[t, u(t)]\, dt + \int_{t_k}^{t_{k+1}} d_n(t)\, dW_n(t) \Bigg], \tag{B3}$$

with

$$c_n[t, u(t)] = e^{\nu k_n^2 (t - t_k)} \{ B_n[u(t)] + f_n(t) \}, \tag{B4}$$

and

$$d_n(t) = e^{\nu k_n^2 (t - t_k)} b_n. \tag{B5}$$

Taylor-expanding $d_n(t)$ as

$$d_n(t) = e^{\nu k_n^2 (t - t_k)} b_n = \left\{ 1 + \nu k_n^2 (t - t_k) + O[(t - t_k)^2] \right\} b_n \tag{B6}$$

and then substituting into the time-integral yields

$$\begin{aligned} &\int_{t_k}^{t_{k+1}} d_n(t)\, dW_n(t) \\ &= b_n \Delta W_n(t_k) + \nu k_n^2 b_n \int_{t_k}^{t_{k+1}} (t - t_k)\, dW(t) + O[(\Delta t)^{5/2}] \\ &= b_n \Delta W_n(t_k) + \nu k_n^2 b_n [\Delta t \Delta W_n(t_k) - \Delta Z_n(t_k)] \\ &\quad + O[(\Delta t)^{5/2}] \end{aligned} \tag{B7}$$

by an integration by parts.

To similarly expand $c_n[t, u(t)]$ we must use the Itō formula

$$\begin{aligned} c_n[t, u(t)] = c_n[t_k, u(t_k)] &+ \int_{t_k}^{t} ds\, (\partial_s + L) c_n[s, u(s)] \\ &+ \sum_m \int_{t_k}^{t} ds \Bigg\{ b_m dW_m(s) \frac{\partial c_n}{\partial u_m}[s, u(s)] \\ &+ b_m dW_m^*(s) \frac{\partial c_n}{\partial u_m^*}[s, u(s)] \Bigg\}, \end{aligned} \tag{B8}$$

where L is the forward Kolmogorov operator

$$L = \sum_m \left(a_m \frac{\partial}{\partial u_m} + a_m^* \frac{\partial}{\partial u_m^*} + 2b_m^2 \frac{\partial^2}{\partial u_m \partial u_m^*} \right). \tag{B9}$$

This implies that

$$\int_{t_k}^{t_{k+1}} dt\; c_n[t,u(t)]\,dt = c_n[t_k,u(t_k)]\Delta t + \int_{t_k}^{t_{k+1}} dt \int_{t_k}^{t} ds\; (\partial_s + L)c_n[s,u(s)] + \sum_m \int_{t_k}^{t_{k+1}} dt \int_{t_k}^{t} ds\; b_m \left\{ dW_m(s)\frac{\partial c_n}{\partial u_m}[s,u(s)] + dW_m^*(s)\frac{\partial c_n}{\partial u_m^*}[s,u(s)] \right\}. \tag{B10}$$

Substitution of the Itō formulas for $(\partial_s + L)c_n[s,u(s)]$ and $\frac{\partial c_n}{\partial u_m}[s,u(s)]$ then gives the Itō-Taylor series approximation to the desired order

$$\int_{t_k}^{t_{k+1}} dt\; c_n[t,u(t)]\,dt = c_n[t_k,u(t_k)]\Delta t + \int_{t_k}^{t_{k+1}} dt \int_{t_k}^{t} ds\; (\partial_t + L)c_n[t_k,u(t_k)] + \sum_m \int_{t_k}^{t_{k+1}} dt \int_{t_k}^{t} ds\; b_m \left\{ dW_m(s)\frac{\partial c_n}{\partial u_m}[t_k,u(t_k)] + dW_m^*(s)\frac{\partial c_n}{\partial u_m^*}[t_k,u(t_k)] \right\} + R, \tag{B11}$$

where R is a stochastic remainder term. Straightforward calculations using Eq. (B4) then give

$$\begin{aligned}\int_{t_k}^{t_{k+1}} dt\; c_n[t,u(t)] &= \Delta t\{B_n[t_k,u(t_k)] + f_n(t_k)\} + \frac{1}{2}(\Delta t)^2\big(\nu k_n^2\{B_n[t_k,u(t_k)] + f_n(t_k)\} + \dot{f}_n(t_k)\big) \\ &\quad + \frac{1}{2}(\Delta t)^2 \sum_m \left\{ a_m \frac{\partial B_n}{\partial u_m}[t_k,u(t_k)] + a_m^* \frac{\partial B_n}{\partial u_m^*}[t_k,u(t_k)] + 2b_m^2 \frac{\partial^2 B_n}{\partial u_m \partial u_m^*}[t_k,u(t_k)] \right\} \\ &\quad + \sum_m b_m \left\{ \Delta Z_m(t_k)\frac{\partial B_n}{\partial u_m}[t_k,u(t_k)] + \Delta Z_m^*(t_k)\frac{\partial B_n}{\partial u_m^*}[t_k,u(t_k)] \right\} + R.\end{aligned} \tag{B12}$$

Putting it all together gives the integration scheme

$$\begin{aligned}u_n(t_{k+1}) &= e^{-\nu k_n^2 \Delta t}\Bigg(u_n(t_k) + \Delta t\{B_n[t_k,u(t_k)] + f_n(t_k)\} + \frac{1}{2}(\Delta t)^2\big(\nu k_n^2\{B_n[t_k,u(t_k)] + f_n(t_k)\} + \dot{f}_n(t_k)\big) \\ &\quad + \frac{1}{2}(\Delta t)^2 \sum_m \left\{ a_m \frac{\partial B_n}{\partial u_m}[t_k,u(t_k)] + a_m^* \frac{\partial B_n}{\partial u_m^*}[t_k,u(t_k)] + 2b_m^2 \frac{\partial^2 B_n}{\partial u_m \partial u_m^*}[t_k,u(t_k)] \right\} \\ &\quad + \sum_m b_m \left\{ \Delta Z_m(t_k)\frac{\partial B_n}{\partial u_m}[t_k,u(t_k)] + \Delta Z_m^*(t_k)\frac{\partial B_n}{\partial u_m^*}[t_k,u(t_k)] \right\} + b_n\big[(1+\nu k_n^2\Delta t)\Delta W_n(t_k) - \Delta Z_n(t_k)\big] \Bigg).\end{aligned} \tag{B13}$$

This result may be compared with Eq. (6.1) of Ref. [103].

For the Sabra shell model, the only nonvanishing first-derivatives are

$$\begin{aligned}\frac{\partial B_n}{\partial u_{n-2}} &= \frac{1}{2}ik_{n-1}u_{n-1}, & \frac{\partial B_n}{\partial u_{n+2}} &= ik_{n+1}u_{n+1}^* \\ \frac{\partial B_n}{\partial u_{n-1}} &= \frac{1}{2}ik_{n-1}u_{n-2}, & \frac{\partial B_n}{\partial u_{n+1}} &= -\frac{1}{2}ik_n u_{n-1}^* \\ \frac{\partial B_n}{\partial u_{n-1}^*} &= -\frac{1}{2}ik_n u_{n+1}, & \frac{\partial B_n}{\partial u_{n+1}^*} &= ik_{n+1}u_{n+2},\end{aligned} \tag{B14}$$

while for all m

$$\frac{\partial^2 B_n}{\partial u_m \partial u_m^*} = 0. \tag{B15}$$

Substituting these results into Eq. (B13) yields our numerical scheme Eq. (3.18) for the noisy Sabra model.

APPENDIX C: CONVERGENCE OF STEADY-STATE AVERAGES

Convergence of steady-state averages for our numerical study required a sufficiently large averaging time T and proper resolution of the dynamics required a sufficiently large truncation wave number N and sufficiently small time step Δt. Here we describe the tests we have made that our choices of those parameters were sufficient.

In Sec. III B 3 we already addressed at length the convergence of transition probabilities with respect to the high-wave-number shell truncation N. Such convergence of transition probabilities implies convergence of the averages with respect to truncation wave number. The time step was chosen as $\Delta t = 10^{-5}$ to be smaller than the viscous time $t_{\rm visc} = 1/\nu k_N^2$ for the highest shell number N. Setting the external forcing to zero, $f_n = 0$ for all shells n, guarantees the Gaussian Gibbs distribution Eq. (3.10) and we checked that the time step $\Delta t = 10^{-5}$ sufficed to reproduce that distribution to excellent accuracy for all shells, whereas reducing the step size to $\Delta t = 1 \times 10^{-4} \sim 3 \times 10^{-4}$ introduced errors for n near N. In the forced simulation with f_n chosen as in Eq. (4.2), it was likewise found that the same choice $\Delta t = 10^{-5}$ sufficed to produce Gaussian thermal equilibrium very accurately at the highest two shells (see Fig. 6) and further produced accurately the known stretched-exponential decay in the deterministic model run (see insets in Fig. 9). These

consistency checks confirmed that our time step $\Delta t = 10^{-5}$ was sufficiently small.

The total averaging time T was taken to be 300 large eddy turnover times, based on convergence tests of the statistical averages presented in Sec. IV. Dividing the total time into ten subintervals of times $T/10$ and calculating averages separately over each led to negligible changes, which suggested that we had acceptable convergence for $-0.9 < p < 6$. This was confirmed by the good agreement of our scaling exponents with the very accurate values obtained in Ref. [56], as shown in Fig. 10. Our work was not focused on high-precision of inertial-range scaling exponents, so that this was acceptable accuracy for our purposes. Crucially, the profound differences that we observed in the dissipation range between the statistics of the deterministic Sabra model Eq. (3.1) and of the noisy Sabra model Eq. (3.8) lie very far outside all error bars on the numerical calculations.

[1] C.-L. M. H. Navier, Mémoire sur les lois du mouvement des fluides, Mem. Acad. Roy. Sci. **6**, 389 (1823).

[2] O. Reynolds, On the dynamical theory of turbulent incompressible viscous fluids and the determination of the criterion, Proc. R. Soc. London Ser. I **56**, 40 (1894).

[3] A. N. Kolmogorov, The local structure of turbulence in incompressible viscous fluid for very large reynolds number, Akad. Nauk SSSR Dokl. **30**, 301 (1941).

[4] A. N. Kolmogorov, Dissipation of energy in locally isotropic turbulence, Akad. Nauk SSSR Dokl. **32**, 16 (1941).

[5] C. Bardos, F. Golse, and D. Levermore, Fluid dynamic limits of kinetic equations. I. Formal derivations, J. Stat. Phys. **63**, 323 (1991).

[6] C. Bardos, F. Golse, and C. D. Levermore, Fluid dynamic limits of kinetic equations. II. Convergence proofs for the Boltzmann equation, Commun. Pure Appl. Math. **46**, 667 (1993).

[7] J. Quastel and H.-T. Yau, Lattice gases, large deviations, and the incompressible Navier-Stokes equations, Ann. Math. **148** 51 (1998).

[8] S. Corrsin, Outline of some topics in homogeneous turbulent flow, J. Geophys. Res. **64**, 2134 (1959).

[9] U. Frisch, *Turbulence: The Legacy of A. N. Kolmogorov* (Cambridge University Press, Cambridge, UK, 1995)

[10] J. Leray, Sur le mouvement d'un liquide visqueux emplissant l'espace, Acta Math. **63**, 193 (1934).

[11] J. Leray and R. Terrell, Translation of "On the motion of a viscous liquid filling space," arXiv:1604.02484.

[12] C. L. Fefferman, Existence and smoothness of the Navier-Stokes equation, Millen. Prize Prob. **57**, 67 (2000).

[13] J. O. de Zarate and J. Sengers, *Hydrodynamic Fluctuations in Fluids and Fluid Mixtures* (Elsevier Science, Amsterdam, 2006).

[14] R. Schmitz, Fluctuations in nonequilibrium fluids, Phys. Rep. **171**, 1 (1988).

[15] L. D. Landau and E. M. Lifshitz, *Fluid Mechanics*, Course of Theoretical Physics (Addision-Wesley, Reading, MA, 1959), Vol. 6.

[16] D. Forster, D. R. Nelson, and M. J. Stephen, Long-Time Tails and the Large-Eddy Behavior of a Randomly Stirred Fluid, Phys. Rev. Lett. **36**, 867 (1976).

[17] D. Forster, D. R. Nelson, and M. J. Stephen, Large-distance and long-time properties of a randomly stirred fluid, Phys. Rev. A **16**, 732 (1977).

[18] F. B. Usabiaga, J. B. Bell, R. Delgado-Buscalioni, A. Donev, T. G. Fai, B. E. Griffith, and C. S. Peskin, Staggered schemes for fluctuating hydrodynamics, Multiscale Model. Simul. **10**, 1369 (2012).

[19] A. Donev, A. Nonaka, Y. Sun, T. Fai, A. Garcia, and J. Bell, Low mach number fluctuating hydrodynamics of diffusively mixing fluids, Commun. Appl. Math. Comput. Sci. **9**, 47 (2014).

[20] A. Nonaka, Y. Sun, J. Bell, and A. Donev, Low mach number fluctuating hydrodynamics of binary liquid mixtures, Commun. Appl. Math. Comput. Sci. **10**, 163 (2015).

[21] To prevent confusion, we note that the fluctuating hydrodynamics equations are essentially different, both physically and mathematically, from the Navier-Stokes equation with a spatially smooth white-in-time force added to represent large-scale stirring [201–203]. When the forcing spectrum decays rapidly at high wave numbers, then the random stirring in the latter case inputs energy which cascades inertially to small scales. Mathematically, one can then safely take any UV cutoff Λ to infinity with fixed viscosity ν and obtain a well-defined limit defined by a stochastic partial differential equation (SPDE) [22,204]. On the contrary, the fluctuating hydrodynamic equations have stochastic forcing prescribed by the fluctuation-dissipation relation, so that the statistical steady state is thermal equilibrium with time-reversible dynamics; see Appendix A. Because the forcing spectrum is now *growing* with wave number, it is not at all obvious how to define a limiting SPDE as $\Lambda \to \infty$ [22]. In fact, the bare viscosity is now renormalized by the thermal fluctuations and becomes a scale-dependent quantity ν_Λ [16,17]. These important differences are discussed at greater length in the text.

[22] G. Da Prato and M. Röckner (Eds.), *SPDE in Hydrodynamics: Recent Progress and Prospects: Lectures Given at the C.I.M.E. Summer School Held in Cetraro, Italy, August 29–September 3, 2005*, Lecture Notes in Mathematics No. 1942 (Springer, Berlin, 2008).

[23] R. Graham, Onset of cooperative behavior in nonequilibrium steady states, in *Order and Fluctuations in Equilibrium and Nonequilibrium Statistical Mechanics: Proceedings of the XVIIth International Solvay Conference on Physics* (Wiley, New York, 1981), pp. 235–288.

[24] G. L. Eyink, Dissipation and large thermodynamic fluctuations, J. Stat. Phys. **61**, 533 (1990).

[25] D. N. Zubarev and V. G. Morozov, Statistical mechanics of nonlinear hydrodynamic fluctuations, Physica A **120**, 411 (1983).

[26] V. G. Morozov, On the Langevin formalism for nonlinear and nonequilibrium hydrodynamic fluctuations, Physica A **126**, 443 (1984).

[27] P. Español, J. G. Anero, and I. Zúñiga, Microscopic derivation of discrete hydrodynamics, J. Chem. Phys. **131**, 244117 (2009).

[28] I. Hosokawa, Ensemble mechanics for the random-forced Navier-Stokes flow, J. Stat. Phys. **15**, 87 (1976).

[29] D. Ruelle, Microscopic fluctuations and turbulence, Phys. Lett. A **72**, 81 (1979).

[30] M. Macháček, The role of thermal noise in stationary hydrodynamical turbulence, Phys. Lett. A **128**, 76 (1988).

[31] A. N. Kolmogorov, A refinement of previous hypotheses concerning the local structure of turbulence in a viscous incompressible fluid at high Reynolds number, J. Fluid Mech. **13**, 82 (1962).

[32] G. Paladin and A. Vulpiani, Degrees of freedom of turbulence, Phys. Rev. A **35**, 1971 (1987).

[33] W. Heisenberg, Zur statistischen Theorie der Turbulenz, Z. Phys. **124**, 628 (1948).

[34] S. Chandrasekhar, Theory of turbulence, Phys. Rev. **102**, 941 (1956).

[35] R. H. Kraichnan, The structure of isotropic turbulence at very high Reynolds numbers, J. Fluid Mech. **5**, 497 (1959).

[36] U. Frisch and R. Morf, Intermittency in nonlinear dynamics and singularities at complex times, Phys. Rev. A **23**, 2673 (1981).

[37] C. Foias, O. Manley, and L. Sirovich, Empirical and Stokes eigenfunctions and the far-dissipative turbulent spectrum, Phys. Fluids **2**, 464 (1990).

[38] L. Sirovich, L. Smith, and V. Yakhot, Energy Spectrum of Homogeneous and Isotropic Turbulence in Far Dissipation Range, Phys. Rev. Lett. **72**, 344 (1994).

[39] R. H. Kraichnan, Intermittency in the very small scales of turbulence, Phys. Fluids **10**, 2080 (1967).

[40] U. Frisch and M. Vergassola, A prediction of the multifractal model: The intermediate dissipation range, Europhys. Lett. **14**, 439 (1991).

[41] S. Khurshid, D. A. Donzis, and K. R. Sreenivasan, Energy spectrum in the dissipation range, Phys. Rev. Fluids **3**, 082601(R) (2018).

[42] A. Gorbunova, G. Balarac, M. Bourgoin, L. Canet, N. Mordant, and V. Rossetto, Analysis of the dissipative range of the energy spectrum in grid turbulence and in direct numerical simulations, Phys. Rev. Fluids **5**, 044604 (2020).

[43] D. Buaria and K. R. Sreenivasan, Dissipation range of the energy spectrum in high Reynolds number turbulence, Phys. Rev. Fluids **5**, 092601(R) (2020).

[44] P. K. Yeung, X. M. Zhai, and K. R. Sreenivasan, Extreme events in computational turbulence, Proc. Natl. Acad. Sci. USA **112**, 12633 (2015).

[45] P. K. Yeung and K. Ravikumar, Advancing understanding of turbulence through extreme-scale computation: Intermittency and simulations at large problem sizes, Phys. Rev. Fluids **5**, 110517 (2020).

[46] M. Farazmand and T. P. Sapsis, A variational approach to probing extreme events in turbulent dynamical systems, Sci. Adv. **3**, e1701533 (2017).

[47] D. Buaria, A. Pumir, E. Bodenschatz, and P.-K. Yeung, Extreme velocity gradients in turbulent flows, New J. Phys. **21**, 043004 (2019).

[48] D. Buaria, A. Pumir, and E. Bodenschatz, Self-attenuation of extreme events in Navier–Stokes turbulence, Nat. Commun. **11**, 5852 (2020).

[49] D. Buaria, E. Bodenschatz, and A. Pumir, Vortex stretching and enstrophy production in high Reynolds number turbulence, Phys. Rev. Fluids **5**, 104602 (2020).

[50] F. Nguyen, J.-P. Laval, and B. Dubrulle, Characterizing most irregular small-scale structures in turbulence using local Hölder exponents, Phys. Rev. E **102**, 063105 (2020).

[51] P. Debue, D. Kuzzay, E.-W. Saw, F. Daviaud, B. Dubrulle, L. Canet, V. Rossetto, and N. Wschebor, Experimental test of the crossover between the inertial and the dissipative range in a turbulent swirling flow, Phys. Rev. Fluids **3**, 024602 (2018).

[52] P. Debue, V. Valori, C. Cuvier, F. Daviaud, J.-M. Foucaut, J.-P. Laval, C. Wiertel, V. Padilla, and B. Dubrulle, Three-dimensional analysis of precursors to nonviscous dissipation in an experimental turbulent flow, J. Fluid Mech. **914**, A9 (2021).

[53] R. Betchov, On the fine structure of turbulent flows, J. Fluid Mech. **3**, 205 (1957).

[54] R. Betchov, Thermal agitation and turbulence, in *Rarefied Gas Dynamics*, edited by L. Talbot (Academic Press, New York, 1961), pp. 307–321, in *Proceedings of the 2nd International Symposium on Rarefied Gas Dynamics, held at the University of California, Berkeley, CA, 1960*.

[55] R. Betchov, Measure of the intricacy of turbulence, Phys. Fluids **7**, 1160 (1964).

[56] V. S. L'vov, E. Podivilov, A. Pomyalov, I. Procaccia, and D. Vandembroucq, Improved shell model of turbulence, Phys. Rev. E **58**, 1811 (1998).

[57] V. S. L'vov, E. Podivilov, and I. Procaccia, Hamiltonian structure of the Sabra shell model of turbulence: Exact calculation of an anomalous scaling exponent, Europhys. Lett. **46**, 609 (1999).

[58] D. Bandak, G. Eyink, A. Mailybaev, and N. Goldenfeld, Thermal noise competes with turbulent fluctuations at millimeter scales, arXiv:2107.03184.

[59] F. Flandoli, An introduction to 3D stochastic fluid dynamics, in *Proceedings of the SPDE in Hydrodynamics: Recent Progress and Prospects: Lectures given at the C.I.M.E. Summer School held in Cetraro, Italy, August 29–September 3, 2005*, Lecture Notes in Mathematics, edited by G. Da Prato and M. Röckner (Springer, Berlin, 2008), Vol. 1942.

[60] This problem is solved in principle by the Green-Kubo formulas for the transport coefficients obtained in the microscopic derivations of the fluctuating hydrodynamic equations, such as Eq. (2.56) of Ref. [25] or Eq. (48) of Ref. [27]. However, evaluation of those formulas itself requires microscopic molecular dynamics simulations.

[61] J. M. Burgers, On the application of statistical mechanics to the theory of turbulent fluid motion. VII. K. Ned. Akad. Wet. **36**, 620 (1933).

[62] T. D. Lee, On some statistical properties of hydrodynamical and magneto-hydrodynamical fields, Q. Appl. Math. **10**, 69 (1952).

[63] L. Onsager, Statistical hydrodynamics, Nuovo Cimento Suppl. **6**, 279 (1949).

[64] E. Hopf, Statistical hydromechanics and functional calculus, J. Ration. Mech. Analysis **1**, 87 (1952).

[65] R. H. Kraichnan, Helical turbulence and absolute equilibrium, J. Fluid Mech. **59**, 745 (1973).

[66] There is no assumption made here that the r.m.s. velocity $u_{\rm rms} \sim U$ and their ratio could be Re-dependent.

[67] J. R. Garratt, *The Atmospheric Boundary Layer*, Cambridge Atmospheric and Space Science Series (Cambridge University Press, Cambridge, UK, 1994).

[68] T. Von Kármán, Progress in the statistical theory of turbulence, Proc. Natl. Acad. Sci. USA **34**, 530 (1948).

[69] D. A. Donzis and K. R. Sreenivasan, The bottleneck effect and the Kolmogorov constant in isotropic turbulence, J. Fluid Mech. **657**, 171 (2010).

[70] J. Von Neumann, Recent theories of turbulence (unpublished report to the Office of Naval Research, 1949), in *Collected Works of John Von Neumann, Vol. 6: Theory of Games, Astrophysics, Hydrodynamics and Meteorology*, edited by A.H. Taub (Pergamon Press, Oxford, UK, 1963), pp. 437.

[71] See Supplemental Material at http://link.aps.org/supplemental/10.1103/PhysRevE.105.065113 for evaluation of the thermal equilibration scale from the theory of the intermediate-dissipation range spectrum and extreme burst event given to full doubleprecision accuracy.

[72] Z.-S. She and E. Leveque, Universal Scaling Laws in Fully Developed Turbulence, Phys. Rev. Lett. **72**, 336 (1994).

[73] V. Yakhot, Mean-field approximation and a small parameter in turbulence theory, Phys. Rev. E **63**, 026307 (2001).

[74] M. Tarpin, L. Canet, and N. Wschebor, Breaking of scale invariance in the time dependence of correlation functions in isotropic and homogeneous turbulence, Phys. Fluids **30**, 055102 (2018).

[75] M. H. Jensen, Multiscaling and Structure Functions in Turbulence: An Alternative Approach, Phys. Rev. Lett. **83**, 76 (1999).

[76] V. Shukla, P. D. Mininni, G. Krstulovic, P. C. di Leoni, and M. E. Brachet, Quantitative estimation of effective viscosity in quantum turbulence, Phys. Rev. A **99**, 043605 (2019).

[77] R. H. Kraichnan, Remarks on turbulence theory, Adv. Math. **16**, 305 (1975).

[78] C. Cichowlas, P. Bonaïti, F. Debbasch, and M. Brachet, Effective Dissipation and Turbulence in Spectrally Truncated Euler Flows, Phys. Rev. Lett. **95**, 264502 (2005).

[79] A. J. Majda and A. L. Bertozzi, *Vorticity and Incompressible Flow*, Cambridge Texts in Applied Mathematics (Cambridge University Press, Cambridge, UK, 2002).

[80] K. Kadau, C. Rosenblatt, J. L. Barber, T. C. Germann, Z. Huang, P. Carlès, and B. J. Alder, The importance of fluctuations in fluid mixing, Proc. Natl. Acad. Sci. USA **104**, 7741 (2007).

[81] G. I. Taylor, Statistical theory of turbulence, Proc. R. Soc. London A **151**, 421 (1935).

[82] If relation $x^2e^x = 1/\theta_\eta$ is solved for $x = k\eta, \theta_\eta$, then satisfying it for $x' = 2x, \theta'_\eta$ requires $1/\lambda = \theta_\eta/\theta'_\eta = 4e^x$.

[83] U. Frisch and G. Parisi, On the singularity structure of fully developed turbulence, in *Turbulence and Predictability in Geophysical Fluid Dynamics and Climate Dynamics* (Elsevier, Amsterdam, 1985), pp. 84–88.

[84] J. C. Bowman, C. R. Doering, B. Eckhardt, J. Davoudi, M. Roberts, and J. Schumacher, Links between dissipation, intermittency, and helicity in the GOY model revisited, Physica D **218**, 1 (2006).

[85] L. Canet, V. Rossetto, N. Wschebor, and G. Balarac, Spatiotemporal velocity-velocity correlation function in fully developed turbulence, Phys. Rev. E **95**, 023107 (2017).

[86] G. L. Eyink, Turbulence Theory, Course Notes, Johns Hopkins University, https://www.ams.jhu.edu/~eyink/Turbulence/notes.html.

[87] K. P. Iyer, K. R. Sreenivasan, and P. K. Yeung, Scaling exponents saturate in three-dimensional isotropic turbulence, Phys. Rev. Fluids **5**, 054605 (2020).

[88] The meaning of statistics here is in the sense of "local thermodynamic equilibrium." Thus, the region of diameter $\eta_h(\mathbf{x}, t)$ centered at $\mathbf{x}$ at time t may be partitioned into $(\eta_h/\ell)^3$ subregions of diameter ℓ and the distribution of values $\bar{\mathbf{u}}_\ell$ over the subregions should be the given Gaussian distribution (2.30) for $\ell_{intp} \ll \ell \ll \eta_h$.

[89] M. Gross, M. E. Cates, F. Varnik, and R. Adhikari, Langevin theory of fluctuations in the discrete Boltzmann equation, J. Stat. Mech. (2011) P03030.

[90] X. Xue, L. Biferale, M. Sbragaglia, and F. Toschi, A lattice Boltzmann study on Brownian diffusion and friction of a particle in a confined multicomponent fluid, J. Comput. Sci., **47** 101113 (2020).

[91] E. B. Gledzer, System of hydrodynamic type admitting two quadratic integrals of motion, Sov. Phys. Dokl. **18**, 216 (1973).

[92] K. Ohkitani and M. Yamada, Temporal intermittency in the energy cascade process and local Lyapunov analysis in fully developed model turbulence, Prog. Theor. Phys. **81**, 329 (1989).

[93] L. Biferale, Shell models of energy cascade in turbulence, Annu. Rev. Fluid Mech. **35**, 441 (2003).

[94] D. Vincenzi and J. D. Gibbon, How close are shell models to the 3D Navier–Stokes equations? Nonlinearity **34**, 5821 (2021).

[95] P. Constantin, B. Levant, and E. S. Titi, Analytic study of shell models of turbulence, Physica D **219**, 120 (2006).

[96] P. Constantin, B. Levant, and E. S. Titi, Regularity of inviscid shell models of turbulence, Phys. Rev. E **75**, 016304 (2007).

[97] P. D. Ditlevsen, *Turbulence and Shell Models* (Cambridge University Press, Cambridge, UK, 2010).

[98] H. Bessaih and B. Ferrario, Invariant Gibbs measures of the energy for shell models of turbulence: The inviscid and viscous cases, Nonlinearity **25**, 1075 (2012).

[99] M. Kardar, G. Parisi, and Y.-C. Zhang, Dynamic Scaling of Growing Interfaces, Phys. Rev. Lett. **56**, 889 (1986).

[100] N. Schörghofer, L. Kadanoff, and D. Lohse, How the viscous subrange determines inertial range properties in turbulence shell models, Physica D **88**, 40 (1995).

[101] A. A. Mailybaev, Spontaneous stochasticity of velocity in turbulence models, Multiscale Model. Simul. **14**, 96 (2016).

[102] V. S. L'vov, I. Procaccia, and D. Vandembroucq, Universal Scaling Exponents in Shell Models of Turbulence: Viscous Effects are Finite-Sized Corrections to Scaling, Phys. Rev. Lett. **81**, 802 (1998).

[103] G. J. Lord and J. Rougemont, A numerical scheme for stochastic PDEs with Gevrey regularity, IMA J. Numer. Anal. **24**, 587 (2004).

[104] D. Pisarenko, L. Biferale, D. Courvoisier, U. Frisch, and M. Vergassola, Further results on multifractality in shell models, Phys. Fluids **5**, 2533 (1993).

[105] E. Platen and W. Wagner, On a Taylor formula for a class of Itō processes, Prob. Math. Stat. **3**, 87 (1982).

[106] P. E. Kloeden and E. Platen, *Numerical Solution of Stochastic Differential Equations*, Stochastic Modelling and Applied Probability (Springer, Berlin, 2013).

[107] S. Becker, A. Jentzen, and P. E. Kloeden, An exponential Wagner–Platen type scheme for spdes, SIAM J. Numer. Anal. **54**, 2389 (2016).

[108] P. E. Kloeden, G. J. Lord, A. Neuenkirch, and T. Shardlow, The exponential integrator scheme for stochastic partial differential equations: Pathwise error bounds, J. Comput. Appl. Math. **235**, 1245 (2011).

[109] T. N. Palmer, Stochastic weather and climate models, Nat. Rev. Phys. **1**, 463 (2019).

[110] S. Chen, G. Doolen, J. R. Herring, R. H. Kraichnan, S. A. Orszag, and Z. S. She, Far-Dissipation Range of Turbulence, Phys. Rev. Lett. **70**, 3051 (1993).

[111] J. Schumacher, K. R. Sreenivasan, and V. Yakhot, Asymptotic exponents from low-Reynolds-number flows, New J. Phys. **9**, 89 (2007).

[112] J. Schumacher, Sub-Kolmogorov-scale fluctuations in fluid turbulence, Europhys. Lett. **80**, 54001 (2007).

[113] Note that it is possible that $N(4t_{\rm avg}) > N(t_{\rm avg})$ because a new strong "burst" may enter the dissipation range between the times $t_{\rm avg}$ and $4t_{\rm avg}$.

[114] J. I. Marden, Hypothesis testing: From p values to Bayes factors, J. Am. Stat. Assoc. **95**, 1316 (2000).

[115] D. Agostini and C. Améndola, Discrete Gaussian distributions via theta functions, SIAM J. Appl. Algebra Geom. **3**, 1 (2019).

[116] S. Roux and M. H. Jensen, Dual multifractal spectra, Phys. Rev. E **69**, 016309 (2004).

[117] Whereas we averaged over 300 large-eddy turnover times, Ref. [56] averaged over several thousand such times. We could not afford to do likewise, because our much better-resolved dissipation range forced us to use a much smaller time step.

[118] E. D. Siggia, Model of intermittency in three-dimensional turbulence, Phys. Rev. A **17**, 1166 (1978).

[119] A. A. Mailybaev, Blowup as a driving mechanism of turbulence in shell models, Phys. Rev. E **87**, 053011 (2013).

[120] L. Biferale, A note on the fluctuation of dissipative scale in turbulence, Phys. Fluids **20**, 031703 (2008).

[121] M. Hairer, Solving the KPZ equation, Ann. Math., **178** 559 (2013).

[122] Here we neglect, however, scale-dependence of the renormalized viscosity $\nu(k)$. If this viscosity decreases as k grows, then $k_{\rm coup}$ is correspondingly lowered. A kinematic viscosity on order of magnitude $\nu \sim \lambda_{\rm micr} c_{\rm th}$ follows, as is well-known, from the kinetic theories of Boltzmann and Enskog. This is a reasonable estimate of the "bare viscosity" at length scales of order the mean free path, before it is dressed or renormalized by thermal fluctuations. Indeed, it is well-known that the Boltzmann-type kinetic equations neglect the effects of thermal fluctuation, which must be incorporated by additional Langevin terms; see Refs. [205–207] and, for more recent work, Refs. [174,208]. Furthermore, this estimate of the "bare viscosity" is in agreement with the study of Ref. [19]; see their Appendix C, Fig. 8.

[123] N. N. Bogoliubov, *Problem Dinamicheskoi Theorii v Statisticheskoi Fiziki* (Gostekhizdat, Moscow-Leningrad, 1946) translated into English as N. N. Bogoliubov, "Problems of a Dynamical Theory in Statistical Physics," in *Studies in Statistical Mechanics*, edited by J. de Boer and G. E. Uhlenbeck (North-Holland, Amsterdam, 1962), Vol. 1, p. 1.

[124] H. Grad, On the kinetic theory of rarefied gases, Commun. Pure Appl. Math. **2**, 331 (1949).

[125] D. Bandak, G. L. Eyink, N. Goldenfeld, and A. Mailybaev, Spontaneous stochasticity in fluid turbulence from thermal noise: How the "swerve" of molecules influences weather and climate (unpublished).

[126] G. Krstulovic and M.-É. Brachet, Two-fluid model of the truncated Euler equations, Physica D **237**, 2015 (2008).

[127] S. S. Ray, U. Frisch, S. Nazarenko, and T. Matsumoto, Resonance phenomenon for the Galerkin-truncated Burgers and Euler equations, Phys. Rev. E **84**, 016301 (2011).

[128] S. D. Murugan, D. Kumar, S. Bhattacharjee, and S. S. Ray, Many-Body Chaos in Thermalized Fluids, Phys. Rev. Lett. **127**, 124501 (2021).

[129] A. J. Majda and I. Timofeyev, Remarkable statistical behavior for truncated Burgers–Hopf dynamics, Proc. Natl. Acad. Sci. USA **97**, 12413 (2000).

[130] D. Venkataraman and S. Sankar Ray, The onset of thermalization in finite-dimensional equations of hydrodynamics: Insights from the Burgers equation, Proc. R. Soc. A **473**, 20160585 (2017).

[131] P. Clark Di Leoni, P. D. Mininni, and M. E. Brachet, Dynamics of partially thermalized solutions of the Burgers equation, Phys. Rev. Fluids **3**, 014603 (2018).

[132] S. D. Murugan, U. Frisch, S. Nazarenko, N. Besse, and S. S. Ray, Suppressing thermalization and constructing weak solutions in truncated inviscid equations of hydrodynamics: Lessons from the Burgers equation, Phys. Rev. Res. **2**, 033202 (2020).

[133] U. Frisch, S. Kurien, R. Pandit, W. Pauls, S. S. Ray, A. Wirth, and J.-Z. Zhu, Hyperviscosity, Galerkin Truncation, and Bottlenecks in Turbulence, Phys. Rev. Lett. **101**, 144501 (2008).

[134] U. Frisch, S. S. Ray, G. Sahoo, D. Banerjee, and R. Pandit, Real-Space Manifestations of Bottlenecks in Turbulence Spectra, Phys. Rev. Lett. **110**, 064501 (2013).

[135] D. Banerjee and S. S. Ray, Transition from dissipative to conservative dynamics in equations of hydrodynamics, Phys. Rev. E **90**, 041001(R) (2014).

[136] R. Agrawal, A. Alexakis, M. E. Brachet, and L. S. Tuckerman, Turbulent cascade, bottleneck, and thermalized spectrum in hyperviscous flows, Phys. Rev. Fluids **5**, 024601 (2020).

[137] P. D. Ditlevsen and I. A. Mogensen, Cascades and statistical equilibrium in shell models of turbulence, Phys. Rev. E **53**, 4785 (1996).

[138] T. Gilbert, V. S. L'vov, A. Pomyalov, and I. Procaccia, Inverse Cascade Regime in Shell Models of Two-Dimensional Turbulence, Phys. Rev. Lett. **89**, 074501 (2002).

[139] B. Levant, F. Ramos, and E. S. Titi, On the statistical properties of the 3D incompressible Navier-Stokes-Voigt model, Commun. Math. Sci. **8**, 277 (2010).

[140] R. Tom and S. S. Ray, Revisiting the Sabra model: Statics and dynamics, Europhys. Lett. **120**, 34002 (2017).

[141] S. S. Ray, Thermalized solutions, statistical mechanics and turbulence: An overview of some recent results, Pramana **84**, 395 (2015).

[142] T. Matsumoto, M. Otsuki, O. Takeshi, S. Goto, and A. Nakahara, Response function of turbulence computed via

fluctuation-response relation of a Langevin system with vanishing noise, Phys. Rev. E **89**, 061002(R) (2014).
[143] R. H. Kraichnan, Convergents to turbulence functions, J. Fluid Mech. **41**, 189 (1970).
[144] J. B. Bell, A. Nonaka, A. L. Garcia, and G. Eyink, Thermal fluctuations in the dissipation range of homogeneous isotropic turbulence, J. Fluid Mech. **939**, A12 (2022).
[145] H. Sadeghi, P. Lavoie, and A. Pollard, Effects of finite hot-wire spatial resolution on turbulence statistics and velocity spectra in a round turbulent free jet, Exp. Fluids **59**, 40 (2018).
[146] M. Raffel, C. E. Willert, F. Scarano, C. J. Kähler, S. T. Wereley, and J. Kompenhans, *Particle Image Velocimetry: A Practical Guide*, Experimental Fluid Mechanics (Springer International Publishing, Berlin, 2018).
[147] B. Dubrulle, Giant von Kármán experiment, https://www-llb.cea.fr/Pisp/berengere.dubrulle/projects//EXPLOIT/Gallery.htm.
[148] A. Donev, J. B. Bell, A. L. Garcia, and B. J. Alder, A hybrid particle-continuum method for hydrodynamics of complex fluids, Multiscale Model. Simul. **8**, 871 (2010).
[149] T. Li, S. Kheifets, D. Medellin, and M. G. Raizen, Measurement of the instantaneous velocity of a Brownian particle, Science **328**, 1673 (2010).
[150] S. Kheifets, A. Simha, K. Melin, T. Li, and M. G. Raizen, Observation of Brownian motion in liquids at short times: Instantaneous velocity and memory loss, Science **343**, 1493 (2014).
[151] S. Tan, A. Salibindla, A. U. M. Masuk, and R. Ni, Introducing OpenLPT: New method of removing ghost particles and high-concentration particle shadow tracking, Exp. Fluids **61**, 47 (2020).
[152] J. Czarske and L. Büttner, Micro laser doppler velocimetry (μ-LDV), in *Encyclopedia of Microfluidics and Nanofluidics*, edited by D. Li (Springer Science, New York, 2013).
[153] A. Donev, T. G. Fai, and E. Vanden-Eijnden, A reversible mesoscopic model of diffusion in liquids: From giant fluctuations to Fick's law, J. Stat. Mech. (2014) P04004.
[154] A. Chaudhri, J. B. Bell, A. L. Garcia, and A. Donev, Modeling multiphase flow using fluctuating hydrodynamics, Phys. Rev. E **90**, 033014 (2014).
[155] M. Gallo, F. Magaletti, D. Cocco, and C. M. Casciola, Nucleation and growth dynamics of vapour bubbles, J. Fluid Mech. **883**, A14(2020).
[156] A. Lemarchand and B. Nowakowski, Fluctuation-induced and nonequilibrium-induced bifurcations in a thermochemical system, Mol. Simul. **30**, 773 (2004).
[157] A. K. Bhattacharjee, K. Balakrishnan, A. L. Garcia, J. B. Bell, and A. Donev, Fluctuating hydrodynamics of multispecies reactive mixtures, J. Chem. Phys. **142**, 224107 (2015).
[158] I. O. Götze and G. Gompper, Mesoscale simulations of hydrodynamic squirmer interactions, Phys. Rev. E **82**, 041921 (2010).
[159] D. A. Donzis, K. R. Sreenivasan, and P. K. Yeung, The Batchelor spectrum for mixing of passive scalars in isotropic turbulence, Flow, Turbul. Combust. **85**, 549 (2010).
[160] M. P. Clay, D. Buaria, P. K. Yeung, and T. Gotoh, GPU acceleration of a petascale application for turbulent mixing at high schmidt number using openmp 4.5, Comput. Phys. Commun. **228**, 100 (2018).
[161] D. Buaria, M. P. Clay, K. R. Sreenivasan, and P. K. Yeung, Turbulence is an Ineffective Mixer when Schmidt Numbers are Large, Phys. Rev. Lett. **126**, 074501 (2021).
[162] I. Saito and T. Gotoh, Turbulence and cloud droplets in cumulus clouds, New J. Phys. **20**, 023001 (2018).
[163] S. Elghobashi, Direct numerical simulation of turbulent flows laden with droplets or bubbles, Annu. Rev. Fluid Mech. **51**, 217 (2019).
[164] F. Milan, L. Biferale, M. Sbragaglia, and F. Toschi, Sub-Kolmogorov droplet dynamics in isotropic turbulence using a multiscale lattice Boltzmann scheme, J. Comput. Sci. **45**, 101178 (2020).
[165] K. R. Sreenivasan, Possible effects of small-scale intermittency in turbulent reacting flows, Flow, Turbul. Combust. **72**, 115 (2004).
[166] J. F Driscoll, Turbulent premixed combustion: Flamelet structure and its effect on turbulent burning velocities, Prog. Energy Combust. Sci. **34**, 91 (2008).
[167] T. Echekki and E. Mastorakos, *Turbulent Combustion Modeling: Advances, New Trends and Perspectives*, Fluid Mechanics and Its Applications (Springer, Netherlands, 2010).
[168] W. M. Durham, E. Climent, M. Barry, F. De Lillo, G. Boffetta, M. Cencini, and R. Stocker, Turbulence drives microscale patches of motile phytoplankton, Nat. Commun. **4**, 2148 (2013).
[169] J. D. Wheeler, E. Secchi, R. Rusconi, and R. Stocker, Not just going with the flow: The effects of fluid flow on bacteria and plankton, Annu. Rev. Cell Dev. Biol. **35**, 213 (2019).
[170] L. Caffarelli, R. Kohn, and L. Nirenberg, Partial regularity of suitable weak solutions of the Navier-Stokes equations, Commun. Pure Appl. Math. **35**, 771 (1982).
[171] H. M. Mott-Smith, The solution of the Boltzmann equation for a shock wave, Phys. Rev. **82**, 885 (1951).
[172] H. W. Liepmann, R. Narasimha, and M. T. Chahine, Structure of a plane shock layer, Phys. Fluids **5**, 1313 (1962).
[173] E. Salomons and M. Mareschal, Usefulness of the Burnett Description of Strong Shock Waves, Phys. Rev. Lett. **69**, 269 (1992).
[174] F. Bouchet, Is the Boltzmann equation reversible? A large deviation perspective on the irreversibility paradox, J. Stat. Phys. **181**, 515 (2020).
[175] S.-H. Yu, Hydrodynamic limits with shock waves of the Boltzmann equation, Commun. Pure Appl. Math. **58**, 409 (2005).
[176] G. L. Eyink, Review of the Onsager "ideal turbulence" theory, arXiv:1803.02223.
[177] G. L. Eyink and T. D. Drivas, Cascades and Dissipative Anomalies in Compressible Fluid Turbulence, Phys. Rev. X **8**, 011022 (2018).
[178] T. D. Drivas and G. L. Eyink, An Onsager singularity theorem for turbulent solutions of compressible Euler equations, Commun. Math. Phys. **359**, 733 (2018).
[179] R. Zwanzig, Memory effects in irreversible thermodynamics, Phys. Rev. **124**, 983 (1961).
[180] H. Grabert, *Projection Operator Techniques in Nonequilibrium Statistical Mechanics*, Springer Tracts in Modern Physics (Springer, Berlin, 2006).
[181] A. J. Chorin, O. H. Hald, and R. Kupferman, Optimal prediction and the Mori–Zwanzig representation of irreversible processes, Proc. Natl. Acad. Sci. USA **97**, 2968 (2000).

[182] C. Hijón, P. Español, E. Vanden-Eijnden, and R. Delgado-Buscalioni, Mori–Zwanzig formalism as a practical computational tool, Faraday Discuss. **144**, 301 (2010).
[183] H. Spohn, *Large Scale Dynamics of Interacting Particles*, Theoretical and Mathematical Physics (Springer, Berlin, 2012).
[184] P. Luchini, Receptivity to thermal noise of the boundary layer over a swept wing, AIAA J. **55**, 121 (2017).
[185] A. Fedorov and A. Tumin, Receptivity of high-speed boundary layers to kinetic fluctuations, AIAA J. **55**, 2335 (2017).
[186] A. A. Mailybaev, Spontaneously stochastic solutions in one-dimensional inviscid systems, Nonlinearity **29**, 2238 (2016).
[187] N. Vladimirova, M. Shavit, S. Belan, and G. Falkovich, Second harmonic generation as a minimal model of turbulence, Phys. Rev. E **104**, 014129 (2021).
[188] M. Shavit and G. Falkovich, Singular Measures and Information Capacity of Turbulent Cascades, Phys. Rev. Lett. **125**, 104501 (2020).
[189] O. Feliachi and F. Bouchet, Dynamical large deviations for homogeneous systems with long range interactions and the Balescu-Guernsey-Lenard equation, J. Stat. Phys. **186**, 22 (2022).
[190] J. A. Krommes, Projection-operator methods for classical transport in magnetized plasmas. part 1. Linear response, the Braginskii equations and fluctuating hydrodynamics, J. Plasma Phys. **84**, 925840401 (2018).
[191] J. A. Krommes, Projection-operator methods for classical transport in magnetized plasmas. part 2. Nonlinear response and the Burnett equations, J. Plasma Phys. **84**, 905840601 (2018).
[192] S. Xu and A. Lazarian, Magnetohydrodynamic turbulence and turbulent dynamo in partially ionized plasma, New J. Phys. **19**, 065005 (2017).
[193] G. Satten and D. Ronis, Fluctuations in finite systems: Time reversal symmetry, surface onsager reciprocal relations and fluctuating hydrodynamics, Physica A **125**, 281 (1984).
[194] G. L. Eyink and A. Jafari, High Schmidt-number turbulent advection and giant concentration fluctuations, Phys. Rev. Research (to be published).
[195] R. H. Kraichnan, Convection of a passive scalar by a quasi-uniform random straining field, J. Fluid Mech. **64**, 737 (1974).
[196] P. K. Yeung, S. Xu, D. A. Donzis, and K. R. Sreenivasan, Simulations of three-dimensional turbulent mixing for Schmidt numbers of the order 1000, Flow, Turbul. Combust. **72**, 333 (2004).
[197] M. P. Clay, Strained Turbulence and Low-Diffusivity Turbulent Mixing using High Performance Computing, Ph.D. thesis, Georgia Institute of Technology (2017).
[198] A. Vailati and M. Giglio, Giant fluctuations in a free diffusion process, Nature (London) **390**, 262 (1997).
[199] A. Vailati, R. Cerbino, S. Mazzoni, C. J. Takacs, D. S. Cannell, and M. Giglio, Fractal fronts of diffusion in microgravity, Nat. Commun. **2**, 290 (2011).
[200] J. D. Ramshaw and K. Lindenberg, Augmented Langevin description of multiplicative noise and nonlinear dissipation in Hamiltonian systems, J. Stat. Phys. **45**, 295 (1986).
[201] S. F. Edwards, The statistical dynamics of homogeneous turbulence, J. Fluid Mech. **18**, 239 (1964).
[202] E. A. Novikov, Functionals and the random-force method in turbulence theory, Sov. Phys. JETP **20**, 1290 (1965).
[203] S. F. Edwards and W. D. McComb, Statistical mechanics far from equilibrium, J. Phys. A: Gen. Phys. **2**, 157 (1969).
[204] M. I. Vishik and A. V. Fursikov, *Mathematical Problems of Statistical Hydromechanics*, Mathematics and its Applications (Springer, Berlin, 1988), Vol. 9.
[205] M. Bixon and R. Zwanzig, Boltzmann-Langevin equation and hydrodynamic fluctuations, Phys. Rev. **187**, 267 (1969).
[206] R. F. Fox and G. E. Uhlenbeck, Contributions to nonequilibrium thermodynamics. II. Fluctuation theory for the Boltzmann equation, Phys. Fluids **13**, 2881 (1970).
[207] H. Spohn, Fluctuation theory for the Boltzmann equation, in *Nonequilibrium Phenomena I: The Boltzmann Equation* (North-Holland Publishing, Amsterdam, 1983), pp. 225–251.
[208] T. Bodineau, I. Gallagher, L. Saint-Raymond, and S. Simonella, Statistical dynamics of a hard sphere gas: Fluctuating Boltzmann equation and large deviations, arXiv:2008.10403.

Supplemental Material

A Evaluation of the thermal equilibration scale from the theory of the intermediate-dissipation range spectrum

In this section of the Supplemental Material we estimate the equilibration scale using the Frisch-Vergassola theory of the "intermediate-dissipation range" (IDR) [40], rather than the exponential decay ansatz (II.20). We recall that the Frisch-Vergassola theory is built on the assumption of a range of dissipation lengths $\eta_h = LRe^{-\frac{1}{1+h}}$, for each Hölder exponent h with multifractal dimension spectrum $D(h)$. For deterministic Navier-Stokes turbulence, [40] arrived at the model energy spectrum exhibiting "pseudo-algebraic decay" in the IDR:

$$\begin{cases} E(k) = C_K u_{rms}^2 L (kL)^{-1-\zeta_2}, \ \text{ for } \ k < \eta_2^{-1}, \\ E(k) = C_K u_{rms}^2 L (kL)^{-1-2h(k)-3+D(h(k))}, \qquad \text{for } \ \eta_2^{-1} < k < \eta_\infty^{-1}, \end{cases} \tag{1}$$

with $h(k) = -1 + \frac{\log(Re)}{\log(kL)}$ and with $\eta_p = \eta_{h_p}$ for $h_p = d\zeta_p/dp$. Here h_∞ is the minimum Hölder singularity, often denoted $h_{\min}$. In the far-dissipation range $k > 1/\eta_\infty$, [40] supposed a rapidly decaying spectrum "possibly of exponential type". We shall therefore supplement the above model with an exponential-decay spectrum in the FDR

$$E(k) = C_K u_{rms}^2 k^{-1} e^{-\beta \eta_\infty k}, \ \text{ for } \ \eta_\infty^{-1} < k, \tag{2}$$

where $\beta = [2h_\infty + (3 - D(h_\infty)] \ln(L/\eta_\infty)$ so that it continuously joins onto the IDR spectrum. In fact, we shall see that this ansatz of exponential decay in the FDR plays no essential role in the estimation of the thermal equilbration scale, because the spectral decay in the IDR is already extremely rapid. In fact, it is straightforward to show using the IDR model that

$$\frac{\partial \ln E(k)}{\partial \ln(kL)} = -2 + D(h(k)) - p(h(k))(h(k) + 1) \tag{3}$$

with $p(h) = D'(h)$ so that $\left.\frac{\partial \ln E(k)}{\partial \ln(kL)}\right|_{k=1/\eta_\infty} = -\infty$ unless $h_\infty = -1$. Thus, in a log-log plot, the local slope of the energy spectrum at the upper end of the IDR is $-\infty$ and the spectral decay is infinitely steep. We now illustrate these points with several popular multifractal models [31,71,72].

We begin with the She-Lévêque log-Poisson model [71], according to which the scaling exponents ζ_p are given by

$$\zeta_p = \frac{p}{9} + 2 - 2\big(2/3\big)^{p/3} \tag{4}$$

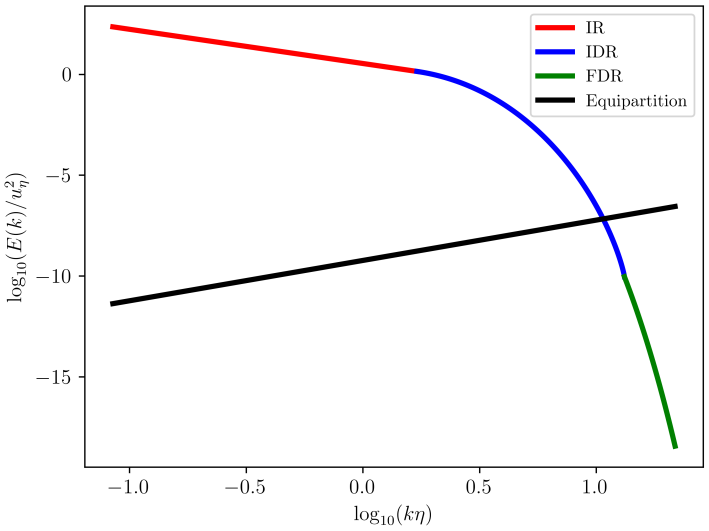

Figure 1: Model energy spectrum for the She-Lévêque model, including the inertial range (IR), intermediate-dissipation range (IDR), far-dissipation range (FDR), and the equipartition spectrum.

and $h_\infty = 1/9$. In that case, the Hölder exponent as a function of order p is

$$h_p = \frac{d\zeta_p}{dp} = \frac{1}{9} + \ln(3/2)(2/3)^{\frac{p}{3}+1}. \tag{5}$$

Inverting this expression to get $p(h)$ we obtain

$$p(h) = \frac{3}{\ln(\frac{3}{2})} \ln\left(\frac{\frac{2}{3}\ln(\frac{3}{2})}{h - \frac{1}{9}}\right) \tag{6}$$

Then the fractal dimension as a function of Hölder exponent is

$$D(h) = hp(h) + 3 - \zeta_{p(h)} = 1 + 3\left(1 + \ln\left(\frac{\frac{2}{3}\ln\frac{3}{2}}{h - \frac{1}{9}}\right)\right)\frac{h - \frac{1}{9}}{\ln(\frac{3}{2})} \tag{7}$$

Substituting these results into the IDR model (1) yields the spectrum plotted in Figure 1 using Kolmogorov dissipation-range units. Here we have taken $C_K = 1.6$, and the parameter values u_{rms}, L were chosen to correspond to those from the main text of the paper. Note that the IDR is fairly short, covering less than a decade of scales for $Re \sim 10^6$ appropriate to the ABL, but the "pseudo-algebraic" spectral decay over this range is very steep.

The second model we consider is the Yakhot mean-field model [72] with structure function exponents given as

$$\zeta_p = \frac{ap}{b + cp} \tag{8}$$

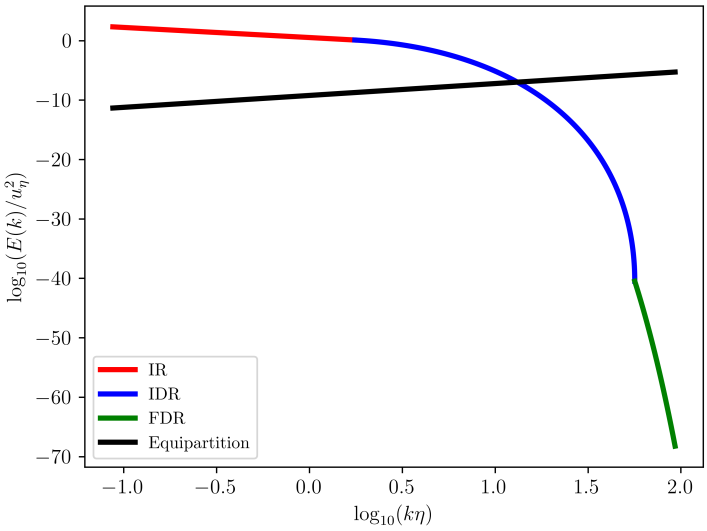

Figure 2: Model energy spectrum for the Yakhot mean-field model, including the inertial range (IR), intermediate-dissipation range (IDR), far-dissipation range (FDR), and the equipartition spectrum.

for $a = 0.185$, $b = 0.473$, and $c = 0.0275$. Then the Hölder exponent as a function of order p is

$$h_p = \frac{d\zeta_p}{dp} = \frac{ab}{(b + cp)^2} \tag{9}$$

and

$$p(h) = \frac{1}{c}\left(\frac{ab}{h}\right)^{1/2} - \frac{b}{c} \tag{10}$$

We thus arrive at the fractal dimension as a function Hölder exponent

$$D(h) = hp(h) + 3 - \zeta_{p(h)} = 3 - \frac{b}{c}\left(\left(\frac{a}{b}\right)^{1/2} - h^{1/2}\right)^2 \tag{11}$$

Substituting this into the Eq.1 results in the spectrum plotted in Figure 2 using dissipation-range units. Note that $h_\infty = 0$ here, smaller than the value $h_\infty = 1/9$ for the log-Poisson model. Thus, the IDR is longer, covering almost two decades of scales for $Re \sim 10^6$ but the energy spectrum again falls off very steeply here.

The last model we consider is the Kolmogorov lognormal model [31] with structure function exponents given as

$$\zeta_p = \frac{p}{3} - \frac{\mu}{18}p(p-3), \tag{12}$$

for $\mu = 0.25$. Performing the same steps as for the two previous models

$$h_p = \frac{d\zeta_p}{dp} = \frac{1}{3} - \frac{\mu}{18}(2p-3), \tag{13}$$

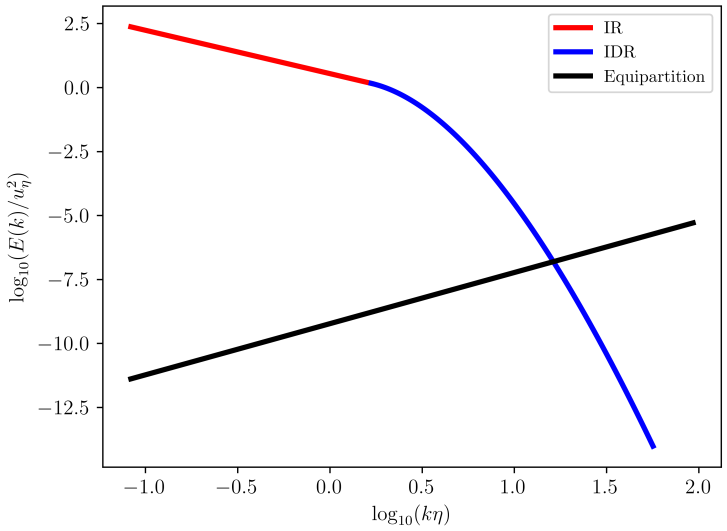

Figure 3: Model energy spectrum for the Kolmogorov lognormal model, including the inertial range (IR), intermediate-dissipation range (IDR), and the equipartition spectrum.

$$p(h) = \frac{3}{2} + \frac{9}{\mu}(\frac{1}{3} - h), \tag{14}$$

$$D(h) = hp(h) + 3 - \zeta_{p(h)} = 3 - \frac{1}{2\mu}\Big(1 + \frac{\mu}{2} - 3h\Big)^2, \tag{15}$$

we arrive at the spectrum plotted in Figure 3, also in dissipation-range units. In this model formally $h_\infty = -\infty$, although $\eta_h = 0$ already for $h = -1$ and thus only $h > -1$ are physically relevant. In this model the IDR becomes infinitely long and so we added no FDR exponential-decay range.

As is clearly seen from the Figures 1, 2, and 3, the equipartition spectrum $E(k) = \frac{\theta_K k^2}{4\pi^4}$ with the value $\theta_K = 2.83\times10^{-8}$ from the main text, appropriate to the ABL, crosses the deterministic model spectra at a scale just a factor of $\simeq 6.3$, 7.9 and 10.0 below the Kolmogorov scale η respectively. Not only is the correction to the estimate in the main text of the paper of order unity, but also the equilibration scale is closer to the Kolmogorov scale for the She-Leveque and Yakhot mean-field theories. Note that in all three cases the crossover to thermal equipartition occurs in the IDR range and not in the FDR range with exponentially decaying energy spectrum. This is an illustration of the point made in the main text that the equilibration scale is robust with respect to exact details of the fluctuations below the Kolmogorov scale, and must appear around $\eta_K/10$. This will be true, up to factors of order unity, for any model of the turbulent energy spectrum which exhibits very rapid decay in the dissipation range, so that the amplitude of the turbulent velocity fluctuations quickly becomes of the same order as the thermal fluctuations.

B Extreme Burst Event

Here we give to full double-precision accuracy the extreme burst event that we used for convergence tests in the main text of the paper:

$$
\begin{aligned}
(&-18.849526195188336 - 23.050633157318 46i,\\
&-2.783369994139593 - 26.903742403718077i,\\
&-18.31205838300695 - 21.761423345252606i,\\
&-11.773634233964085 - 18.445715311506376i,\\
&-16.79185981909443 - 17.759878017576444i,\\
&-8.46269922283849 - 13.662493157995428i,\\
&2.9499477133177474 - 12.573345649311605i,\\
&9.39311352232625 - 16.645759217187404i,\\
&13.165496151785879 - 1.6424477622763587i,\\
&7.923466581725228 + 9.062137712120846i,\\
&5.077361321839786 + 15.805823258118155i,\\
&-10.891820549933136 + 12.156351830237558i,\\
&-9.698457257518518 - 9.736257942800322i,\\
&10.304053079351213 + 8.065004934238564i,\\
&6.211864121538015 - 1.8230069634584574i,\\
&-1.4093348240188477 + 1.5700620722441085i,\\
&-1.3676684827038674 - 1.1009625173074413i,\\
&-0.0657630170592099 + 0.101405418447494i,\\
&-0.0002542426626073849 + 0.006533617008375689i,\\
&-0.00029773367792373663 + 0.00012256324898515924i,\\
&0.00023489945398114735 + 9.415521350520184 \times 10^{-5}i,\\
&-0.00011252714872981789 - 0.00026933372836924737i,\\
&9.142826562445602 \times 10^{-5} - 0.0001509544819947159i)
\end{aligned}
$$